PLASTICITY IN LATERAL AMYGDALA AFTER PAVLOVIAN FEAR CONDITIONING – A Computational Study

---

A Dissertation

presented to

the Faculty of the Graduate School

University of Missouri – Columbia

In Partial Fulfillment

of the Requirement for the Degree

Doctor of Philosophy

---

by

DONGBEOM KIM

Dr. Satish S. Nair, Dissertation Supervisor

July 2013

The undersigned, appointed by the dean of the Graduate School, have examined the dissertation entitled

PLASTICITY IN LATERAL AMYGDALA AFTER PAVLOVIAN CONDITIONING-A COMPUTATIONAL STUDY

presented by Dongbeom Kim,

a candidate for the degree of doctor of philosophy,

and hereby certify that, in their opinion, it is worthy of acceptance.

Professor Satish S. Nair

Professor Dominic Ho

Professor Jae Wan Kwon

Professor Yunxin Zhao

ACKNOWLEDGEMENTS

I want to appreciate my advisor Dr. Satish Nair for his guidance and support. Without him this work would not have been accomplished. I also thank Dr Jae Wan Kwon, Dr Dominic Ho and Dr Yunxin Zhao for being a part of my Ph.D. program committee.

Above all things, I appreciate my family, my wife Jooyoung and my precious two daughters, Diane and Danielle.

I am also grateful to group members who are always ready to help me in every possible way.

Lastly I would like to thank my parents for their blessings that have made me the person that I am today.

TABLE OF CONTENTS

CHAPTER 3

LIST OF FIGURES

Chapter 4

Chapter 5

LIST OF TABLES

ABSTRACT

Computational neuroscience provides tools to abstract and generalize principles of neuronal function using mathematics and computers. This dissertation reports a computational model of a specific neuronal sub-circuit that provide insights into fear memory formation in vertebrates, including methods to develop biologically realistic reduced order models of single neurons.

One of the main contributions of the dissertation is an explanation of how and why certain neurons are recruited into a memory trace. For this, we developed a biophysical model of the rodent lateral amygdala (LA) and then examined how particular LA neurons are assigned to the fear memory trace, i.e., how fear memory is formed in a rodent brain, after Pavlovian fear conditioning. The model revealed that neurons with high intrinsic excitability are more likely to be integrated into the memory trace but that competitive synaptic interactions also play a critical role. We also examined the relative contributions of plasticity in auditory afferent (thalamic, cortical) neurons vs. within LA. This revealed that plasticity in afferent pathways to LA is required for fear memory formation, but that once formed, the plasticity in afferent pathways was not needed. The model then provided insights into how 'competition' was implemented at the single cell level, including the role of excitatory connections among neurons, of disynaptic inhibition, and of neuromodulation. These principles should also apply to other forms of memory in brains. We then investigated another related concept of specificity of memory, i.e., how does memory of fear to a particular tone prevented from being elicited by another tone. Analysis showed that formation of tone fear memory in LA involves

plasticity in intrinsic excitatory and inhibitory connections within LAd and this intrinsic plasticity also ensures specificity for that memory.

Neuronal network models presently use simplified single cells models with either one or two compartments. This is largely due to the fact that computational overheads become prohibitive with more detailed models. We also report a procedure to develop a reduced order model matching passive properties, current injection traces, and preserving some synaptic integration features. Comparisons are made at both single cell and at 100-cell network model levels. Analysis showed that a model with three compartments provides a good compromise between biological realism and ease of computation.

CHAPTER 1

INTRODUCTION AND OBJECTIVES

1.1. BACKGROUND AND MOTIVATION

I still remember the scary story my grandmother recited to me and my older sister when we were kids. I also remember being deeply saddened when she passed away, and at that time thought that such emotions rose from the heart. Now, more than 30 years later, I spent my days and nights, trying to figure out how brains work, especially how they help make emotional memory.

Computational neuroscience is the study of brain function in terms of the information processing properties of the neurons and synapses that make up the nervous system. A neuron is modeled as a nonlinear electrical element with capacitance and variable resistances, and many neurons were combined to form networks and circuits. Using biologically realistic and reduced order models, system theoretic concepts are used to investigate how such neurons/network circuits implement functions. The particular circuit studied in this dissertation is the mammalian fear circuit. This circuit is essential for the survival of any organism, since an organism that cannot fear 'appropriately' will not be able to escape from dangers. Malfunction of such circuits is thought to be the cause for many of the anxiety disorders including post-traumatic stress disorder. For that reason, there is considerable interest among numerous research agencies in understanding how the mammalian fear circuit works. Studies of such circuits are typically performed by neuroscientists using rodents as the animal model, and Pavlovian fear conditioning as

the paradigm. A key element of the mammalian fear circuit is the amygdala which has about 24,000 neurons in rodents. This structure is the focus of this dissertation.

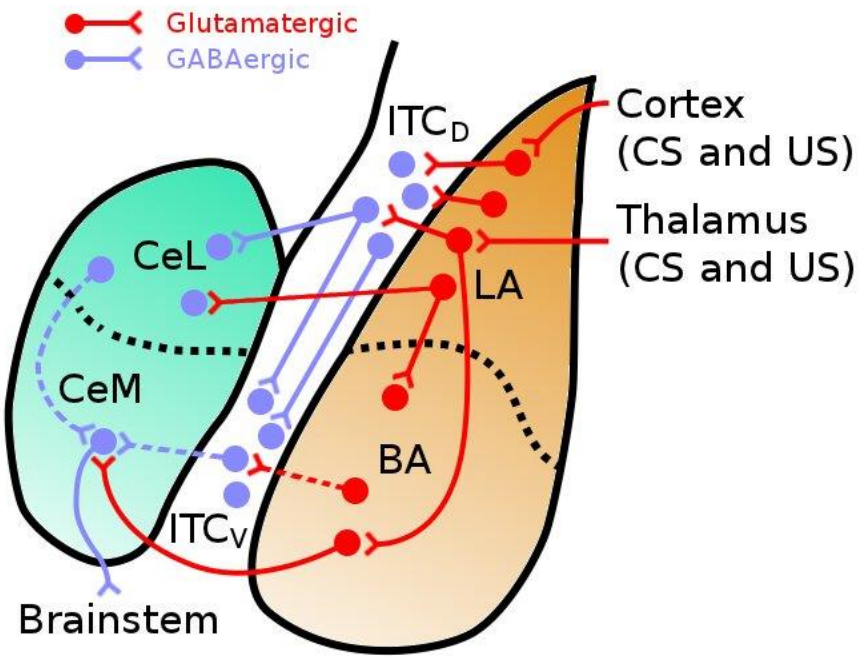

Fig. 1. Amygdalar pathways relevant to auditory fear. Tone and shock information arrive at LA via thalamic and cortical routes. LA projects to BA and also to ITC_D and Ce_L. Based on our present understanding (Amano et al., 2011), LA projects to BA, ITC_D and CeL. BA fear neurons project to Ce_M and BA extinction neurons project to ITC_V (fear recall circuit in bold and extinction recall in dashed line type). Ce represents the amygdalar output which projects to the brainstem and other regions eliciting fear.

In Pavlovian auditory fear conditioning, an initially neutral conditioned acoustic stimulus (CS), after being associated with an aversive unconditioned stimulus (US), typically electric shock, acquires the ability to induce conditioned fear responses (Pavlov,1927). The components of the amygdala which are critical for fear conditioning

are the lateral nucleus (LA), the basal nucleus (BL), and the central nucleus (CE). The LA is believed to be a storage site for such fear memories. In auditory fear conditioning, convergence of tone (conditioned stimulus, CS) and foot-shock (unconditioned stimulus, US) inputs from the auditory cortex and auditory thalamus in LA leads to potentiation of CS inputs, resulting in larger tone responses in LA. Increased LA responses are relayed to the CE via the basal nuclei, and the intercalated (ITC) cell masses, eliciting fear responses via successive projections to brain stem and hypothalamic sites. As a result, rats learn to freeze to tones that predict foot-shock. Repeated subsequent presentation of the tone without shock leads to a decrease in fear which eventually goes down to habituation levels, and this process is called extinction. It has been shown that extinction is not just erasure of fear memory but the formation of a different memory. This dissertation focuses on how the lateral amygdala stores fear and extinction memories via the potentiation of particular synapses within the amygdala.

1.2 OVERVIEW OF DISSERTATION AND OBJECTIVES

This dissertation deals with four related studies that involve computational models of neurons and neuronal networks at varying levels of complexity and biological realism. Each study is presented in the form of a stand-alone journal article, as described below.

Chapter 2. *Mechanisms contributing to the induction and storage of pavlovian fear memories in the lateral amygdala*. We developed a 1000-neuron biophysical model of LAd that reproduced the cellular correlates of auditory fear memory formation, as seen experimentally. It examined the relative contributions of plasticity in auditory afferent (thalamic, cortical) neurons vs. within LA. This revealed that plasticity in afferent

pathways to LA is required for fear memory formation. However, once induced, thalamocortical plasticity is no longer required because the fear memory is maintained by changes in synaptic efficacy within LA. We then investigated the role of plasticity at the afferent synapses onto LA neurons themselves, and of the plasticity at synapses between LA neurons. Analysis revealed that efficacy of the synapses that thalamic and cortical neurons form with LA cells augments considerably and are important to maintain the memory, and that plasticity at synapses between LA neurons plays a minor role in maintaining the fear memory.

Chapter 3. *Assignment of lateral amygdala neurons to the fear memory trace depends on competitive synaptic interactions*

The study then examined how particular LA neurons are assigned to the fear memory trace. For instance, when fear is being learned during the Pavlovian fear conditioning protocol, only 20% of the LA neurons end up storing this memory, but it is not clear how this 20% are selected. This study revealed that neurons with high intrinsic excitability are more likely to be integrated into the memory trace but that competitive synaptic interactions also play a critical role. In particular, these results indicate that subsets of projection cells effectively band together by virtue of their excitatory interconnections to suppress plasticity in other principal neurons via the recruitment of inhibitory interneurons.

Chapter 4. *Synaptic mechanisms related to competition and specificity of amygdalar fear*.

After studying how memory formation depended on the excitability of principal cells and their connections, we go to a lower level in this chapter and explore of how competition

between lateral amygdala neurons is implemented via plasticity in the network at the single cell level. Another related issue studies is how does such plasticity enable the animal to distinguish between to related stimuli. That is, if the animal is fear conditioned to a particular tone, will it also fear another tone that has overlapping frequency components, and would it also fear some other stimuli such as smell in case a subset of the same LA neurons are utilized by that stimulus. The model suggested that both completion and stimulus specificity are related, and that the plasticity that is caused by competition also helps preserve stimulus specificity.

Chapter 5. *Single cell model selection for network simulations*. Biologically realistic multi-compartmental models of single neurons typically have compartments ranging from 1 to over 500. Neuronal network models typically use simplified single cells models with either one or two compartments presently. This is largely due to the fact that computational times become prohibitive if detailed cell models are used. Although other model such as the Izhikevich model that preserves neuro-computational properties do provide attractive alternatives, they are not suited for detailed biological studies that require realistic synapses, neuromodulation, and morphology to represent transmission of signals from dendrites to soma and vice versa. We report a procedure to develop a reduced order model which provides a good compromise between biological realism and ease of computation. We compare the model with a very detailed model, and investigate the roles of inhibition, neuromodulation and plasticity.

Chapter 6. The final chapter summarizes the dissertation and suggests areas for future research.

CHAPTER 2

MECHANISMS CONTRIBUTING TO THE INDUCTION AND STORAGE OF PAVLOVIAN FEAR MEMORIES IN THE LATERAL AMYGDALA

ABSTRACT

The relative contributions of plasticity in the amygdala vs. its afferent pathways to conditioned fear remain controversial. Some believe that thalamic and cortical neurons transmitting information about the conditioned stimulus (CS) to the lateral amygdala (LA) serve a relay function. Others maintain that thalamic and/or cortical plasticity is critically involved in fear conditioning. To address this question, we developed a large-scale biophysical model of the lateral amygdala (LA) that could reproduce earlier findings regarding the cellular correlates of fear conditioning in LA. We then conducted model experiments that examined whether fear memories depend on (1) training-induced increases in the responsiveness of thalamic and cortical neurons projecting to LA, (2) plasticity at the synapses they form in LA, and/or (3) plasticity at synapses between LA neurons. These tests revealed that training-induced increases in the responsiveness of afferent neurons are required for fear memory formation. However, once the memory has been formed, this factor is no longer required because the efficacy of the synapses that thalamic and cortical neurons form with LA cells has augmented enough to maintain the

memory. In contrast, our model experiments suggest that plasticity at synapses between LA neurons plays a minor role in maintaining the fear memory.

INTRODUCTION

The ability to associate fear responses to new stimuli or circumstances on the basis of experience is necessary for survival. The experimental paradigm typically used to study this process is Pavlovian fear conditioning, where an initially neutral stimulus (conditioned stimulus-CS) acquires the ability to elicit conditioned fear responses after pairing with a noxious unconditioned stimulus (US). While there is evidence that fear conditioning induces widespread synaptic plasticity in the brain, including at thalamic and cortical levels (Letzkus et al., 2011; Weinberger, 2011), there is also data indicating that the dorsal portion of the lateral amygdala (LAd) is a critical site of plasticity for the storage of CS-US associations (LeDoux, 2000; reviewed in Pape and Paré, 2010).

For instance, unit recording studies have revealed that auditory fear conditioning increases the CS responsiveness of LAd neurons (Quirk et al., 1995; Collins and Paré, 2000; Repa et al., 2001; Goosens et al., 2003). In the most dorsal part of LAd (LAdd), neurons display increases in CS responsiveness that last for only a few trials ("transient cells") whereas in more ventrally located LAd (LAdv) neurons ("long-term plastic cells"), CS responses are persistently increased, even resisting extinction training (Repa et al., 2001). This has led to the proposal that the two cell types are involved in the initiation of learning vs. long-term storage of the fear memory, respectively (Repa et al., 2001). However, the mechanisms contributing to the formation of these two response types remain unknown.

Similarly, although it is well established that fear conditioning increases the CS responsiveness of thalamic and cortical neurons projecting to LA (reviewed in Weinberger, 2011), the contributions of CS afferent pathways to conditioned fear memories remain controversial. In particular, it has been impossible to determine the relative importance of plasticity within LA versus CS inputs to LA. To address these questions, we developed a biologically realistic computational model of LAd that could reproduce the transient and long-term plastic LAd cells previously observed by Repa et al. (2001) and then conducted a series of experimentally impossible manipulations to probe the contributions of plasticity in CS afferent pathways versus within LAd to conditioned fear.

RESULTS

We have developed a biophysically-realistic model of LAd to investigate the mechanisms underlying the different temporal patterns of increased tone responsiveness displayed by neurons in the dorsal and ventral parts of LAd during fear conditioning (Repa et al., 2001). The simulated LAd network included conductance-based models of 800 principal cells and 200 interneurons that reproduced the electroresponsive properties of these cell types, as observed experimentally (**Fig. 1**; reviewed in Sah et al., 2003), and neuromodulatory inputs from brainstem dopaminergic and noradrenergic neurons (Johnson et al., 2011). In addition, based on previous in vitro experiments (Samson and Paré, 2006), the model network integrated spatially differentiated patterns of excitatory and inhibitory connections within LA (**Fig. 2**). Last, all the glutamatergic synapses in the

model could undergo both short-term and long-term activity-dependent plasticity, except for those delivering shock or background inputs (see Materials and Methods).

The training paradigm we used is shown in **figure 2C.** In figures 3 to 7, all data points represent a block of four trials, except for the first, which is the average of the final six habituation trials, as in Repa et al. (2001). All reported values are averages ± s.e.m. expressed as percent change from control and tone responses (see representative examples in Fig. S1) are computed as spikes per tone within 200 ms of tone onset.

Impact of fear conditioning on the tone responsiveness of LAd neurons

There is a long-standing controversy in the field regarding the relative contributions of plasticity in the amygdala vs. CS afferent pathways to conditioned fear (Paré, 2002). One view posits that thalamic and cortical neurons transmitting CS information to LA merely serve as sensory relays. Another stipulates that thalamic and/or cortical plasticity is critical for fear conditioning (reviewed in Weinberger, 2011). Thus, we first examined whether our model could reproduce the findings of Repa et al. (2001) when the CS responsiveness of thalamic and cortical neurons relaying tone information to LAd remained unchanged at 20 Hz (habituation level) through conditioning.

In these conditions (**Fig. 3**, empty triangles), the model could not reproduce the findings of Repa et al. (2001; **Fig. 3**, solid circles). Indeed, whereas Repa et al. (2001) observed that 24% of LAd cells developed increased tone responses as a result of fear conditioning, only 9% (or 75 of 800) did so in the model experiment with thalamic and cortical tone-evoked firing rates unchanged at 20 Hz through conditioning. Moreover, when we considered cells that showed significant increases in tone responsiveness, as

identified using the criterion of Repa et al. (2001), their average tone responses were much lower (<50%) than seen experimentally (**Fig. 3**). Various modifications to the model, including the distribution or strength of thalamic and cortical inputs, the Ca^{2+}-dependence of synaptic plasticity in LAd neurons, as well as the intrinsic connectivity within LAd, failed to alter this basic conclusion **(Fig. S2)**.

Since many studies reported that fear conditioning does increase the tone responsiveness of CS afferent neurons and that such changes play a critical role in the formation of conditioned fear memories (Quirk et al., 1997; Hennevin and Maho, 2005; Letzkus et al., 2011; Weinberger, 2011), we next ran the same "behavioral" protocol but increased the firing rate of thalamic inputs during the CS from 20 to 40 Hz after one conditioning trial, and after six trials for cortical inputs, in keeping with prior experimental observations (Quirk et al., 1997).With this modification (**Fig. 3**, gray squares), the model successfully replicated the impact of fear conditioning and extinction training on the CS responsiveness of principal LAd cells, as described in Repa et al. (2001).

To assess the model's ability to reproduce these earlier results (**Fig. 4A 1,2,** black curves), we relied on the criteria used by Repa et al. (2001) to analyze the behavior of LAd cells. That is, as a first step, model neurons were classified as plastic if their CS-elicited firing during any of the 4-trial conditioning blocks was higher than the habituation level using a t-test with a significance threshold of $p<0.05$. In a second step, a 'persistence' value was calculated for each plastic cell by dividing the increase in CS responses during late conditioning (final 8 trials) by that seen during early conditioning (first 8 trials), both relative to habituation. As in Repa et al. (2001), plastic cells with

persistence values of less than 0.75 were classified as *transiently plastic* (TP) cells (**Fig. 4A1**, red), and those with persistence values greater than 0.75 were classified as *long-term plastic* (LP) cells (**Fig. 4A2**, blue).

In the model, 24.7% (198/800) of principal LAd cells were plastic cells (LP and TP cells), which is similar to experimental observations (24/100, Repa et al., 2001) with 12% (96/800) being TP cells and 12.7% (102/800) being LP cells, again similar to experimental values (12% for each type; Repa et al., 2001). Moreover, whereas TP cells were largely found in LAdd (**Fig. 5**; 75 of 96), model LP cells were more widely distributed in LAd (**Fig. 5**; 47 and 55 of 102 in LAdd and LAdv, respectively), as again seen experimentally (5 and 7 of 12, in Fig. 8 of Repa et al. 2001). Last, model TP and LP neurons reproduced the behavior of the corresponding cell types during extinction, as seen experimentally (**Fig. 4A**). That is, the tone responses of TP cells were at habituation levels except during the first block of extinction (**Fig. 4A1**; $p<0.001$). In contrast, LP cells retained higher levels of tone responsiveness throughout extinction (**Fig. 4A2**; $p<0.001$).

While the above suggests that conditioning-induced increases in the CS responsiveness of thalamic and cortical neurons are required for the emergence of LP and TP cells (**Fig. 3, 4B**), it remains unclear whether the altered CS responsiveness of LAd neurons, once induced, remains dependent on an augmented signaling of the CS by thalamic and cortical neurons. To address this question, we ran the same simulation as above with the exception that the firing rates of thalamic and cortical CS inputs during the CS were returned to habituation levels during the recall test. Unexpectedly, this manipulation did not alter the average tone responses of TP (**Fig. 4C1**, squares**)** and LP

cells (**Fig. 4C2**, squares), only causing a small and statistically insignificant decrease (10%; p = 0.33) in their tone responses. Overall, the above simulations indicate that increases in the CS responsiveness of thalamic and cortical neurons projecting to LAd are required for the development of the LAd plasticity but that, once induced, it is plasticity in LAd that mainly contributes to maintain the increased tone responsiveness of TP and LP cells.

Role of input connectivity in the formation of TP and LP cells

To determine whether the emergence of TP and LP cells was dependent on the particular connections they formed, we compared their intrinsic and extrinsic connectivity. Since TP and LP cells were more prevalent in LAdd vs. LAdv, respectively (**Fig. 5**; TP, red; LP, blue), we first compared the inputs to principal cells in these two LAd regions. The reader is reminded that the model's intrinsic connectivity was not set arbirarily but adjusted to reproduce the pattern of intra-LAd connections infered in a previous electrophysiological study (Samson and Paré, 2006). This analysis revealed that the average ratio of excitatory to inhibitory connections for an LAd principal cell was significantly lower in LAdd (0.84 ± 0.03) than in LAdv (1.1 ± 0.04, $p<0.0001$). This difference was even more pronounced between TP cells in LAdd (1.07±0.05) and LP cells in LAdv (1.5±0.08).

However, TP and LP cells were similar in other respects. For instance, both types received at least one tone input and most received direct shock inputs (TP, 93%; LP, 96%). Yet, a higher proportion of the tone inputs originated from the thalamus for TP (86%) than LP cells (58%) and the opposite for cortical inputs (TP, 40%; LP, 91%; X^2 =

23.5, $p<0.001$). Since previous unit recordings in rats have revealed that the CS responsiveness of auditory cortical neurons increases slowly during conditioning (Quirk et al., 1997), the latter difference probably contributed to the distinct temporal profiles seen in model TP and LP cells. Consistent with this, ablating cortical inputs to LAdv and LAdd neurons drastically reduced the tone responsiveness of LP cells (**Fig. 6A2**; $p<0.001$), with only marginal effects on TP cells (**Fig. 6A1**; $p=0.55$).

To test whether the differences in intrinsic connectivity between TP and LP cells play a role in shaping their spatial distribution and responsiveness, we carried out additional simulations using a random uniform connectivity (see details in legend of Fig. 6) or by selectively removing all connections from LAdd to LAdv (**Fig. 6B**). In TP cells, the random uniform connectivity resulted in an unchanged tone responsiveness during habituation but a marked increase by the end of conditioning (225±18%; $p<0.0001$) and late extinction (49±4%; $p<0.05$; **Fig. 6B1**, empty red circles and dashed lines). In contrast, the tone responses of LP cells were reduced by 46±3% ($p<0.05$) during late conditioning and by 37±3% ($p<0.01$) during late extinction, with no significant change during habituation ($p=0.23$; **Fig. 6B2**, empty blue circles and dashed line). As explained below, these divergent changes in tone responsiveness of TP and LP cells were due to a shift in dorsoventral connectivity. Indeed, by converting the model's connectivity from biology-based to random, the number of ventral to dorsal principal cell connections (which were sparse in the control case) increased, while dorsal to ventral connections (which were high in the control case) decreased.

In a second test, the model's connectivity was returned to its initial state with the exception that we selectively removed all connections from LAdd to LAdv. This resulted

in a decrease in tone responses of LP cells during late conditioning (43±3%; $p<0.001$) and late extinction (36±3%; $p<0.001$), with no significant change during habituation ($p=0.2$), (**Fig. 6B2**, triangles), and, as expected, no significant change in the tone responsiveness of TP cells ($p=0.79$; **Fig. 6B1**, triangles).

Last, we directly tested the hypothesis put forward by Repa et al. (2001), namely that TP and LP cells are involved in the initiation of learning vs. long-term storage of the fear memory, respectively. To this end, we ran simulations with the synaptic strengths of TP cells clamped at habituation levels (by disabling plasticity) during conditioning (**Fig. 7A1**). Although this manipulation only had a marginal effect on the number of LP cells (from 102 to 98), it greatly reduced their responses to the CS (**Fig. 7A2**) during late conditioning (41±3% from control; $p<0.001$) and late extinction (29±3%; $p<0.001$).Overall, these simulations support the model set forth by Repa et al. (2001) and indicate that that the heterogeneous intrinsic connectivity of LAd plays a critical role in shaping the behavior of LAd neurons during fear conditioning.

Role of afferent and intrinsic LAd synapses in storing fear memories

Overall, the model experiments presented so far suggest that formation of auditory conditioned fear memories depends on several interacting factors including (1) conditioning-induced increases in the tone responsiveness of afferent thalamic and cortical neurons, (2) a heterogeneous termination pattern of these cells in LAd, and (3) spatially differentiated intrinsic connections within LAd. However, the above tests did not address the question of what amygdala synapses are critical for storing the fear memory. As mentioned above, when the tone-evoked activity of thalamic and cortical neurons was artificially returned to habituation levels during the recall test, the number of

plastic LAd cells as well as the magnitude of their tone-evoked responses were essentially unaltered (**Fig. 4C**). This indicates that a population of synapses within the amygdala maintains the memory.

Candidate synapses include those between tone afferents and LAd neurons as well as those between LAd neurons themselves. To identify the critical synapses, we next ran simulations where, after fear conditioning, the weight of various types of synapses was returned to habituation levels, one type at a time. We then examined the impact of these manipulations on the responsiveness of TP and LP cells when the CS was presented alone. As shown in **figure 7B**, returning the weight of tone afferents to habituation levels had a dramatic impact, reverting the tone evoked responses of TP and LP cells to pre-training levels (paired t-tests: TP 66±5%, $p < 0.001$; LP 80±6%, $p<0.001$). In contrast, the same manipulation at all amygdala synapses simultaneously caused a marginal *increase* in the tone responses of TP (26 ± 2%) and LP cells (11 ± 1%) (**Fig. 7C**). Only the former effect reached significance (paired t-test, $p<0.01$). Importantly, restricting the latter tests to synapses involving plastic cells yielded the same results.

Selection of model parameters.

As cited in methods, available biological data were used to constrain the single cell models, connectivity, and the effects of neuromodulation, as in other similar models (e.g., Dyhrfjeld-Johnsen et al., 2007). However, synaptic strengths and plasticity parameters are not well understood presently. Two conditioning-induced factors affect afferent (thalamus/cortex to LAd) and intrinsic (within LAd) plasticity during conditioning: (i) change in excitability of thalamic and cortical cells, and (ii) change in neuromodulator

concentrations. As we have demonstrated with the model, these two factors were critical for matching experimental data in Repa et al. (2001) for the numbers of plastic cells and the magnitudes of their tone responses. Various modifications to other parameters such as distributions of afferents, plasticity parameters, or intrinsic connectivity within LAd failed to reproduce the experimental data for the numbers of plastic cells and/or their tone responsiveness (e.g., Fig. S2, S3) if only one effect were present. Furthermore, with both effects present, we did find a second model (model 2, see section S2.2 of Suppl Matls.) that was similar in all respects to the present model except for different intra-LAd parameters (initial intra- synaptic strengths and plasticity parameters). Model 2 outputs were also similar in all cases except for decreased inhibitory transmission in the amygdala after fear conditioning as has been reported in some experiments (Rea et. al., 2009), in contrast to the small increase seen in model 1. Both thalamic/cortical plasticity and neuromodulator effects were critical for model 2 also. Taken together, all these constitute evidence that the network might not be inadvertently 'tuned' in the process of development.

DISCUSSION

We have developed a biophysically-realistic model of LAd to shed light on fundamental, yet unresolved questions regarding the mechanisms of Pavlovian fear memory formation, storage, and expression. These questions include the respective contributions of plasticity in LAd vs. CS afferent pathways, and the role of the intrinsic LAd network in the initiation and storage of fear memories. Below, we discuss the insights that emerged from our simulations.

Initiation vs. storage of fear memory by different types of LAd neurons: contributing mechanisms

During fear conditioning, the temporal profile of changes in CS responsiveness is not uniform in LAd (Repa et al., 2001). Some neurons, concentrated in LAdd, display augmented CS responses for only a few trials whereas others, typically in LAdv, show persistently increased CS responses that resist extinction. This led Repa et al. (2001) to speculate that the two cell types (transient –TP; long-term – LP) are involved in the initiation of learning vs. long-term storage of the fear memory, respectively. Our model could reproduce these observations including the two cell types, their incidence, as well as differential distribution in LAd. Our analyses revealed that a number of interacting factors contributed to the emergence of the two cell types in LAd.

Intrinsic connectivity. Differences in the intrinsic connectivity of principal cells in LAdd and LAdv appeared to play a determining role in the emergence of TP and LP cells. Indeed, our model featured heterogeneous intrinsic connections based on the findings of a prior electrophysiological study (Samson and Paré, 2006). As a result of this heterogeneous connectivity, the ratio of excitatory to inhibitory inputs to principal cells was lower in LAdd than LAdv, and this difference was particularly marked between TP and LP cells. When this heterogeneous intrinsic connectivity was replaced with random uniform connections, the model could no longer reproduce the observations of Repa et al. (2001). LAdd to LAdv connections appeared to play a critical role in this respect since selective ablations of these connections greatly attenuated the CS responsiveness of LP cells. Moreover, in support of the notion that TP and LP cells are respectively involved in

the initiation of learning vs. long-term storage of the fear memory, we observed that clamping the CS responsiveness of TP cells at habituation levels during learning blunted the increase in the CS responses of LP cells produced by fear conditioning.

Tone and shock inputs. Another aspect of the model's connectivity that played a determining role was the distribution of tone and shock inputs. Compared to non-plastic cells, a higher proportion of TP and LP cells received tone and shock inputs in the model. However, TP and LP cells tended to derive their tone inputs from different sources: prevalently from the thalamus for TP cells vs. the cortex for LP cells. Since the CS responsiveness of auditory cortical neurons increases slowly during conditioning (Quirk et al., 1997), this difference is likely a major determinant of the contrasting temporal profiles of increased CS responsiveness seen in model TP and LP cells.

Contributions of the amygdala and CS afferent neurons to fear memory formation and storage

Despite incontrovertible evidence that fear conditioning leads to plasticity not only in the amygdala but also in CS afferent pathways (≈25 papers from numerous laboratories), the role of thalamic and cortical neurons in fear memory formation is often overlooked in the literature (reviewed in Weinberger, 2011). In part, this is due to the difficulty of disentangling thalamocortical vs. amygdala contributions to fear memory. However, computational models allow experimentally impossible manipulations that can shed light on this question.

Here, we compared how our model LAd network behaved when the firing rates of thalamic and cortical neurons during the CS were clamped at habituation levels

throughout the behavioral protocol or allowed to increase during conditioning, as observed experimentally. These simulations revealed that unless thalamic and cortical CS responsiveness increased during conditioning, the model could not reproduce learning-induced changes in the behavior of LAd neurons, as observed experimentally (Repa et al., 2001). While this suggests that an augmented thalamic and cortical CS responsiveness is required for the induction of amygdala plasticity, is it also required for fear expression after learning? To address this question, we allowed the CS responsiveness of thalamic and cortical neurons to increase during conditioning but returned it to habituation levels during the recall test. Unexpectedly, the CS responses of LAd neurons were marginally altered by this manipulation.

Overall, these results support the view that increases in the CS responsiveness of thalamic and cortical neurons are required for fear learning, but that later on, they are no longer critical because the fear memory can be maintained by learning-induced changes in synaptic efficacy within the amygdala. To identify what population of synapses are critical for storing Pavlovian fear memories, we next ran simulations where, after fear conditioning, the weight of various types of synapses was returned to habituation levels, one type at a time. This revealed that the critical sites of plasticity are tone inputs from the thalamus and cortex to LAd neurons. Indeed, suppressing plasticity at these synapses returned the tone responses of TP and LP cells to habituation levels. In contrast, abolishing plasticity at all synapses between amygdala neurons caused an unexpected *increase* in CS responsiveness. It may be that plasticity in the intrinsic LAd network leads to a potentiation of feedforward inhibition that limits the size of the population of

plastic cells. Such a phenomenon might contribute to maintain the specificity of fear memories. A challenge for future studies will be to test this prediction.

Finally, it should be noted that the model did not address the question of whether the amygdala is involved in altering the tone responsiveness of thalamic and/or cortical neurons in the first place. This possibility appears likely given the abundance of data indicating that the amygdala can facilitate synaptic plasticity in various structures of the brain either directly, or via the recruitment of modulatory systems (McGaugh, 2002; Paré, 2003).

MATERIALS AND METHODS

We developed a biophysical model of LAd. A brief overview is presented here. See Supplementary materials for details (S1-S3).

Single cell models

To reproduce the diversity of spike frequency adaptation seen in principal LA neurons (reviewed in Sah et al., 2003), we modeled three types of regular spiking principal cells, with high (type-A), intermediate (type-B), or low (type-C) spike frequency adaptation, due to the differential expression of a Ca^{2+}-dependent K^+ current. LA also contains local GABAergic interneurons that exhibit various firing patterns, even among neurochemically-homogeneous subgroups (Lang and Paré, 1998; Rainnie et al., 2006; Sosulina et al., 2006; Woodruff and Sah, 2007; Jasnow et al., 2009). However, the majority displays a fast-spiking pattern, which was reproduced in the model.

The principal cell model had three compartments representing a soma (diameter 24.75 µm; length 25 µm), an apical dendrite (dia 2.5 µm; length 296 µm) on which synapses were placed, and another dendrite (dia 5 µm; length 400 µm) that helped match passive properties. Values of specific membrane resistance, membrane capacity and cytoplasmic (axial) resistivity were, respectively, R_m = 55 KΩ-cm^2, C_m= 1.2-2.4 µF/cm^2, and R_a= 150-200 Ω-cm. Leakage reversal potential (E_L) was set to -67 mV. The resulting V_{rest} was – 69.5 mV, input resistance (R_{IN}) was ~150 MΩ, and τ_m was 30 ms, all of which were within the ranges reported in previous physiological studies (Washburn and Moises, 1992; Faber et al., 2001). All compartments had the following currents: leak (I_L), voltage-gated persistent muscarinic (I_M), high-voltage activated Ca^{2+} (I_{Ca}), spike-generating

sodium (I_{Na}), potassium delayed rectifier (I_{DR}) and A-type potassium (I_A) (Li et al., 2009; Power et al., 2011). In addition, the dendrites had a hyperpolarization-activated nonspecific cation (I_h) currents and a slow apamin-insensitive, voltage-independent afterhyperpolarization current (I_{sAHP}) (Power et al., 2011). See sections S1.4 and S1.5 of the supplementary materials as well as Tables S1-2 for current equations and densities.

Figure 1A shows the voltage response of the three principal cell models to depolarizing (two left panels) and hyperpolarizing (right panel) current injection. The three model cells could reproduce previous experimental observations (Sah et al., 2003) including the temporal dynamics of repetitive firing produced by membrane depolarization as well as their responses to membrane hyperpolarization.

The interneuron model had two compartments, a soma (dia 15 µm; length 15 µm) and a dendrite (dia 10 µm; length 150 µm). Each compartment contained a fast Na^+ (I_{Na}) and a delayed rectifier K^+ (I_{DR}) currents with kinetics (Durstewitz et al., 2000) that reproduced the much shorter spike duration that is characteristic of fast-spiking cells. The passive membrane properties were as follows: R_m = 20 KΩ-cm^2, C_m=1.0 µF/cm^2, R_a= 150 Ω-cm, and E_L = -70 mV. As shown in **figure 1B**, the interneuron model could reproduce the non-adapting repetitive firing behavior of fast spiking cells, as observed experimentally (Lang and Paré, 1998; Woodruff and Sah, 2007).

Network structure and connectivity

It was estimated that there are 24,000 principal cells in LAd (Tuunanen and Pitkänen, 2000). To keep computation times practical while capturing the complexity of the intra-LAd network, we modeled a scaled down (30:1) version of LAd that included 800

principal cells. Because the proportion of interneurons to principal cells is 20:80 (McDonald and Augustine, 1993), the model included 200 interneurons. Principal cells and interneurons were distributed randomly in a realistic tri-dimensional representation of the horn-shaped LAd (**Fig. 2A**).

By comparing the responses of LA cells to local applications of glutamate at various positions with respect to recorded neurons, Samson and Paré (2006) inferred general principles of connectivity among principal cells, as well as between local-circuit and principal neurons. In particular, Samson and Paré (2006) determined that excitatory connections between principal cells prevalently run ventrally and medially with significant rostrocaudal divergence. In contrast, inhibitory connections prevalently run mediolaterally in the horizontal plane and have no preferential directionality in the coronal plane. Samson and Paré (2006) also recognized that principal LA neurons located along the external capsule (in the "shell" region of LA) form different connections than those found more medially (in the "core" region of LA; shell thickness of 100 μm). In the shell region, inhibitory neurons only affect nearby principal neurons whereas excitatory connections between principal cells are spatially less limited. While not providing precise connectivity data, this information could be used to infer critical estimates about directionality and ratio of excitation to inhibition. Using the directionality information from the Samson and Paré (2006) study, and a third of the connectivity numbers, a model principal cell had, on average, 21.4 mono- and 40.6 di-synaptic excitatory inputs, and 22.2 mono-synaptic inhibitory inputs. These average figures result from the implementation of directionally heterogeneous connections, as described below.

Coronal plane. Within a 100 μm coronal slice, principal shell neurons excite shell cells located 300-400 μm more ventrally with 10% probability (**Fig. 2B1**; note that these are for mono-synaptic connectivity). Core to shell connections occur with a much lower probability (2%). In addition, principal shell neurons are inhibited by more dorsally-located interneurons (23% connectivity for cells within 300 μm; **Fig. 2B2**). In the core region, excitatory connections between principal cells have a greater extent in the lateromedial direction (50-800 μm, 2-6%, connectivity; **Fig. 2B3**) than in the mediolateral direction (50-200 μm, 5% connectivity; **Fig. 2B3**), whereas inhibitory connections have similar strengths in all directions (interneurons formed inhibitory inputs with 10-24% of principal cells at a distance of 50-600 μm; **Fig. 2B4**).

Horizontal plane. Within a 100 μm horizontal slice, connections were set in the following manner. Connection probability increased with distance for lateromedial connections, and the opposite for mediolateral connections (see details in **Fig. 2B5**). As to inhibitory connections, they prevalently run in the mediolateral direction with 8-20% connectivity in the range 50-600 μm and 5-20% connectivity in the lateromedial direction within a distance of 50-600 μm (**Fig. 2B6**). Principal cells project to all interneurons within a spherical radius of 100 μm.

Activity-dependent synaptic plasticity

Fear conditioning induces changes in the efficacy of synapses conveying CS inputs to LA (McKernan and Shinnick-Gallagher, 1997; Rumpel et al., 2005). Also, activity-dependent long-term potentiation (LTP) can be induced at thalamic (Huang et al., 2000; Humeau et al., 2005; Tsvetkov et al., 2004) and cortical (Huang and Kandel, 1998;

Humeau et al., 2003; Humeau et al., 2005; Tsvetkov et al., 2002) inputs to principal LA neurons. Furthermore, it has been shown that fear conditioning and LTP share a common set of mechanisms (Miserendino et al., 1990; Kim et al., 1991; Campeau et al., 1992; Huang and Kandel, 1998; Bauer et al., 2002), and that fear conditioning occludes LTP of cortical inputs to LA cells (Tsvetkov et al., 2002). These findings, coupled to the fact that intra-amygdala infusion of NMDA receptor antagonists blocks the induction of conditioned fear in vivo and of LTP in vitro provided the basis for the hypothesis that NMDA receptor-mediated LTP represents a cellular substrate of fear conditioning (reviewed in Pape and Paré, 2010). Induction of LTP at thalamic and cortical inputs to principal cells has been found to depend on postsynaptic depolarization allowing influx of Ca^{2+} ions via NMDA receptors (Bauer et al., 2002; Tsvetkov et al., 2002) and/or voltage-dependent L-type Ca^{2+} channels (Bauer et al., 2002; Humeau et al., 2005; Weisskopf et al., 1999). In addition, it was reported that excitatory glutamatergic synapses from the thalamus or cortex onto interneurons exhibit NMDA-receptor-dependent potentiation (Bauer and LeDoux, 2004). This potentiation is also AMPA-receptor-dependent because AMPA receptors on inhibitory neurons lack the GluR2 subunit, making them calcium-permeable (Mahanty and Sah, 1998). It was further shown that inhibitory inputs onto pyramidal cells are modifiable via a Ca^{2+}-dependent mechanism (Bauer and LeDoux, 2004). In addition to LTP, long-term depression (LTD) can be readily induced at excitatory amygdala synapses by low-frequency stimulation of the lateral nucleus at 1 Hz for 15 min (Wang and Gean, 1999).

To reproduce these experimental findings, all AMPA synapses in the model were endowed with long-term postsynaptic plasticity except for those delivering shock or

background inputs. Also, all GABA synapses had long-term plasticity. This form of plasticity was implemented using a learning rule that uses the concentration of a post-synaptic calcium pool at each modifiable synapse (Kitajima and Hara, 1997; Shouval et al., 2002; Li et al., 2009). Calcium entered post-synaptic pools at excitatory synapses via NMDA receptors (and AMPA receptors for interneurons) and voltage-gated calcium channels (VGCCs). Similarly, calcium for pools at inhibitory synapses came from post-synaptic intra-cellular stores and VGCCs (Li et al., 2009). For both types of synapses, the synaptic weight decreased when the calcium concentration of the pool was below a lower threshold and increased when it exceeded an upper threshold. Equations and details related to the learning rule are provided in S1.6 of the supplementary materials.

All model AMPA and GABA synapses also exhibited short-term presynaptic plasticity, with short-term depression at interneuron to principal cell and principal cell to interneuron connections modeled after the experimental findings of Woodruff and Sah (2007) in the basolateral amygdala. In the absence of experimental data about the short-term dynamics of synapses between principal LAd neurons, we relied on data obtained between regular spiking cortical cells to implement short-term frequency dependent depression (Markram et al., 2004). For convenience in modeling, these were implemented by multiplying the synaptic conductances of the relevant AMPA and GABA synapses after each spike with appropriate frequency-dependent factors (Varela et. al 1997). See section S1.7 of the supplementary materials for equations.

Neuromodulator effects

Neuromodulators have long been implicated in fear and anxiety, and are known to regulate Pavlovian fear learning and synaptic plasticity in LA (Bissière, 2003; Tully and Bolshakov, 2001). Conditioned aversive stimuli alter the activity of ventral tegmental area and locus coeruleus neurons (Feenstra et al., 2001), which in turn modulate fear and anxiety through their widespread forebrain projections, including to the amygdala (Guarraci and Kapp, 1999). Therefore, the model incorporated the effects of dopamine (DA) and norepinephrine (NE) on LAd cells, based on prior experimental reports as outlined in S1.1 of supplementary materials**.**

Inputs

LA receives auditory inputs directly from the posterior intralaminar nucleus and the medial sector of the medial geniculate nucleus (LeDoux et al., 1985; Linke et al., 2000; Shinonaga et al., 1994; Turner and Herkenham, 1991; Woodson et al., 2000) as well as indirectly via temporal auditory cortical fields (Romanski and LeDoux, 1993ab; Mascagni et al., 1993; Shi and Cassell, 1997). Moreover, the same posterior thalamic regions that send auditory inputs to LA also receive inputs from the spinothalamic tract (LeDoux et al., 1987) and probably send convergent CS and US inputs to LA. Accordingly, the model was endowed with CS and US inputs represented as glutamatergic synapses acting at AMPA and NMDA receptors. Based on the experimental literature, we modeled two types of CS inputs: thalamic and cortical, both at 20 Hz during habituation and 40 Hz after conditioning (Bordi and LeDoux, 1994; Quirk et al., 1997). These two tone inputs were differentially distributed in LAd, as described below.

Background synaptic inputs. LA projection neurons have low spontaneous firing rates in control conditions (Gaudreau and Paré, 1996). To reproduce this, Poisson-distributed, random excitatory background inputs were delivered to all model cells, resulting in average spontaneous firing rates of 0.7 Hz for principal cells and 7.2 Hz for interneurons.

Tone and shock inputs. Auditory fear conditioning is commonly thought to depend on the convergence of inputs relaying information about the CS (tone) and US (footshock) in LA (reviewed in Pape and Paré 2010). In the model, the CS and US inputs were represented by glutamatergic synapses acting via AMPA and NMDA receptors. The frequency of thalamic and cortical tone inputs during habituation was set to 20 Hz (Quirk et al., 1997). The tone inputs also included noise represented by random Poisson spikes with an average frequency of 2 Hz. The density of both cortical and thalamic tone inputs to LAd was determined iteratively (see S1.2 of supplementary materials). The following distribution of inputs was used for the simulations described in the Results section: uniform total tone density throughout LAd with 70% of the LAdd cells receiving thalamic and 35% receiving cortical tone projections, and the opposite for LAdv, i.e., 35% of LAdv cells receiving thalamic and 70% receiving cortical tone projections. The shock inputs continued to be distributed uniformly to 70% of LAd cells.

Conditioning protocol used in simulations

The schedule of tone and shock inputs in the simulations was based on in vivo studies (Repa et al., 2001; Quirk et al. 1995). We scaled down the timing of the auditory fear conditioning protocol so that it would be suitable for computational studies (**Fig. 2C**). The protocol included three phases (habituation, conditioning and extinction), comprised

of 8, 16 and 20 trials, respectively. Each trial featured a 0.5 sec tone CS followed by a 3.5 sec gap. Only during conditioning, a shock was administered 100 msec prior to the end of the tone, so that they co-terminated. In light of evidence that fear conditioning leads to plasticity in CS afferent pathways (reviewed in Weinberger, 2011), the frequency of thalamic and cortical tone inputs was increased to 40 Hz after the first and sixth conditioning trials, respectively. Simulations were performed using the NEURON modeling package (Carnevale and Hines, 2006).

Generalization of model outputs

To ensure that the model outputs were consistent across random runs using the same network size, we ran three additional cases with different (i) distribution of cells (types A, B, C) in the 3D space, (ii) connectivity, and (iii) delays, all selected with different random seeds. All these cases yielded consistent numbers for the total plastic cells in the control case (avg. 196.6±4), and for the individual cell groups: TP cells (93.6±4.1), LP cells (103±1.7). Moreover, all the other behaviors discussed were similar, suggesting that the model output is robust to all these parameters.

REFERENCES

Amano T, Duvarci S, Popa D, Paré D. 2011. The fear circuit revisited: contributions of the basal amygdala nuclei to conditioned fear. *J Neurosci* **31**: 15481-15489.

Bauer EP, Schafe GE, LeDoux JE. 2002. NMDA receptors and L-type voltage gated calcium channels contribute to long-term potentiation and different components of fear memory formation in the lateral amygdala. *J Neurosci* **22**: 5239-5249.

Bauer EP, LeDoux JE. 2004. Heterosynaptic long-term potentiation of inhibitory interneurons in the lateral amygdala. *J Neurosci* **24**: 9507-9512.

Bissière S, Humeau Y, Luthi A. 2003. Dopamine gates LTP induction in lateral amygdala by suppressing feedforward inhibition. *Nat Neurosci* **6**: 587-592.

Boatman JA, Kim JJ. 2006. A thalamo-cortico-amygdala pathway mediates auditory fear conditioning in the intact brain. *Eur J Neurosci* **24**: 894-900.

Bordi F, LeDoux JE. 1994. Response properties of single units in areas of rat auditory thalamus that project to the amygdala. I. Acoustic discharge patterns and frequency receptive fields. *Exp Brain Res* **98**: 261-274.

Bush D, Caparosa EM, Gekker A, LeDoux JE. 2010. Beta-adrenergic receptors in the lateral nucleus of the amygdala contribute to the acquisition but not the consolidation of auditory fear conditioning. *Front Behav Neurosci* **4**: 154.

Campeau S, Miserendino MJD, Davis M. 1992. Intraamygdala infusion of the N-methyl-D-aspartate receptor antagonist AP5 blocks acquisition but not expression of fear-potentiated startle to an auditory conditioned-stimulus. *Behav Neurosci* **106**: 569-574.

Carnevale NT, Hines ML. 2006. *The NEURON book*. Cambridge University Press, Cambridge, UK.

Ciocchi S, Herry C, Grenier F, Wolff SB, Letzkus JJ, Vlachos I, Ehrlich I, Sprengel R, Deisseroth K, Stadler MB, Müller C, Lüthi A. 2010. Encoding of conditioned fear in central amygdala inhibitory circuits. *Nature* **468**: 277-282.

Collins DR, Paré D. 2000. Differential fear conditioning induces reciprocal changes in the sensory responses of lateral amygdala neurons to the CS(+) and CS(-). *Learn Mem* **7**: 97-103.

Durstewitz D, Seamans JK, Sejnowski TJ. 2000. Dopamine-mediated stabilization of delay-period activity in a network model of prefrontal cortex. *J Neurophysiol*. **83**: 1733-1750.

Duvarci S, Popa D, Paré D. 2011. Central amygdala activity during fear conditioning. *J Neurosci* **31**: 289-294.

Dyhrfjeld-Johnsen J, Santhakumar V, Morgan RJ, Huerta R, Tsimring L, Soltesz I. 2007. Topological determinants of epileptogenesis in large-scale structural and functional models of the dentate gyrus derived from experimental data. *J Neurophysiol* **97**: 1566-1587.

Faber ES, Callister RJ, Sah P. 2001. Morphological and electrophysiological properties of principal neurons in the rat lateral amygdala in vitro. *J Neurophysiol* **85**: 714-723.

Faber ES, Sah P. 2003. Ca2+-activated K+ (BK) channel inactivation contributes to spike broadening during repetitive firing in the rat lateral amygdala. *J Physiol* **552**: 483-497.

Feenstra MG, Vogel M, Botterblom MH, Joosten RN, de Bruin JP. 2001. Dopamine and noradrenaline efflux in the rat prefrontal cortex after classical aversive conditioning to an auditory cue. *Eur J Neurosci* **13**: 1051–1054.

Gaudreau H, Paré D. 1996. Projection neurons of the lateral amygdaloid nucleus are virtually silent throughout the sleep-walking cycle. *J Neurophysiol* **75**: 1301–1305.

Gaiarsa JL, Caillard O, Ben-Ari Y. 2002. Long-term plasticity at GABAergic and glycinergic synapses: mechanisms and functional significance. *Trends Neurosci* **25**: 564-570.

Goosens KA, Hobin JA, Maren S. 2003. Auditory-evoked spike firing in the lateral amygdala and Pavlovian fear conditioning: mnemonic code or fear bias? *Neuron* **40**:1013-1022.

Guarraci FA, Kapp BS. 1999. An electrophysiological characterization of ventral tegmental area dopaminergic neurons during differential Pavlovian fear conditioning in the awake rabbit. *Behav Brain Res* **99**: 169-179.

Hennevin E, Maho C. 2005. Fear conditioning-induced plasticity in auditory thalamus and cortex: to what extent is it expressed during slow-wave sleep? *Behav Neurosci* **110**: 1277-1289.

Huang YY, Kandel ER. 1998. Postsynaptic induction and PKA-dependent expression of LTP in the lateral amygdala. *Neuron* **21**: 169-178.

Huang YY, Martin KC, Kandel ER. 2000. Both protein kinase A and mitogen activated protein kinase are required in the amygdala for the macromolecular synthesis-dependent late phase of long-term potentiation. *J Neurosci* **20**: 6317-6325.

Humeau Y, Shaban H, Bissiere S, Luthi A. 2003. Presynaptic induction of heterosynaptic associative plasticity in the mammalian brain. *Nature* **426**: 841-845.

Humeau Y, Herry C, Kemp N, Shaban H, Fourcaudot E, Bissiere S, Luthi A. 2005. Dendritic spine heterogeneity determines afferent-specific hebbian plasticity in the amygdala. *Neuron* **45**: 119-131.

Jasnow AM, Ressler KJ, Hammack SE, Chhatwal JP, Rainnie DG. 2009. Distinct subtypes of cholecystokinin (CCK)-containing interneurons of the basolateral amygdala identified using a CCK promoter-specific lentivirus. *J Neurophysiol* **101**: 1494-506

Johnson LR, Hou M, Prager EM, LeDoux JE. 2011. Regulation of the fear network by mediators of stress: norepinephrine alters the balance between cortical and subcortical afferent excitation of the lateral amygdala. *Front Behav Neurosci* **5**: 23.

Kim JJ, DeCola JP, Landeira-Fernandez J, Fanselow MS. 1991. N-methyl-D-aspartate receptor antagonist APV blocks acquisitionbut not expression of fear conditioning. *Behav Neurosci* **105**: 126-133.

Kitajima T, Hara K. 1997. An integrated model for activity-dependent synaptic modifications. *Neural Networks* **10**: 413-421.

Komatsu Y. 1996. GABAB receptors, monoamine receptors, and postsynaptic inositol trisphosphate-induced Ca2_ release are involved in the induction of long-term potentiation at visual cortical inhibitory synapses. *J Neurosci* **16**, 6342–6352.

Lang EJ, Paré D. 1998**.** Synaptic responsiveness of interneurons of the cat lateral amygdaloid nucleus. *Neurosci* 83: 877-899.

LeDoux JE, Sakaguchi A, Iwata J, Reis DJ. 1985. Auditory emotional memories: establishment by projections from the medial geniculate nucleus to the posterior neostriatum and/or dorsal amygdala. *Ann NY Acad Sci* **444**: 463-464

LeDoux JE, Ruggiero DA, Forest R, Stornetta R, Reis DJ. 1987. Topographic organization of convergent projections to the thalamus from the inferior colliculus and spinal cord in the rat. *J Comp Neurol* **264**: 123-146.

LeDoux JE. 2000. Emotional circuits in the brain. *Annu Rev Neurosci* **23**: 155-184.

Letzkus JJ, Wolff SB, Meyer EM, Tovote P, Courtin J, Herry C, Lüthi A. 2011. A disinhibitory microcircuit for associative fear learning in the auditory cortex. *Nature* **480**: 331-335.

Li G, Nair S, Quirk GJ. 2009. A biologically realistic network model of acquisition and extinction of conditioned fear associations in lateral amygdala neurons. *J Neurophysiol* **101**: 1629-1646.

Linke R, Braune G, Schwegler H. 2000. Differential projection of the posterior paralaminar thalamic nuclei to the amygdaloid complex in the rat. *Exp Brain Res* **134**: 520-532.

Mahanty NK, Sah P. 1998. Calcium-permeable AMPA receptors mediate long-term potentiation in interneurons in the amygdala. *Nature* **394**: 683-687.

Markram H, Toledo-Rodriguez M, Wang Y, Gupta A, Silberberg G,Wu C. 2004. Interneurons of the neocortical inhibitory system. *Nat Rev Neurosci* **5**, 793-807.

Mascagni F, McDonald AJ, Coleman JR. 1993. Corticoamygdaloid and corticocortical projections of the rat temporal cortex: a Phaseolus vulgaris leucoagglutinin study. *Neurosci* **57**: 697-715.

McDonald AJ, Augustine JR. 1993. Localization of GABA-like immunoreactivity in the monkey amygdala. *Neuroscience* **52**: 281–294.

McGaugh JL. 2002. Memory consolidation and the amygdala: a systems perspective. *Trends Neurosci* **25**: 456-461.

McKernan MG, Shinnick-Gallagher P. 1997. Fear conditioning induces a lasting potentiation of synaptic currents in vitro. *Nature* **390**: 607-611.

Miserendino MJD, Sananes CB, Melia KR, Davis M. 1990.Blocking of acquisition but not expression of conditioned fear-potentiated startle by NMDA antagonists in the amygdala. *Nature* **345**: 716-718.

Pape HC, Paré, D. 2010. Plastic synaptic networks of the amygdala for the acquisition, expression, and extinction of conditioned fear. *Physiol Rev* **90**: 419-463.

Paré D. 2002. Mechanisms of Pavlovian fear conditioning: Has the engram been located? *Trends Neurosci* **25**:436-437.

Paré D. 2003. Role of the basolateral amygdala in memory consolidation. *Prog Neurobiol* **70**: 409-420.

Pitkänen A, Pikkarainen M, Nurminen N, Ylinen A. 2000. Reciprocal connections between the amygdala and the hippocampal formation, perirhinal cortex, and postrhinal cortex in rat. *Ann N Y Acad Sci* **911**: 369-391.

Power JM, Bocklisch C, Curby P, Sah P. 2011. Location and function of the slowafterhyperpolarization channels in the basolateral amygdala. *J Neurosci* **31**: 526-537.

Quirk GJ, Repa JC, LeDoux JE. 1995. Fear conditioning enhances short latency auditory responses of lateral amygdala neurons: parallel recordings in the freely behaving rat. *Neuron* **15**: 1029-1039.

Quirk GJ, Armorny JL, LeDoux JE. 1997. Fear conditioning enhance different temporal component of tone-evoked spike trains in auditory cortex and lateral amygdala. *Neuron* **19**: 613-624.

Rainnie DG, Mania I, Mascagni F, McDonald AJ. 2006. Physiological and morphological characterization of parvalbumin-containing interneurons of the rat basolateral amygdala. *J Comp Neurol* **498**: 142-161.

Rea K, Lang Y, Finn DP. 2009. Alterations in extracellular levels of gamma-aminobutyric acid in the rat basolateral amygdala and periaqueductal gray during conditioned fear, persistent pain and fear-conditioned analgesia. *J Pain* 10(10):1088-98.

Repa JC, Muller J, Apergis J, Desrochers TM, Zhou Y, LeDoux JE. 2001. Two different lateral amygdala cell populations contribute to the initiation and storage of memory. *Nat Neurosci* **4**: 724-731.

Romanski LM, LeDoux JE. 1993a. Information cascade from primary auditory cortex to the amygdala: corticocortical and corticoamygdaloid projections of temporal cortex in the rat. *Cerebral Cortex* **3(6):** 515-532.

Romanski LM, LeDoux JE. 1993b. Organization of rodent auditory cortex: anterograde transport of PHA-L from MGv to temporal neocortex. *Cerebral Cortex* **3**: 499-514.

Rumpel S, LeDoux J, Zador A, Malinow R. 2005. Postsynaptic receptor trafficking underlying a form of associative learning. *Science* **308**: 83–88.

Sah P, Faber ES, Lopez de Armentia M, Power J. 2003. The amygdaloid complex: anatomy and physiology. *Physiol Rev* **83**: 803-834.

Samson RD, Paré D. 2006. A spatially structured network of inhibitory and excitatory connections directs impulse traffic within the lateral amygdala. *Neuroscience* **141**: 1599–1609.

Shi CJ, Cassell MD. 1997. Cortical, thalamic, and amygdaloid projections of rat temporal cortex. *J Comp Neurol* **382**: 153-175.

Shinonaga Y, Takada M, Mizuno N. 1994. Direct projections from the non-laminated divisions of the medial geniculate nucleus to the temporal polar cortex and amygdala in the cat. *J Comp Neurol* **340**: 405-426.

Sosulina L, Meis S, Seifert G, Steinhauser C, Pape HC. 2006. Classification of projection neurons and interneurons in the rat lateral amygdala based upon cluster analysis. *Mol Cell Neurosci* **33**: 57–67.

Shouval HZ, Castellani GC, Blais BS, Yeung LC, Cooper LN. 2002a. Converging evidence for a simplified biophysical model of synaptic plasticity. *Biol Cybern* **87**: 383-391.

Tsvetkov E, Carlezon WA, Benes FM, Kandel ER, Bolshakov VY. 2002. Fear conditioning occludes LTP-induced presynaptic enhancement of synaptic transmission in the cortical pathway to the lateral amygdala. *Neuron* **34**: 289-300.

Tsvetkov E, Shin RM, Bolshakov VY. 2004. Glutamate uptake determines pathway specificity of long-term potentiation in the neural circuitry of fear conditioning. *Neuron* **41**: 139-151.

Tully K, Bolshkov VY. 2001. Emotional enhancement of memory: how norepinephrine enables synaptic plasticity. *Mol Brain* **3**: 15.

Tully K, Li Y, Tsvetkov E, Bolshkov VY. 2007. Norepinephrine enables the induction of associative long-term potentiation at thalamo-amygdala synapses. *Proc Natl Acad Sci* **104**: 14146-14150.

Turner BH, Herkenham M. 1991. Thalamoamygdaloid projections in the rat: a test of the amygdala's role in sensory processing. *J Comp Neurol* **313**: 295-325.

Tuunanen J, Pitkänen A. 2000. Do seizures cause neuronal damage in rat amygdala kindling? *Epilepsy Res* **39**: 171-176.

Varela J, Sen K, Gibson J, Fost J, Abbott L, Nelson S. 1997. A quantitative description of short-term plasticity at excitatory synapses in layer 2/3 of rat primary visual cortex. *J Neurosci* **17**: 7926–7940.

Wang SJ, Gean PW. 1999. Long-term depression of excitatory synaptic transmission in the rat amygdala. *J Neurosci* **19**: 10656-10663.

Warman EN, Durand DM, Yuen GLF. 1994. Reconstruction of hippocampal CA1 pyramidal cell electrophysiology by computer simulation. *J Neurophysiol* **71**: 2033-2045.

Washburn MS, Moises H.C. 1992. Electrophysiological and morphological properties of rat basolateral amygdaloid neurons in vitro. *J Neurosci* **12**: 4066-4079.

Weinberger NM. 2011. The medial geniculate, not the amygdala, as the root of auditory fear conditioning. *Hear Res* **274**: 61-74.

Weisskopf MG, Bauer EP, LeDoux JE. 1999. L-type voltage-gated calcium channels mediate NMDA-independent associate long-term potentiation at thalamic input synapses to the amygdala. *J Neurosci* **19**: 10512-10519.

Woodruff AR, Sah P. 2007. Networks of parvalbumin-positive interneurons in the basolateral amygdala. *J Neurosci* **27**: 553–563.

Woodson W, Farb CR, Ledoux JE. 2000. Afferents from the auditory thalamus synapse on inhibitory interneurons in the lateral nucleus of the amygdala. *Synapse* **38**: 124-137.

FIGURES

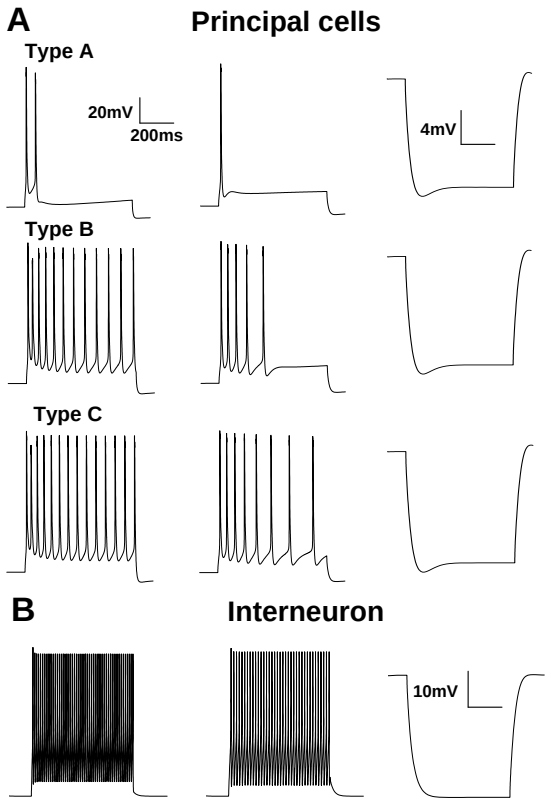

Figure 1. Electroresponsive properties of model LA neurons.Voltage responses of model cells to intracellular current injection. (**A**) The responses of the three types of principal cells (types A, B and C) to current injections (left: 400 pA; middle: 300 pA; right: -100 pA; duration 600 ms) are similar to those reported in Faber et al. (2001). (**B**) Voltage responses of the interneuron model to 200-ms current injections of the same magnitude as in A.

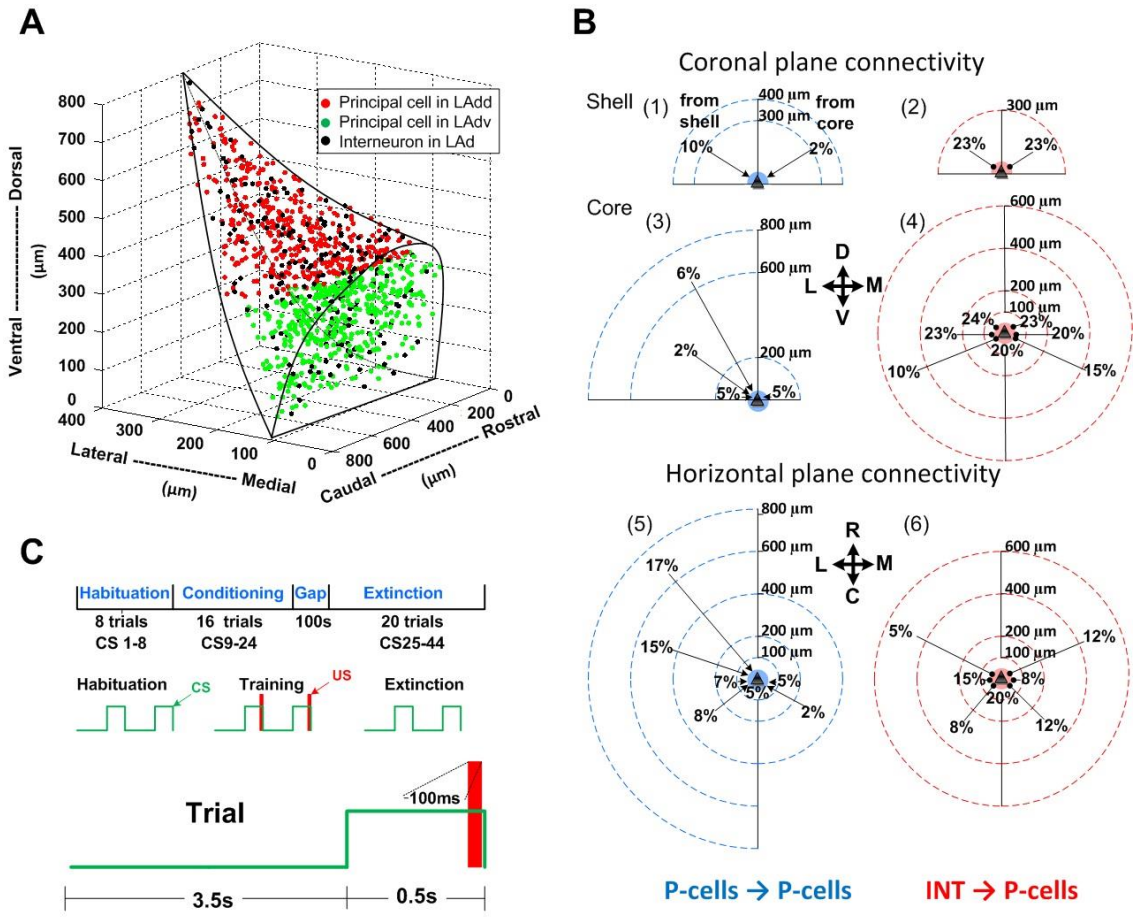

Figure 2. Spatial structure, intrinsic connectivity and fear conditioning protocol for the LAd network model.**(A)** The model consists of 800 principal cells (red and green dots, 400 each, represent principal cells in LAdd and LAdv, respectively) and 200 interneurons (black dots). The principal cells in the model were populated randomly in the horn shaped tridimensional structure with dimensions of 800 μm in the rostral-caudal, 800 μm in the ventral-dorsal, and 400 μm in the medial-lateral directions.**(B)** Intrinsic connectivity of the model in the coronal and horizontal planes**. Blue**, glutamatergic connections to principal cells; **red**, GABAergic connections to principal cells. Excitatory connections to principal cells were different in shell and core regions of LAd. (1) Shell neurons in dorsal region excited principal cells in the ventral region (e.g., for cells separated by 300-400 μm, the connectivity was 10%). (2) Principal cells in ventral shell region are inhibited by interneurons in the dorsal region (for distances between 50-300 μm, the connectivity was 23%). (3) Within the core region, cells in the dorsolateral region excited principal cells in the ventromedial region (e.g., cells within a radius of 200 μm dorsal-lateral had 5% connection probability; see text). (4) Inhibitory connections were provided to all cells within a radius of 100 μm from the interneuron, with 20% connection probability. Inhibitory connectivity changed as a function of distance and direction (see text). (5) Excitatory connections in the horizontal plane prevalently ran in

the lateromedial direction. The connection probability was a function of the distance between the cells (5-17% connectivity was changed depending on the distance of 50-800 μm in lateromedial direction, and 2-5% connectivity for those separated by 50-400 μm in mediolateral direction) (6)Interneuron-principal cell connections were higher in the mediolateral direction (8-20% connectivity was assumed for those separated by 0-600 μm) than in the lateromedial direction (5-20% connectivity was assumed for those separated by 0-600 μm). **(C)** Fear conditioning protocol. As in the experiments of Repa et al. (2001), the "behavioral" protocol included habituation, conditioning and extinction phases, with 8, 16 and 20 trials, respectively.

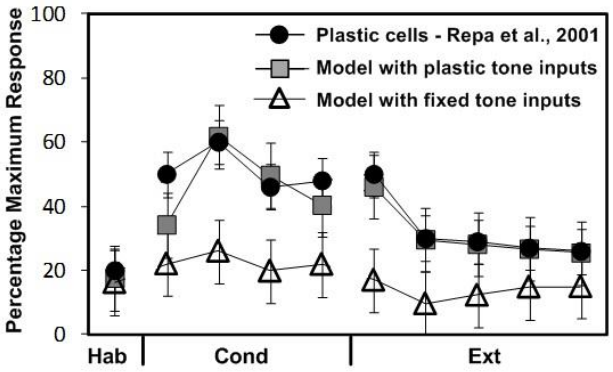

Figure 3. Plasticity of tone inputs is required to generate plastic cells in LAd. With no plasticity in thalamic and cortical inputs, i.e., frequency fixed to 20 Hz, the number of plastic cells decreased (N=89/800) and their CS responsiveness also decreased by 61±3% (triangles, $p<0.001$), compared to experimental (black circles; N=24/100; from Repa et al., 2001) and control model (gray squares, N=198/800) values.

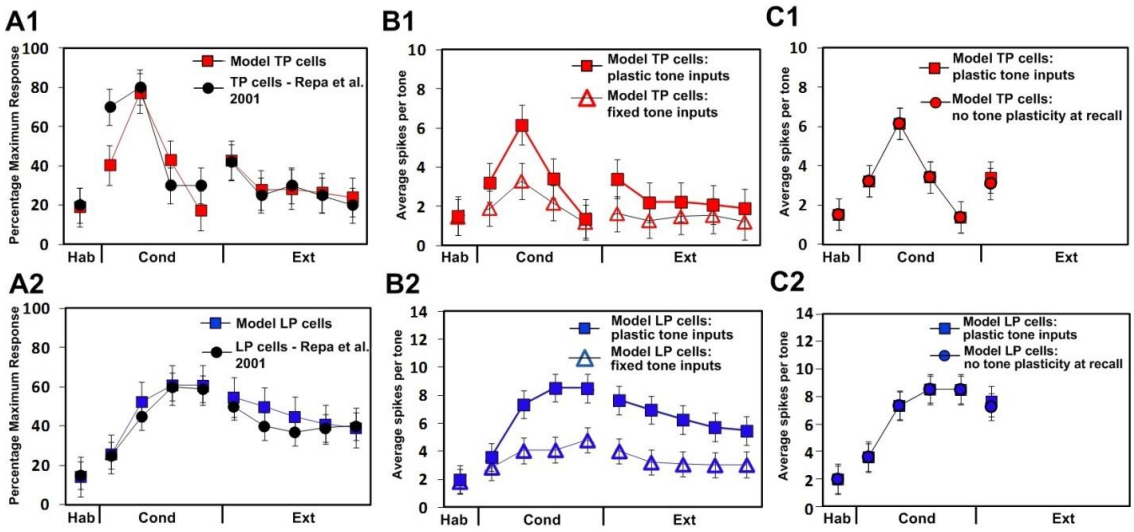

Figure 4. Impact of various manipulations (**A-C**) on the tone responses of TP (**1**) and LP (**2**) cells. (**A**) Tone responses of LAd cells during the different phases of the behavioral protocol. (**A1**) Model (red, N=96/800) and experimental (black; N=12/100; from Repa et al., 2001) tone responses of TP cells show a sudden increase during early conditioning, and then drop to habituation levels during late conditioning. (**A2**) Model (blue; N=102/800) and experimental (black; N=12/100) tone responses of LP cells increase gradually with conditioning and persist during extinction. (**B)** Tone responsiveness of model TP **(B1**, red**)** or LP **(B2**, blue**)** cells with (squares) or without (triangles) plasticity at tone inputs. Data shown includes only cells where conditioning induced significant changes in CS responsiveness, using the criterion in Repa et al. (2001). (**C**) Tone responsiveness of model TP **(C1**, red**)** or LP **(C2**, blue**)** cells in two conditions: with plasticity of tone inputs during conditioning and the recall test (squares; from 20 to 40 Hz) or only during conditioning (circles). In the latter case, tone inputs were returned to habituation levels (20 Hz) during the recall test.

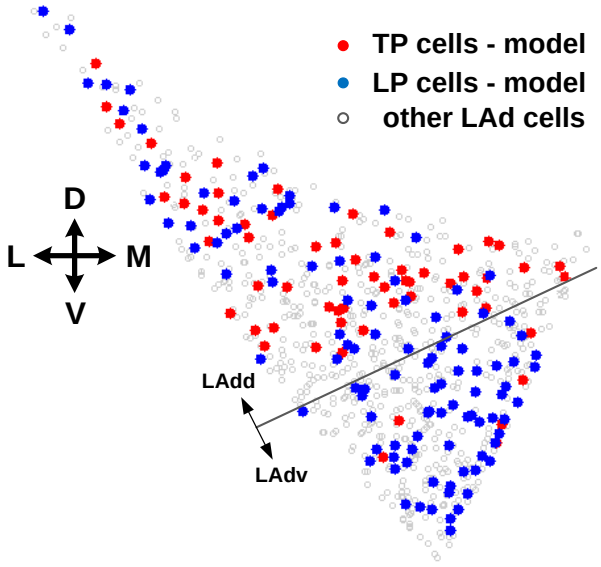

Figure 5. Coronal view of LAd showing the location of TP cells (red) and LP cells (blue) in LAd. The distribution of TP and LP cells was similar to that seen experimentally (see fig. 8 in Repa et al., 2001).

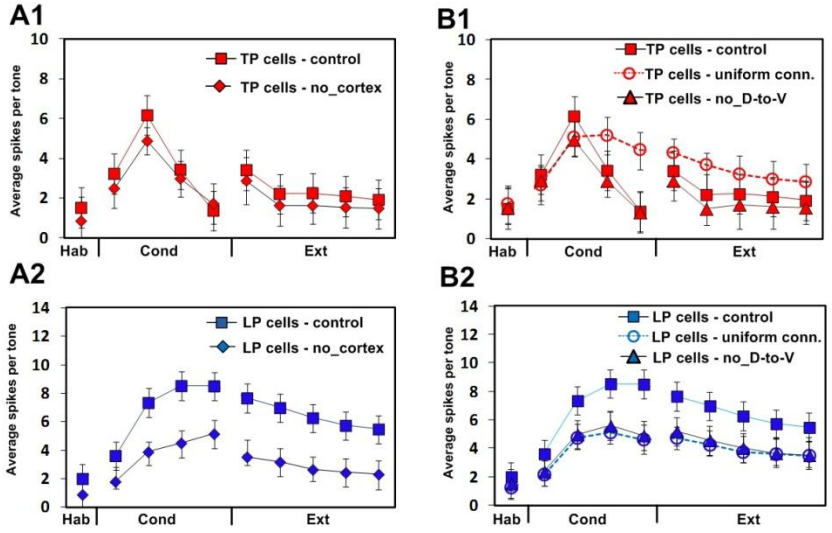

Figure 6. **(A)** Cortical inputs are necessary for the formation of LP cells. Spikes per tone (mean ±s.e.m.) of plastic LAd model cells. (**A1)** TP (red) and (**A2)** LP cells (blue), for the following cases: control (square) and no cortical input (diamond). **(B)** Intrinsic connectivity contributes to the generation of the two cell types in LAd. Spikes per tone (mean ±s.e.m.) of LAd model cells. (**B1)** TP (red) and (**B2)** LP cells (blue), for the following cases: control (squares), uniform connectivity (circles; see below) and no LAdd to LAdv connectivity (triangles). Random uniform connectivity was implemented as follows: 3% excitatory connectivity within a 50-400 μm radius of a principal cell, and a 35% inhibitory connectivity within a 50-200 μm radius for an interneuron, resulting in the average excitatory and inhibitory connections per principal cell to be 21.25 and 20.05, respectively. This ensured that the average excitatory and inhibitory connections to principal cells matched the control case values of 21.4 and 22.2, respectively.

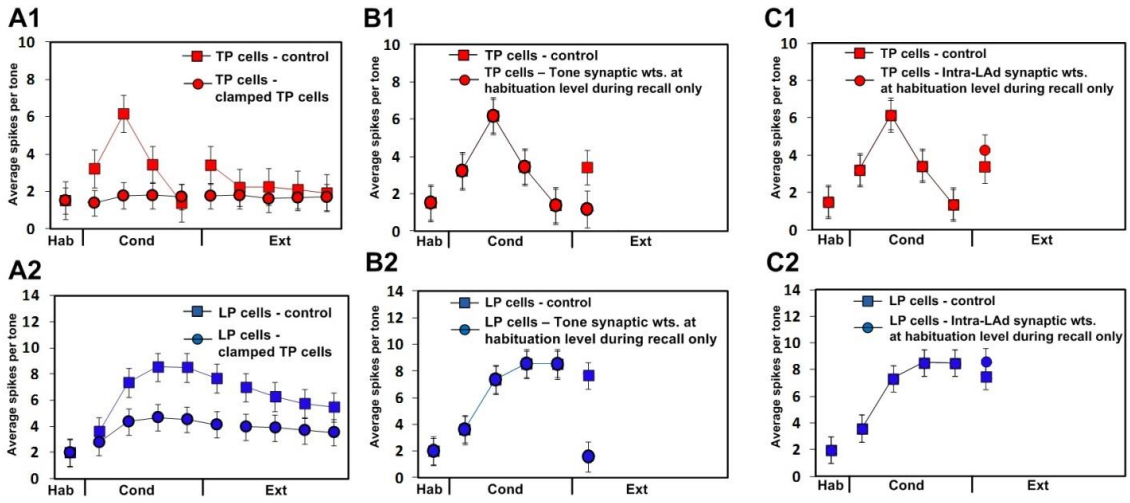

Figure 7. **(A)** Clamping the tone responses of TP cells at habituation levels alters the impact of fear conditioning on LAd cells. Model tone responses in control conditions (squares), or when the tone responses of TP cells were maintained at habituation levels (circles). **(B)** Model tone responses decrease considerably when the tone-pyr weights are set to habituation levels during the recall test (circles). **(C)** Model tone responses are largely unaltered when the synaptic weights between neurons within LAd are set to habituation levels during recall (circles).

SUPPLEMENTARY MATERIALS

S1. DETAILS RELATED TO METHODS

In the sub-sections below, we provide addition information related to methods, including implementation of the effects of neuromodulators, iterative procedures used, and the various mathematical equations. All model runs were performed using parallel NEURON (Carnevale and Hines, 2006) running on a Beowulf supercluster with a time step of 10 μs. Simulation output was analyzed using MATLAB. We have strived to provide all information related to both single cell and network parameters in this document, so as to enable a modeler to recreate the model using packages such as NEURON. We have created a website at our research site from where interested parties will be able to download parts of the codes related to the model. The website is under construction but already features the single cell models. The relevant url is http://engineering.missouri.edu/neuro/research/

S1.1 Modeling neuromodulator effects.

Blockade of DA and NE have been shown to impair the acquisition of fear memory in LA (Bissière et al., 2003; Rodrigues et al. 2009). Other neuromodulators have not been implicated in a similar manner in auditory fear conditioning, although serotonin has been found to be released in the amygdala during fear conditioning. Slice studies seem to indicate that the effects of serotonin overlap with those of DA and NE and hence such effects (and those of others unknown) can be considered to be incorporated into the DA and NE affects that we model.

Dopaminergic modulation of LA. The amygdala receives dopaminergic inputs from the ventral tegmental area and substantia nigra pars compacta. DA receptors are present on 70% of principal cells in LA (Muller et al., 2009). Accordingly, we populated these receptors randomly on 70% of LAd model cells. D_1 receptors (D_1Rs) have an affinity between 500 nM and 5 μM (low affinity) and D_2 receptors (D_2Rs) have affinity between 5 nM and 500 nM (high affinity; Martina and Bergeron, 2008). We assumed that both D_1Rs and D_2Rs are present on cells modeled with DA receptors, but are activated differentially depending on DA levels. D_1Rs are activated at high concentrations (late conditioning and early extinction) while D_2Rs are activated at all concentrations levels (early conditioning, late conditioning and early extinction). In principal cells, D_1R activation decreases the spike threshold from -40.1mV to -43mV, and causes a 20-30% reduction in the slowly inactivating K^+ current (Kroner et al., 2004). These effects were modeled by shifting the activation curve of Na^+ channels by a maximum of -1.5 mV, and decreasing the maximum conductance of the slowly inactivating K^+ current ($g_{Kd,max}$) by 20% during shock. D_1R activation was reported to reduce NMDA current amplitudes by 20-30% in LA (Martina and Bergeron, 2008). This effect was modeled by decreasing $g_{NMDA,max}$ by 20% for connections between principal LAd cells. D_1R activation also increases spontaneous inhibitory network activity as measured by sIPSC frequency (to 151 ± 9% of baseline; Loretan et al., 2004). This was incorporated in the model by increasing $g_{GABA,max}$ for interneuron to principal cell synapses by 60% in the presence of DA. Because D_2R activation reduces inhibition in LAd by 30-40% (Loretan et al., 2004), DA in the model decreased $g_{GABA,max}$ for interneuron to principal cell synapses by up to 30%. D_2Rs are also known to increase the input resistance of principal cells

(Rosenkranz and Grace, 2002), and this was modeled by decreasing g*leak* by up to 20% (Martina and Bergeron, 2008) (see **Table S**3; parameter changes made to develop alternative model 2, if any, are also listed).

Norepinephrine modulation of LA. NE plays an important role in emotional memory formation via stimulation of α and β noradrenergic receptor subtypes (Hu et al., 2007; Sara et al., 2009). NE α and β receptor-mediated effects are seen in 30-50% of principal BLA cells (Farb et al., 2010; Rainbow et al., 1984). Therefore, we populated both types of NE receptors randomly on 50% of all model cells. NE β receptor activation inhibits the slow after-hyperpolarization that follows trains of action potentials and thus facilitates repetitive firing in principal cells (Johnson et al., 2011). This was modeled by reducing g*sAHP,max* by up to 30% in both LAdd and LAdv principal cell models (Tully et al., 2007). In addition, Johnson et al. (2011) reported that NE decreases fEPSP (field excitatory post synaptic potential) amplitudes, whereas administration of selective NE-β agonists increased fEPSP amplitudes. From this, they concluded that NE-α and NE-β receptors modulate excitatory tone and inhibitory synapses in opposite directions. Furthermore, selective activation of NE-β receptors produced a larger potentiation in cortical as compared to thalamic inputs. This led them to propose that NE-β receptors are more prevalent on GABAergic neurons contacted by cortical inputs. We modeled this by differentially activating NE receptors at tone-interneuron synapses depending on the source of the tone (cortical or thalamic) in both LAdd and LAdv regions. Lacking mechanistic information, we chose to model these effects solely via a regulation of the NMDA conductance. Activation of NE-α receptors on thalamic tone-interneuron

synapses inhibits learning and reduced *fEPSP* by 60% during conditioning (Johnson et al., 2011), and this was modeled by increasing $g_{NMDA,max}$ by 30% in thalamic tone-LAdd interneuron synapses. Activation of NE-α receptors on LAd principal cells that receive cortical inputs reduces *fEPSP* amplitudes by 20-35% (Johnson et al., 2011), and this was modeled by decreasing $g_{NMDA,max}$ by 30% in cortical tone-principal cells synapses. The activation of NE-β receptors on LAd interneurons that receive cortical inputs increases plasticity during conditioning by suppressing inhibition on principal cells (Johnson et al., 2011, Tully et al., 2007). This was modeled by decreasing $g_{NMDA,max}$ up to 30% in cortical tone-interneuron synapses. But, activation of NE-β receptors increases activation of principal cells (Johnson et al., 2011) (see Table S3).

S1.2 Iterative determination of the density of thalamic and cortical inputs to LA cells.

We started with a random uniform connectivity of 70% throughout LAd, for both cortical and thalamic tone and shock inputs because experimental studies (Repa et al., 2001; Han et al., 2007) estimated that 70% of LAd cells receive sensory inputs. However, with this approach, the model could not reproduce prior experimental observations. For instance, whereas post-training temporal cortical lesions were reported to completely block conditioned freezing (Boatman and Kim 2006), removal of cortical inputs from the model had only minor effects on the tone responsiveness of model LA neurons. Similarly, although blockade of NE-β receptors during training was reported to prevent acquisition of conditioned fear responses (Bush et al., 2010), the same manipulation in the model had only minor effects of the tone responsiveness of LAd neurons. To

accommodate these effects, we iterated over the thalamic and cortical tone and shock densities and found the following combination that satisfied all experimental observations: uniform total tone density throughout LAd with 70% of the LAdd cells receiving thalamic and 35% receiving cortical tone projections, and the opposite for LAdv, i.e., 35% of LAdv cells receiving thalamic and 70% receiving cortical tone projections. The shock inputs continued to be distributed uniformly to a random 70% of LAd cells.

S1.3 Other model assumptions

Since the degree of convergence in the projections of principal cells to interneurons is unknown, we assumed that each interneuron receives excitatory connections from principal cells within a radius of 50-200 μm with 10% connectivity. Also, in the absence of information about NE and DA concentrations during our fear conditioning protocol, we assumed that they were proportional to the magnitude of conditioned tone responses exhibited by LAdv neurons. We feel this is a reasonable assumption given that LAdv neurons drive conditioned fear responses by exciting, via the basal nuclei (Amano et al., 2011), neurons in the central medial amygdala (Ciocchi et al., 2010; Duvarci et al., 2011) that in turn project to the cell groups contributing DA and NE inputs to LAd (Pitkänen et al., 2000). During early conditioning, when LAdv cell responses are low, we assumed moderate neuromodulator concentrations and this activated only high affinity receptors D_2R and NE-α. During late conditioning and early extinction, neuromodulator concentrations were high. See **Table S3** for details. Neuromodulator concentrations were

the highest during shock with 100% change in neuromodulator effects via the activation of all DA and NE receptors.

Also, initial values of synaptic weights and plasticity thresholds, divergence of the various connections, and neuromodulatory release characteristics, were determined iteratively using the full network model. It is noted that the ultimate test of the model's validity was its ability to reproduce the findings of Repa et al. (2001). This is addressed in the Results section.

S1.4 Mathematical Equations for voltage-dependent ionic currents

The equation for each compartment (soma or dendrite) followed the Hodgkin-Huxley formulations (Byrne and Roberts, 2004) in eqn. S1,

$$C_m dV_s/dt = -g_L(V_s - E_L) - g_c(V_s - V_d) - \sum I_{cur,s}^{int} - \sum I_{cur,s}^{syn} + I_{inj} \qquad \text{(S1)}$$

where V_s/V_d are the somatic/dendritic membrane potential (mV), $I_{cur,s}^{int}$ and $I_{cur,s}^{syn}$ are the intrinsic and synaptic currents in the soma, I_{inj} is the electrode current applied to the soma, C_m is the membrane capacitance, g_L is the is the conductance of leak channel, and g_c is the coupling conductance between the soma and the dendrite (similar term added for other dendrites connected to the soma). The intrinsic current $I_{cur,s}^{int}$, was modeled as $I_{cur,s}^{int} = g_{cur} m^p h^q (V_s - E_{cur})$, where g_{cur} is its maximal conductance, *m* its activation variable (with exponent *p*), *h* its inactivation variable (with exponent *q*), and E_{cur} its reversal potential (a similar equation is used for the synaptic current $I_{cur,s}^{syn}$ but without *m* and *h*). The kinetic equation for each of the gating variables *x* (*m* or *h*) takes the form

$$\frac{dx}{dt} = \frac{x_\infty\left(V,[Ca^{2+}]_i\right)-x}{\tau_x(V,[Ca^{2+}]_i)}$$

(S2)

where x_∞ is the steady state gating voltage- and/or Ca^{2+}- dependent gating variable and τ_x is the voltage- and/or Ca^{2+}- dependent time constant. The equation for the dendrite follows the same format with '*s*' and '*d*' switching positions in eqn. S1. Details related to the model, including types of channels and parameter values are provided in **Tables S1-2**.

S1.5 Mathematical Equations for Synaptic Currents

Excitatory transmission was mediated by AMPA/NMDA receptors, and inhibitory transmission by $GABA_A$ receptors. The corresponding synaptic currents (shown in dendrites below) were modeled by dual exponential functions (Durstewitz et al., 2000), as shown in Eqns. S3-5,

$$I_{AMPA} = \bar{A}w(t)g_{AMPA,max}\frac{\tau_1\tau_2}{\tau_2-\tau_1}[\exp(-t/\tau_2) - \exp(-t/\tau_1)](V - E_{AMPA}) \quad \text{(S3)}$$

$$I_{NMDA} = \bar{A}wg_{NMDA,max}s(V)\frac{\tau_1\tau_2}{\tau_2-\tau_1}[\exp(-t/\tau_2) - \exp(-t/\tau_1)](V - E_{NMDA}) \quad \text{(S4)}$$

$$I_{GABA} = \bar{A}w(t)g_{GABAA,max}\frac{\tau_1\tau_2}{\tau_2-\tau_1}[\exp(-t/\tau_2) - \exp(-t/\tau_1)](V - E_{GABA}) \quad \text{(S5)}$$

where *V* is the membrane potential (mV) of the compartment (dendrite or soma) where the synapse is located, $w(t)$is the adjustable synaptic weight for AMPA synapses (see section S1.7; *w* was held fixed for all NMDA synapses); $\bar{A}$ is a normalization constant chosen so $g_{AMPA,max}$ $g_{NMDA,max}$ and $g_{GABA,max}$ assume maximum values of the conductances; τ_1 and τ_2 are the rise and decay time constants respectively. For AMPA receptor channels, τ_1 = 0.25 ms and τ_2 = 7 ms; for NMDA receptor channels, τ_1 = 3.65 ms and τ_2 = 125.0 ms, and for $GABA_A$ receptors, τ_1 = 0.13ms and τ_2 = 3.75 ms. The voltage-

dependent variable $s(V)$ which implements the Mg^{2+} block was defined as: $s(V) = [1 + 0.33 \exp(-0.06\ V)]^{-1}$ (Zador et al., 1990). The maximal conductances were chosen as: $g_{AMPA,max}$= 1 nS, $g_{NMDA,max}$ = 0.5 nS and $g_{GABA,max}$= 0.6 nS. Synaptic reversal potentials were set as follows: $E_{AMPA} = E_{NMDA} = 0$ mV and E_{GABAA} = -75 mV (Durstewitz et al., 2000).

S1.6 Calcium dynamics and Hebbian learning

Intracellular calcium was regulated by a simple first-order differential equation shown in Eqn. S6 (Warman et al., 1994),

$$\frac{d[Ca^{2+}]_i}{dt} = -f\frac{I'_{Ca}}{zFA} + \frac{[Ca^{2+}]_{rest} - [Ca^{2+}]_i}{\tau_{Ca}} \quad \text{(S6)}$$

where f is the fraction of the Ca^{2+} influx (f =0.024), $V = wA$ with w being the shell thickness (1μm) and A the dendritic/soma surface area, z=2 is the valance of the Ca^{2+} ion, F is the Faraday constant, and τ_{Ca} is the time constant associated with Ca^{2+} removal. The resting Ca^{2+} concentration was $[Ca^{2+}]_{rest}$ =50 nmol/l (Durstewitz et al., 2000).

The biophysical Hebbian rule was implemented by adjusting the synaptic weight w(t) in synaptic conductances (Eqns. S3 and S5) using equation S7,

$$\Delta w_j = \eta([Ca^{2+}]_j)\Delta t(\lambda_1 \Omega([Ca^{2+}]_j) - \lambda_2 \omega_j) \quad \text{(S7)}$$

where η is the Ca^{2+}-dependent learning rate and Ω is a Ca^{2+}-dependent function with two thresholds (θ_d and θ_p; $\theta_d \leq \theta_p$) (for details see Li et al., 2009); λ_1 and λ_2 represent scaling and decay factors respectively; the local calcium level at synapse j is denoted by $[Ca^{2+}]_j$ and Δt is the simulation time step. With this learning rule, the synaptic weight decreases

when $\theta_d < [Ca^{2+}]_j < \theta_p$, and increases when $[Ca^{2+}]_j > \theta_p$, with modulation by the decay term $\lambda_2 w_j$.

Concentration of calcium pools: The concentration of the calcium pool at synapse *j* followed the dynamics in Eq. S6, with f_j= 0.024 (Warman et al. 1994), τ_j = 50 ms (Shouval et al. 2002b), *V* is the volume of a spine head with a diameter of 2 μm (Kitajima and Hara 1997). All the synaptic weights were constrained by upper (W_{max}) and lower (W_{min}) limits (Li et al., 2009). Maximum (f_{max}) and minimum (f_{min}) folds were specified for each modifiable synapse so that W_{max}= f_{max}*w(0) and W_{min} = f_{min}*w(0).

Excitatory synapses onto principal cells. For tone-principal cell, and principal cell-principal cell connections, the calcium influx which determines learning was calculated by using the NMDA current, $I_{Ca}^{N} = P_0 w^{-1} G_{NMDA}(V - E_{Ca})$ (Shouval et al., 2002b), where $G_{NMDA} = \bar{A} w(t) g_{NMDA,max} s(V) \frac{\tau_1 \tau_2}{\tau_2 - \tau_1} \left[\exp\left(-\frac{t}{\tau_2}\right) - \exp\left(-\frac{t}{\tau_1}\right)\right]$ from eqn. S4, the term w^{-1} ensures that it is calculated per synapse, and P_0 = 0.015.

Excitatory synapses onto interneurons. For tone-interneuron, and principal cell-interneuron connections, the calcium influx (used for learning) at the excitatory synapses on interneurons occurs through both NMDA and AMPA receptors (details in Li et al., 2009). In addition to calcium influx through NMDA current I_{Ca}^{N}, the calcium influx through AMPA receptors was calculated as $I_{Ca}^{A} = P_0 w^{-1}(0) G_{AMPA}(V - E_{Ca})$ where G_{AMPA} is the AMPA conductance in eqn. S4 (as described in the earlier para for G_{NMDA}), and *w*(0) is the initial AMPA synaptic weight, P_0 = 0.001. The Ca^{2+} current through the AMPA/NMDA receptors was separated from the total AMPA/NMDA current in this

manner and used for implementation of the learning rule (Kitajima and Hara, 1997; Shouval et al., 2002a; Li et al., 2009).

Inhibitory synapses onto principal cells. Several different mechanisms have been reported for potentiation at GABAergic synapses in other brain regions (e.g., Gaiarsa et al., 2002). A rise in postsynaptic intracellular Ca^{2+} concentration seems to be required in most mechanisms to trigger long-term plasticity. In the neonatal rat hippocampus, potentiation could be induced by Ca^{2+} influx through the voltage-dependent Ca^{2+} channels (VDCCs), whereas in the cortex and cerebellum, this process requires Ca^{2+} release from postsynaptic internal stores that is dependent on stimulation of GABA receptors (Gaiarsa et al., 2002). Thus, both presynaptic activity (GABA receptor stimulation or interneuron firing) and postsynaptic activity (activation of VDCCs by membrane depolarization) contribute to the potentiation of GABA synapses. The process from GABA receptor stimulation to internal Ca^{2+} release involves activating a cascade of complex intracellular reactions (Komatsu 1996). Such a complex process can be simplified by assuming that the Ca^{2+} release is proportional to the stimulation frequency or $GABA_A$ conductance (Li et al., 2009). Hence we modeled this simplified process by considering Ca^{2+} release from the internal stores into a separate Ca^{2+} pool, using an equation similar to that for the AMPA/NMDA case cited above:
$I_{Ca}^{G} = P_0 w^{-1}(t) G_{GABA}(V - E_{Ca})$ with P_0 = 0.01, and G_{GABA} as the $GABA_A$ conductance in Eq. S5 (as described earlier for G_{NMDA}). Note that the current I_{Ca}^{G}, models the dependence of Ca^{2+} release on $GABA_A$ stimulation frequency but not Ca^{2+} influx through the $GABA_A$ channel. The current I_{Ca}^{G}, together with post-synaptic voltage dependent

calcium current (I_{Ca}), contributed towards plasticity. Hence, $I'_{Ca} = I^{G}_{Ca} + 0.01 I_{Ca}$ was used to calculate calcium influx for learning at such synapses. (Li et al., 2009)

S1.7 Short-term presynaptic plasticity

Short term plasticity was implemented as follows (Varela et. al 1997): For facilitation, the factor F was calculated using the equation: $\tau_F * \frac{dF}{dt} = 1 - F$ and was constrained to be ≥ 1. After each stimulus, F was multiplied by a constant, f (≥ 1) representing the amount of facilitation per pre-synaptic action potential, and updated as $F \rightarrow F * f$. Between stimuli, *F* recovered exponentially back toward 1. A similar scheme was used to calculate the factor D for depression: $\tau_D * \frac{dD}{dt} = 1 - D$ and *D* constrained to be ≤ 1. After each stimulus, *D* was multiplied by a constant *d* (≤ 1) representing the amount of depression per pre-synaptic action potential, and updated as $D \rightarrow D * d$. Between stimuli, *D* recovered exponentially back toward 1. We modeled depression using two factors d_1 and d_2 with $d1$ being fast and d_2 being slow subtypes, and $d = d1 * d2$. The parameters for the short-term plasticity models, the initial weights and other learning parameters for the synapses are listed in **Table S4**. Again, parameter changes made to develop alternative model 2, if any, are also listed.

S.2 ADDITIONAL RESULTS

S2.1 Contribution of neuromodulatory inputs to training-induced changes in CS responsiveness

Although removing Ca^{2+}-induced plasticity at synapses to model LAd neurons led to decreases in TP and LP cell responses (**Fig. S3**, circles), this does not necessarily mean that neuromodulators play no role in shaping the tone responsiveness of LA neurons during fear conditioning. Consistent with this, we noted that DA and NA receptors were differentially distributed in TP, LP, and non-plastic cells. Indeed, a higher proportion of TP cells and LP cells had DA and NE receptors (94% of TP cells had DA and 64% had NE receptors; 71% of LP cells had DA and 90% had NE receptors) compared to non-plastic cells (65% had DA and 40% had NE receptors; $X^2 = 3.5$, $p < 0.05$).

To analyze the contribution of neuromodulatory inputs to training-induced changes in CS responsiveness, we separately clamped DA or NE levels at habituation levels (**Fig. S4A**) or selectively blocked DA or NE receptor subtypes (**Fig. S4B,C**). As recent studies (Bissière et al., 2003; Rodrigues et al., 2009) have shown that blockade of DA and NE interfere with the acquisition of fear memory in LA, model significantly reduced tone responses and number of plastic cells. (Dr.Nair, all detail numbers and t-test are in figure 4 legend)In TP cells, preventing the rise in DA release during conditioning greatly attenuated tone responses (**Fig. S4A1**, red circles; see figure legend for statistics). The reduction caused by preventing NE release had a much lower magnitude and did not reach significance (**Fig. S4A1**, red diamonds**)**. In contrast, marked attenuations in the tone responsiveness of LP cells were seen when the rise in DA (**Fig. S4A2**, blue circles) or NA (**Fig. S4A2**, blue diamonds) was prevented, during both conditioning and extinction.

Next, to shed light on the relative contributions of different DA and NE receptors to these effects, we ran additional simulations with selective blockade of particular NE or

DA receptor subtypes (**Fig. S4B,C**). During conditioning, selective block of D1 receptors transformed the transiently increased tone responsiveness of TP cells into persistently enhanced responses (**Fig. S4B1**, empty red circles). In contrast, blocking D2 receptors resulted in a persistent decrease in CS responsiveness of TP cells (**Fig. S4B1**, filled red circles). The protracted increase in the tone responsiveness of TP cells seen following blockade of D1 receptors is likely due to removal of two D1-induced effects, inhibition of NMDA-mediated responses (Martina and Bergeron, 2008) and facilitation of GABA synapses (Loretan et al., 2004; see Table 3). Similarly, the persistent decrease in the tone responsiveness of TP cells following blockade of D2 receptors is likely due to removal of D2-induced suppression of GABA synapses (Loretan et al., 2004; see **Table S3**). In LP cells, paralleling the effect of clamping DA levels at habituation levels (**Fig. S4A2**), blocking D2 (**Fig. S4B2**, filled blue circles) and to a lesser degree D1 (**Fig. S4B2**, empty blue circles) receptors, reduced the tone responsiveness of LP cells during conditioning and extinction. The latter results are likely due to the removal of the D1-induced increase in intrinsic excitability (Kroner et al., 2004), and of the D2-induced inhibition of GABA synapses (Loretan et al., 2004; see **Table S3**).

As to the contribution of NE receptors, consistent with the result of the simulations where we clamped NE release to habituation levels (**Fig. S4A**), blocking α or β NE had a marginal impact on the tone responses of TP cells (**Fig. S4C1**). However, blocking NE-β receptors (**Fig. S4C2**, filled blue diamonds), greatly reduced the tone responses of LP cells during conditioning and extinction. The latter results are likely due to the removal of two NE-β induced effects: inhibition of NMDA-mediated responses in interneurons and

facilitation of NMDA responses to principal cells in the cortical pathway (Johnson et al., 2011; see **Table S3**).

S2.2 Alternative model (Model 2)

Although not in an exhaustive manner, we did investigate whether alternative models might exist that provide output similar to that of the present model. Considering the fact that the distribution of afferents, internal connectivity, and single cell properties were based on data from biology, the only parameters for which we did not have very definitive data were initial synaptic weights and plasticity thresholds. With a different set of initial weights and minor modifications to plasticity thresholds (see Tables S3, S4), we were able to find another model that replicated the findings of the present model very well. The main difference between the output of this model 2 and the one we report was in the intra-LAd synaptic weight changes, which, as cited in the paper, were not found to significantly affect fear memory acquisition or storage. Specifically, we found that inhibitory transmission within amygdala decreased in model 2 (i.e., the interneuron-pyramidal cell connection depressed) by about 20% after conditioning, compared to the present model where it increased slightly after conditioning. Such as decrease in inhibitory transmission in the amygdala after fear conditioning has been reported recently (Rea et al., 2009).

S2.3 Testing the model's predictions

Although the model's predictions are currently hard to test, we predict that they will soon be amenable to experimental confirmation or rejection. Indeed, the last decade has witnessed the introduction of new optogenetic techniques that allow exquisite control of neuronal activity in particular elements of specified circuits, and with a temporal resolution recently thought impossible. With further advances in optogenetics, one can envision how most of the experimentally impossible model experiments described in our study could be performed, in effect allowing the model's prediction to be tested. For instance, using a dual viral strategy similar to the one recently used to selectively manipulate the activity of medial prefrontal neurons projecting to different sites (Xu and Sudhof, 2013), one could make posterior thalamic neurons projecting to the amygdala express channel rhodopsin (ChR2) and/or halorhodopsin so that their firing rates can be modulated up or down by applying light of the proper wavelength during training and recall. Moreover, it will soon be possible to block plasticity in select subsets of LA neurons activated during training. Indeed, Tonegawa and colleagues (Liu et al., 2012) recently introduced a conditional approach that allows selective expression of a transgene in neurons activated during a particular experience. In these experiments, the authors coupled the activity-dependent immediate early gene c-fos to the tetracycline transactivator (tTA), a component of the doxycycline (Dox) system for inducible expression of a gene of interest. Dox inhibited c-fos-promoter driven tTA from binding to its target tetracycline-responsive element site, which in turn prevented it from driving ChR2 expression. In the absence of Dox, training-induced neuronal activity selectively labeled active c-Fos-expressing dentate granule neurons with ChR2–EYFP, which could then be reactivated by light stimulation during testing. Using this approach, the authors

labeled a population of dentate granule neurons activated during contextual fear learning with ChR2 and later optically reactivated these neurons with light in a different context. The mice showed increased freezing only upon light stimulation, indicating light-induced fear memory recall. If one were to replace the transgene (ChR2 in this case) with a protein interfering with the maintenance of activity-dependent synaptic plasticity in LA cells, one could directly test whether increases in the CS responsiveness of thalamic or cortical CS pathways, in the absence of plasticity at synapses onto LA neurons, are sufficient for normal fear learning. Our model predicts that they would not.

S2.4 Supplementary figures and tables

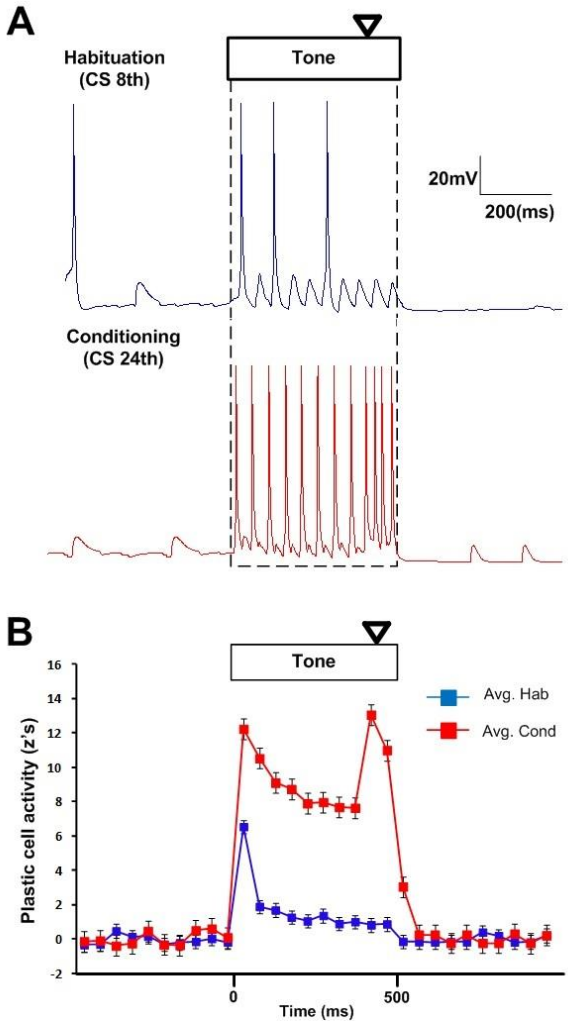

Figure S1. Tone responses of plastic cells in the control case. A : In this representative plastic cell, tone presentation during habituation (last trial) and late conditioning (last trial) elicits barrages of EPSPs. B: Mean peri-event time histogram (PETHs; spikes normalized to the pre-CS baseline; 50ms bins; tone duration 500ms) for the plastic cells (N=198) during habituation (trials 1-8), and conditioning (trials 1-16). Triangle denotes start of shock input during conditioning.

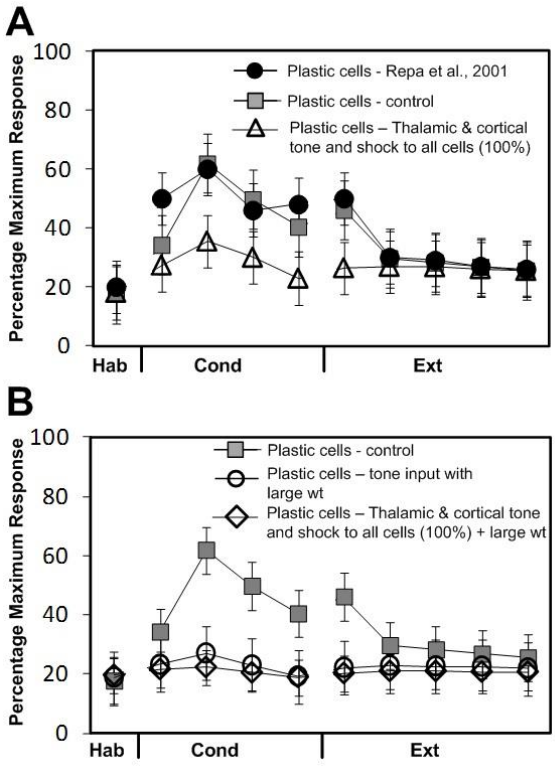

Figure S2. In the absence of tone plasticity, adjustments to model parameters failed to reproduce the findings of Repa et al. (2001; black circles). Three representative cases among several tested are shown here. Control model responses (gray squares) with plastic tone inputs are also shown for comparison. All model responses are normalized to habituation levels as in Repa et al. (2001). **(A)** Increasing the density of both tone and shock inputs to the maximum of 100% (empty triangles; note: biological estimate is 70%) caused a significant decrease in the number of plastic cells (triangles, N=120/800) compared to control (N=198/800). This change also decreased the potentiation in model tone responses during conditioning by 47±4%. **(B)** Increasing the initial synaptic strength (wt ~5) by 100% (wt=10) for the tone inputs only (empty circles) caused a significant decrease in the number of plastic cells (N=72) from control (N=198/800), and decreased the potentiation of model tone responses during conditioning by 64±5%. Increasing both tone and shock distribution to 100% and using larger initial strengths (wt = 10; diamonds) also caused a significant decrease in the number of plastic cells (N=64) from control (N=198/800), and decreased the potentiation of model tone responses during conditioning by 70±6%.

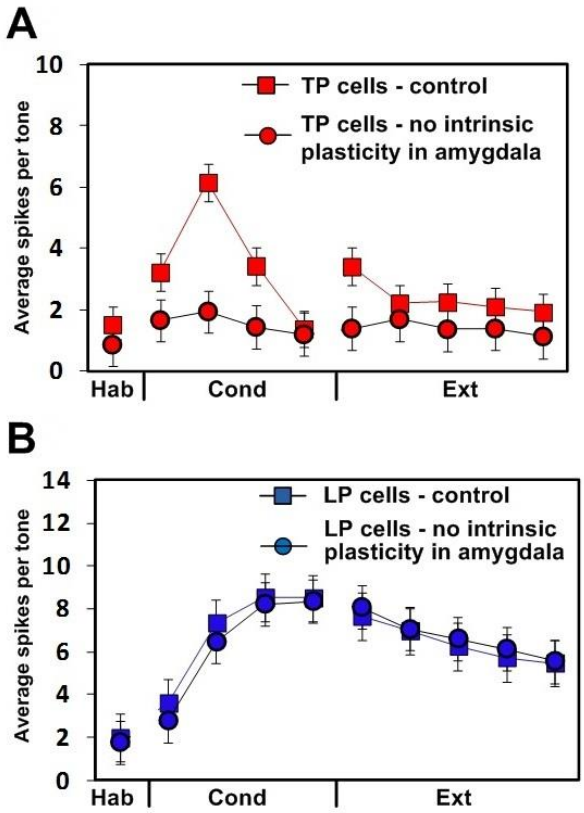

Figure S3. In addition to plasticity of thalamic and cortical tone inputs, plasticity within the amygdala is also necessary for the emergence of TP (A) and LP (B) cells. Spikes per tone (mean ± s.e.m.) of LAd model cells in control conditions (squares) and with suppressed plasticity in the amygdala (circles).

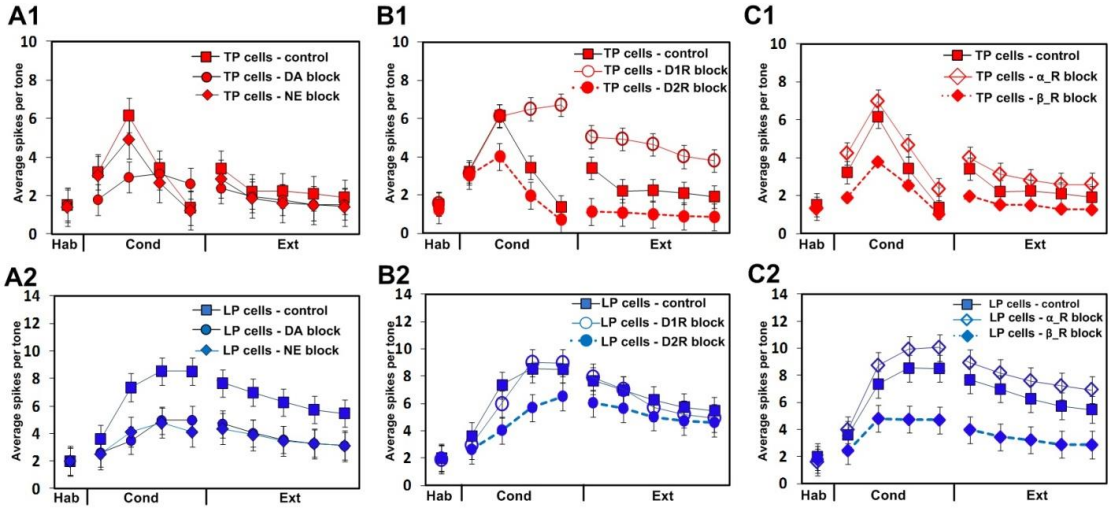

Figure S4. Contributions of neuromodulators to learning-induced changes in the tone responses of LAd cells. Tone responses of TP cells (top, **panels 1 of A-C**) and LP neurons (bottom, **panels 2 of A-C**) during the different phases of the behavioral protocol (x-axis) in the following conditions: (**A**) when the increased release of DA (circles) of NE (diamonds) was blocked; (**B**) when D1 (empty circles) or D2 (solid circles) receptors were blocked; (**C**) when NE-α (empty diamonds) or NE-β (filled diamonds) were blocked. In **A-C**, solid squares represent the control condition with normal neuromodulation. (**A1**) Tone responses of TP cells decreased when the DA (51±4%, $p<0.001$) but not the NE (8±0.6%, $p=0.52$ concentrations were kept at habituation levels; (**A2**) Tone responses of LP cells decreased when DA (61±5%, $p < 0.001$ during conditioning; 56±5%, $p < 0.001$ during extinction) or NE (59±5%, $p < 0.001$ during conditioning; 56±6%, $p < 0.001$ during extinction) concentrations were kept at habituation levels; (**B1**) Tone responses of TP cells increased with blockade of D1Rs (last 4 CS conditioning trials 387±22%, $p < 0.0001$; first 4 CS of extinction trials 97±8%, $p < 0.0001$) and decreased with blockade D2Rs (last 4 CS conditioning trials 48±4%, $p < 0.005$; first 4 CS of extinction trials 56±6%, $p < 0.001$); (**B2**) Tone responses of LP cells changed with selective blockade of either D1Rs (increased by 5±1%, $p=0.23$ during conditioning; decreased by 11±2%, $p<0.05$ during extinction) or D2Rs (decreased by 24±3%, $p<0.01$ during conditioning; decreased by 17±2%, $p<0.05$ during extinction) receptors; (**C1**) Tone responses of TP cells showed marginal increases with selective blockade of NE-α (11±3%, $p=0.3$) and decreases with blockade of NE-β (21±0.9%, $p<0.05$) receptors. (**C2**) Tone responses of LP cells increased with selective blockade of NE-α (empty diamonds; 24±3%, $p<0.05$) and decreased significantly with blockade of NE-β (52±4%, $p<0.001$ during conditioning; 48±4%, $p<0.001$ during extinction) receptors.

Table S1. Gating variables for ion channels used in the single cell models.

Current Type	Gating Variable	α	β	x_∞	τ_x (ms)
I_{Na}	*p=3*	$\frac{-0.4(V+30)}{\exp[-(V+30)/7.2]-1}$	$\frac{0.124(V+30)}{\exp[(V+30)/7.2]-1}$	$\alpha/(\alpha+\beta)$	$\frac{0.6156}{\alpha+\beta}$
	q=1	$\frac{0.03(V+45)}{\exp[-(V+45)/1.5]-1}$	$\frac{0.01(V+45)}{\exp[(V+45)/1.5]-1}$	$\frac{1}{\exp\left[\frac{V+50}{4}\right]+1}$	$\frac{0.6156}{\alpha+\beta}$
I_{DR}	*p=1*	$\exp[-0.1144(V-13)]$	$\exp[-0.08(V-13)]$	$\frac{1}{1+\alpha}$	$\frac{30.78\beta}{1+\alpha}$
I_H	*p=1*	$\exp[0.08316(V+75)]$	$\exp[0.033264(V+75)]$	$\frac{1}{\exp\left[\frac{V+81}{8}\right]+1}$	$\frac{\beta}{0.0473(1+\alpha)}$
I_M	*p=2*	$\frac{0.016}{\exp[-(V+52.7)/23]}$	$\frac{0.016}{\exp[(V-52.7)/18.8]}$	$\alpha/(\alpha+\beta)$	$1/(\alpha+\beta)$
I_{Ca}	*p=2*	$\frac{-15.69(V-81.5)}{\exp[-(V-81.5)/10]-1}$	$0.29\exp[-V/10.86]$	$\alpha/(\alpha+\beta)$	$1/(\alpha+\beta)$
	q=1	—	—	$\frac{0.001}{0.001+[Ca]_i}$	—
I_A **soma**	*p=1*	$exp\left[0.0381(V-11)\left[-1.5-\frac{1}{\exp[(V+40)/5+1]}\right]\right]$	$exp\left[0.021(V-11)\left[-1.5-\frac{1}{\exp[(V+40)/5+1]}\right]\right]$	$\frac{1}{1+\alpha}$	$\frac{6.4826\,\beta}{1+\alpha}$
	q=1	$\exp[0.1144V+56]$	—	$\frac{1}{1+\alpha}$	$0.26(V+50)$
I_A **dend**	*p=1*	$exp\left[-0.0687(V+1)+\frac{0.0382(V+1)}{\exp[(V+40)/5]+1}\right]$	$exp\left[-0.026793(V+1)+\frac{0.014898(V+1)}{\exp[(V+40)/5]+1}\right]$	$\frac{1}{1+\alpha}$	$\frac{3.2413\beta}{1+\alpha}$
	q=1	$\exp[0.1144(V+56)]$	$\exp[0.1144V+56]$	$\frac{1}{1+\alpha}$	$0.26(V+50)$
I_{sAHP}	*p=1*	$\frac{0.0048}{\exp(-5\log_{10}([Ca]_{i2})-17.5)}$	$\frac{0.012}{\exp(2\log_{10}([Ca]_{i2})+20)}$	$\alpha/(\alpha+\beta)$	1000-2000

Table S2. Maximal conductance densities of ion channels.

Conductance (mS/cm^2)		I_{Na}	I_{DR}	I_M	I_H	I_{Ca}	I_A	I_{sAHP}	τ_{Ca}
Principal cell - Type A	Soma	54	3	0.55	-	0.2	1.43	-	-
	Dend	27	3	0.55	0.0286	0.2	0.32	7	1000
Principal cell - Type B	Soma	54	3	0.39	-	0.2	1.43	-	-
	Dend	27	3	0.39	0.0286	0.2	0.32	0.45	1000
Principal cell - Type C	Soma	54	3	0.4	-	0.2	1.43	-	-
	Dend	27	3	0.4	0.0286	0.2	0.32	0.36	1000
Interneuron	Soma	35	8	-	-	-		-	-
	Dend	10	3	-	-	-		-	-

Table S3. Variations in maximal conductances to model neuromodulator effects. (parameter changes made to develop alternative model 2, if any, are listed in parenthesis)

NM	Receptor	Channel	Low level of NM (during trials 2-10 of conditioning)	High level of NM (during trials 11-16 of conditioning and trails 1-4 of extinction)	Highest level of NM (during shock)
Dopamine	D_1Rs (Low affinity)	I_{Kdr}	-	Decrease *gKdr* by 10%	Decrease *gKdr* by 20%
		AP threshold	-	Change activation of Na^+ channel by -0.5mV	Change activation of Na^+ channel by -1.5mV
		NMDA (pyr-pyr)	-	Decrease *gNMDA* by 5% (Decrease *gNMDA* by 20%)	Decrease *gNMDA* by 20% (Decrease *gNMDA* by 30%)
		GABA (interneuron-pyr)	-	Increase *gGABA* by 40% (Increase *gGABA* by 30%)	Increase *gGABA* by 60% (Increase *gGABA* by 40%)
	D_2Rs (High affinity)	Input Resistance	Decrease *gleak* by 5%	Decrease *gleak* by 10%	Decrease *gleak* by 20%
		GABA (interneuron-pyr)	Decrease *gGABA* by 20%	Decrease *gGABA* by 20% (Decrease *gGABA* by 30%)	Decrease *gGABA*,by 30% (Decrease *gGABA* by 60%)
Norepinephrine	NE-α (High affinity)	NMDA (thalamic input to interneuron)	Increase *gNMDA* by 5%	Increase *gNMDA* by 10%	Increase *gNMDA* by 30%
		NMDA (Cortical input to principal cells)	Decrease *gNMDA* by 10%	Decrease *gNMDA* by 30%	Decrease *gNMDA* by 30%
		NMDA (Thalamic input to principal cells)	Decrease *gNMDA* by 5%	Decrease *gNMDA* by 10%	Decrease *gNMDA* by 20%
	NE-β (Low affinity)	I_{sAHP}		Reduce *gK,sAHP* by 20%	Reduce *gK,sAHP* by 30%
		NMDA (Cortical input to principal cells)	-	Increase *gNMDA* by 20%	Increase *gNMDA* by 50%
		NMDA (Cortical input to interneurons)	-	Decrease *gNMDA* by 20%	Decrease *gNMDA* by 30%

Table S4. Model synaptic strengths and learning parameters.
(parameter changes made to develop alternative model 2, if any, are listed in parenthesis)

Long-term postsynaptic plasticity						
Connection	**Initial Weight**	**f_max** (f_min=0.8 for all)	**Learning factor**		**Ca^{2+} Threshold**	
			scaling	**Decay**	**Low**	**High**
Tone to Pyr (Thalamic)	5.5 (5)	3.5 (3)	80 (100)	0.04	0.40 (0.30)	0.53 (0.45)
Tone to Pyr (Cortical)	6 (5)	3.5	10	0.04	0.40 (0.30)	0.53 (0.45)
Tone to Inter (Thalamic)	4.5 (6)	4	5 (4.5)	0.01	0.45	0.5
Tone to Inter (Cortical)	4 (6.5)	4	20	0.01	0.45	0.5
PyrD to PyrD	1 (0.7)	4	80	0.03 (0.04)	0.3 (0.25)	0.55 (0.5)
PyrD to PyrV	1 (0.7)	4	10	0.03	0.3 (0.25)	0.55 (0.5)
PyrV to PyrD	1 (0.7)	4	80	0.03 (0.04)	0.3 (0.25)	0.55 (0.5)
PyrV to PyrV	1 (0.7)	4	10	0.03	0.3 (0.25)	0.55 (0.5)
InterD to PyrD	4.5 (20)	4	4	0.01 (0.04)	0.47 (0.6)	0.52 (0.7)
InterD to PyrV	4.5 (20)	4	2	0.01 (0.04)	0.47 (0.6)	0.52 (0.7)
InterV to PyrD	4.5 (20)	4	4	0.01 (0.04)	0.47 (0.6)	0.52 (0.7)
InterV to PyrV	4.5 (20)	4	2	0.01 (0.04)	0.47 (0.6)	0.52 (0.7)
PyrD to InterD	1.5 (1.0)	3	3	0.01	0.4 (0.3)	0.45 (0.35)
PyrD to InterV	1.5 (1.0)	2	2	0.01	0.4 (0.3)	0.45 (0.35)
PyrV to InterD	1.5 (1.0)	3	3	0.01	0.4 (0.3)	0.45 (0.35)
PyrV to InterV	1.5 (1.0)	3	2	0.01	0.4 (0.3)	0.45 (0.35)

Short-term presynaptic plasticity				
Connection	**Short-term dynamics**	**Parameters**		
		D (Maximum limit)	**d_1/d_2**	**τ_{D1} / τ_{D2} (ms)**
Inter-Pyr	depression	0.6	0.9 / 0.95	40 / 70
Pyr-Pyr	depression	0.5	0.9 / 0.95	40 / 70
Pyr-Inter	depression	0.7	0.9 / 0.95	40 / 70

- Shock synapses do not potentiate (weight =10 for synapses onto both principal cells and interneurons, in thalamic and cortical pathways).

S3. SUPPLEMENTARY REFERENCES

Byrne JH, Roberts JL. 2004. *From Molecules to Networks – An introduction to cellular and molecular neuroscience.* Elsevier Academic Press.

Farb C, Chang W, LeDoux JE. 2010. Ultrastructural characterization of noradrenergic axons and beta-adrenergic receptors in the lateral nucleus of the amygdale. *Front Behav Neurosci* **4**:162.

Hu H, Real E, Takamiya K, Kang M, LeDoux J, Huganir R, Malinow R. 2007. Emotion enhances learning via norepinephrine regulation of AMPA receptor trafficking. *Cell* **131**: 160-173.

Johnson LR, Hou M, Prager EM, LeDoux JE. 2011. Regulation of the fear network by mediators of stress: norepinephrine alters the balance between cortical and subcortical afferent excitation of the lateral amygdala. *Front Behav Neurosci* **5**: 23.

Kroner S, Rosenkranz JA, Grace AA Barrionuevo G. 2004. Dopamine modulates excitability of basolateral amygdala neurons in vitro. *J Neurophysiol* **93**: 1598-1610.

Liu X, Ramirez S, Pang PT, Puryear CB, Govindrajan A, Deisseroth K, Tonegawa S. 2012. Optogenetic stimulation of a hippocampal engram activates fear memory recall. *Nature* **484**: 381-5

Loretan K, Bissiere S, Luthi A 2004. Dopaminergic modulation of spontaneous inhibitory network activity in the lateral amygdale. *Neuropharmacology* **47**: 631-639.

Martina M, Bergeron R. 2008. D1 and D4 dopaminergic receptor interplay mediates coincident G protein-independent and dependent regulation of glutamate NMDA receptors in the lateral amygdala. *J Neurochem* **106**: 2421-2435.

Muller JF, Mascagni F, McDonald AJ. 2009. Dopaminergic innervation of pyramidal cells in the rat basolateral amygdala. *Brain Struct Funct* **213**: 275-288.

Rainbow TC, Parsons B, Wolfe BB. 1984. Quantitative autoradiography of β1- and β2-adrenergic receptors in rat brain. *Proc Natl Acad Sci* **81**: 1585-1589.

Rea K, Lang Y, Finn DP. 2009. Alterations in extracellular levels of gamma-aminobutyric acid in the rat basolateral amygdala and periaqueductal gray during conditioned fear, persistent pain and fear-conditioned analgesia. *J Pain* 10(10):1088-98.

Rodrigues SM, LeDoux JE, Sapolsky RM. 2009. The influence of stress hormones on fear circuitry. *Annu Rev Neurosci* **32**:289-313.

Rosenkranz JA, Grace AA. 2002. Cellular Mechanisms of infralimbic and prelimbic prefrontal cortical inhibition and dopaminergic modulation of basolateral amygdala neurons in vivo. *J Neurosci* **22**: 324-337.

Sara SJ. 2009. The Locus coeruleus and noradrenergic modulation of cognition. *Nat Neurosci Rev* **10**: 211-223.

Shouval HZ, Bear MF, Cooper LN. 2002b. A unified model of NMDA receptor-dependent bidirectional synaptic plasticity. *Proc Natl Aca Sci* **99**: 10831-10836.

Xu W, Sudhof C. 2013. A Neuronal circuit for memory specificity and generalization. *Science* **339**:1290-1295.

Zador A, Koch C, Brown TH. 1990. Biophysical model of a Hebbian synapse. *Proc Natl Acad Sci* **87**: 6718-6722.

CHAPTER 3

ASSIGNMENT OF LATERAL AMYGDALA NEURONS TO THE FEAR MEMORY TRACE DEPENDS ON COMPETITIVE SYNAPTIC INTERACTIONS

We used biophysical modeling to examine how particular lateral amygdala (LA) neurons are assigned to fear memory traces. Neurons with high intrinsic excitability were more likely to be integrated into the memory trace but synaptic competition also played a critical role. Indeed, we found that subsets of these more excitable projection cells effectively band together through their excitatory interconnections to suppress plasticity in other projection cells by recruiting inhibitory interneurons.

It is well established that the dorsal part of the lateral amygdala (LAd) is a critical site of plasticity for the storage of Pavlovian fear memories[1,2]. What is less clear is how particular LAd neurons are assigned to the fear memory trace. Indeed, relatively few LAd neurons (25%) acquire an increased responsiveness to stimuli (conditioned stimuli – CS) predicting adverse outcomes[3-5] even though most receive the necessary inputs[6]. Here, we used a biophysical realistic LAd model[7] (**Fig.1a-d**) to address this question.

LA cells expressing high levels of CREB (adenosine 3',5'-monophosphate response element-binding protein) are preferentially recruited into the memory trace[6,8]. In fact, the proportion of LA cells expressing activated CREB is similar to that acquiring potentiated

responses to the CS in unit recording studies[3-5]. However, when CREB is over-expressed ($CREB^+$) or down-regulated ($CREB^-$) in LA, the proportion of LA neurons recruited into the memory trace does not change, suggesting that assignment of particular LA neurons to the memory trace involves a competitive process[6]. Consistent with this, CREB enhances the intrinsic excitability of principal cells by inhibiting the slow afterhyperpolarization (sAHP) current[9-10], without altering their membrane potential, input resistance, or spike shape[11]. However, it is currently unclear whether CREB increases the likelihood that principal cells will become part of the fear memory by enhancing their intrinsic excitability.

We could address this question with our model because it is endowed with three types of principal cells with high (type-A,50%), intermediate (type-B,30%), or low (type-C,20%) spike frequency adaptation (**Fig.1e**), due to the differential expression of a Ca^{2+}-dependent K^+ current, as observed experimentally[12-14]. Other than their differing intrinsic excitability, Type-A-C neurons are identical; they received the same types and number of inputs (**Table S1**). Therefore, if the model is valid and CREB biases principal cells to become part of the fear memory trace by increasing their intrinsic excitability, one would expect an over-representation of the more excitable principal neurons among the plastic cells.

Consistent with this prediction, we found that a negligible proportion of type-A neurons were plastic cells, compared to around half of type-B and C cells (**Fig.1f**). Furthermore, when we simulated the $CREB^+$ or $CREB^-$ experiments of Han and colleagues[7] by converting a randomly selected subset (25% or 100 cells) of type-A neurons to type-C, or type-B-C neurons to type-A, without altering their connectivity, the

number of plastic cells did not change proportionally to the number of converted cells (**Fig**.**1g**).

To analyze the mechanisms underlying this effect, we compared the extrinsic and intrinsic connectivity of plastic vs. non-plastic cells in the control case. Note that the model's connectivity was not determined arbitrarily[7]. Instead, we used probabilistic gradients of excitatory and inhibitory connectivity so that the model would reproduce prior experimental observations about the spatially heterogeneous intrinsic connectivity that exists in different parts of LA[2].

With respect to extrinsic connections, a higher proportion of plastic cells received tone inputs from the thalamus and/or cortex (100%) than non-plastic type-B or C cells (61%; X^2=6.8,p<0.05). Shock inputs were also more prevalent to plastic (94%) than non-plastic type-B or C cells (47%). Intrinsic connections also differed between the two cell types (**Fig.2**): plastic cells formed more monosynaptic excitatory connections (5.8±0.23) with other plastic cells, as compared to non-plastic cells (4.1±0.15;p<0.0001;**Fig.2a**). In addition, there were more disynaptic connections involving interneurons from plastic to non-plastic cells (131±4.1) compared to such connections between plastic cells (108±4;p<0.0001;**Fig.2b**). Importantly, the same differences in intrinsic connectivity were observed between plastic and non-plastic cells of Types-A-C **(Fig.S1)** as well as in the $CREB^+$ and $CREB^-$ simulations (**Fig.S2**).

As mentioned above, in the $CREB^+$ and $CREB^-$ simulations (**Fig.1g**), the number of plastic cells did not change proportionally to the number of cells whose intrinsic excitability was altered. This occurred because some of the originally plastic cells became non-plastic (hereafter termed "loser-cells") and others, originally non-plastic,

became plastic (hereafter termed "winner-cells"). We reasoned that contrasting the properties of these two cell types would shed light on the factors involved in the competitive process.

This analysis revealed that in the $CREB^+$ and $CREB^-$ simulations, virtually all Type-B/C "loser" (n=47 and 9, respectively) and "winner" (n=45 and 28, respectively) cells received tone and shock inputs. However, as for the control case (**Fig.2a**), Type-B/C "loser-cells" received significantly less monosynaptic excitatory connections from Type-B/C "winner-cells", as compared to such connections between "winner-cells" ($p \leq 0.001$ in both cases; **Fig.2c,e**). Moreover, the disynaptic connections from the "winner-cells" involving interneurons to the "loser-cells" were significantly more numerous than between "winner-cells" ($p \leq 0.015$ in both cases;**Fig. 2d,f)**. Surprisingly however, "loser-cells" lost the competition even though they received as many (and in fact slightly more) excitatory connections from other "loser-cells" than between "winner-cells" (**Fig. 2c,e**). Also, the incidence of disynaptic inhibitory connections between "loser-cells" and "winner-cells" was also comparable (**Fig. 2d,f**). This suggests that pre-existing differences in the connections of the two cell types are not the only factors that bias the cells to win or lose. Consistent with this, the proportion of Type-C cells was significantly higher among "winner-cells" compared to "loser-cells" for the $CREB^+$ and $CREB^-$ cases ($CREB^+$, 96 vs. 47%, X^2=58.9, p<0.0001; $CREB^-$, 64 vs. 33%, X^2=19.2, p<0.0001). All other properties examined did not differ.

To test the robustness of the above findings, we performed additional simulations with different random values for (i) the distribution of the various types of principal cells in 3-D space, (ii) afferent tone and shock connectivity, and (iii) intra-LAd connectivity.

These simulations replicated the results reported above, indicating robustness of the model for these parameters (section S1 of Suppl Matls). Furthermore, we repeated the runs with a second model[7] (model 2, section S2 of Suppl Matls.) that was similar in all respects to the present one except for different initial weights of intra-LAd synapses. Model 2 also replicated the results reported above.

We used computational modeling to test the hypothesis that assignment of particular LAd neurons involves a competitive process[6], a notion based on the following observations. First, during fear conditioning only a minority of principal LA neurons (≈25%) develop potentiated CS responses[3-5] even though most receive the necessary inputs[6]. Second, a similarly low proportion of LA cells displays activated CREB and CREB enhances the likelihood that individual LA neurons are recruited into the fear memory trace[6]. Third, when CREB is over-expressed or down-regulated in LA, the proportion of LA neurons recruited into the memory trace remains constant[6].

Because CREB decreases the sAHP[9-10], we considered the possibility that a higher intrinsic excitability confers a competitive advantage to LA neurons. Consistent with this view, we observed that only 0.7% model LA neurons with high spike frequency adaptation were plastic cells, compared to around half of the intrinsically more excitable neurons. However, if this factor (intrinsic excitability) acted independently, CREB over-expression would result in the recruitment of a higher number of LA cells to the memory trace. Yet, this is not was seen experimentally[6], or in the current model when CREB over-expression was simulated by converting less into more excitable cells. Similarly, CREB down-regulation did not result in a lower number of model cells in the memory trace,

again replicating experimental observations[6]. This suggested that additional factors are involved in the competitive process. Comparative analyses of the intrinsic connectivity of plastic vs. non-plastic cells revealed that a major substrate of this competition is the distribution of excitatory connections between principal cells and the amount of disynaptic inhibition they generate in other projection cells. These two factors conspire to enhance the likelihood that some principal cells will fire more strongly to the CS and US at the expense of others. Effectively, this suggests that subsets of intrinsically more excitable projection cells band together by virtue of their excitatory interconnections to suppress plasticity in other projection cells via the recruitment of inhibitory interneurons. An important challenge for future experiments will be to test these predictions.

REFERENCES

1. LeDoux, J.E. *Annu. Rev. Neurosci.* **23**, 155-184 (2000).
2. Pape, H.C. & Paré, D. *Physiol. Rev.* **90**, 419-463 (2010).
3. Quirk, G.J., Repa, J.C. & LeDoux, J.E. *Neuron* **15**, 1029-1039 (1995).
4. Repa, J.C. *et al. Nat. Neurosci.* **4**, 724-731 (2001).
5. Rumpel, S. et al. *Science* **308**, 83–88 (2005).
6. Han, J.H. *et al. Science* **316**, 457-460 (2007).
7. Kim, D., Pare, D. & Nair S.S. *Learn. Mem.* doi..... (2013).
8. Han, J.H. *et al. Science* **323**, 1492-1496 (2009).
9. Viosca, J. *et al. Learn Mem* **16**, 193-197 (2009).
10. Benito, E., & Barco, A. *Cell* **33**, 230-240 (2010).

11. Zhou, Y. et al. *Nat. Neurosci* **12**, 1438-1443 (2009).

12. Faber, E.S., Callister, R.J. & Sah, P. *J. Neurophysiol.* **85**, 714-723 (2001).

13. Faber, E.S. & Sah, P. *J. Physiol.* **552**, 483-497 (2003).

14. Power, J.M *et al. J. Neurosci*. **31**: 526-537 (2011).

Figures

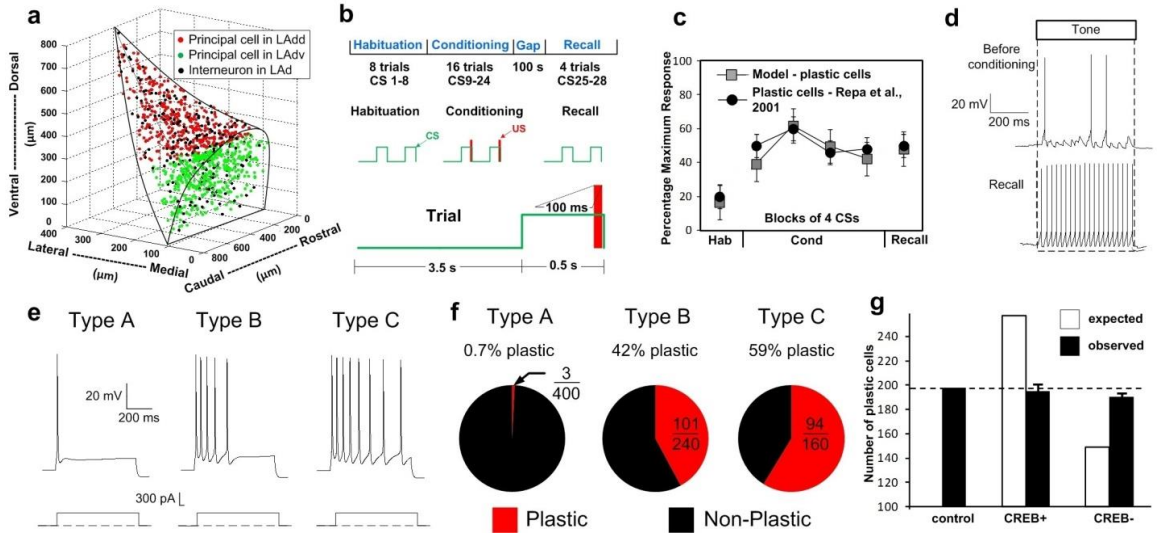

Figure 1. Spatial structure, intrinsic connectivity and fear conditioning protocol for the LAd network model. **(a)** The model consists of 800 principal cells and 200 interneurons populated randomly in the horn-shaped LAd. **(b)** Fear conditioning protocol. **(c)** Average tone responses of plastic LAd cells during the different phases of the behavioral protocol. (**d**) Example of tone responses generated by a plastic cell during habituation (top) and recall test (bottom). (**e**) Repetitive firing dynamics of there types of model projection cells. (**f**) Proportion of plastic cells among the three types of projection cells. (**g**) Expected (white) and observed (black) numbers of model plastic cells for the control, $CREB^{+}$, and $CREB^{-}$ cases. Competition biases the observed numbers towards the control value.

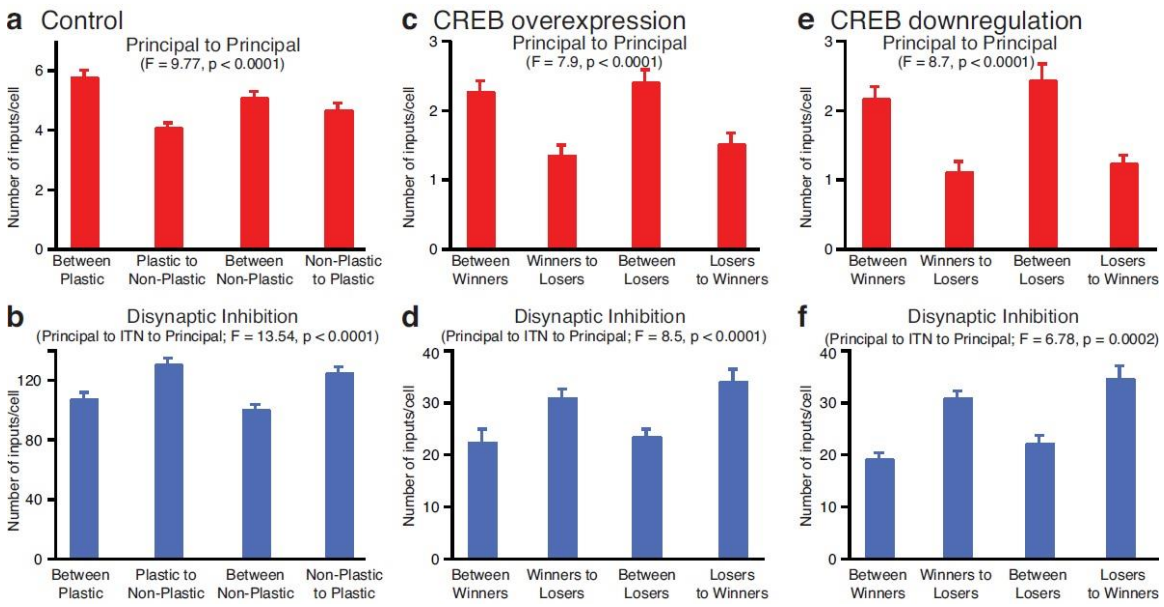

Figure 2. Differential intrinsic connectivity supports competition. Monosynaptic excitatory (**a,c,e**) and disynaptic inhibitory (**b,d,f**) connections among as well as between plastic and non-plastic cells (x-axis) in the control case. (**c-f**) Connections of type B-C "winner" and "loser" cells in the $CREB^{+}$ (**c,d**) and $CREB^{-}$ (**e,f**) simulations. Averages ± SEM. **ITN-local circuit interneurons.**

METHODS

We provide a brief overview of the 1000-cell biophysical LAd model[7].

Single cell models

To reproduce to diversity of spike frequency adaptation seen in principal LA neurons[12-14], we modeled three types of regular spiking principal cells, with high (type-A), intermediate (type-B), or low (type-C) spike frequency adaptation, due to the differential expression of a Ca^{2+}-dependent K^{+} current. LA also contains local GABAergic interneurons that exhibit various firing patterns, even among neurochemically-homogeneous subgroups[2]. However, the majority displays a fast-spiking pattern, which was reproduced in the model.

The principal cell model had three compartments representing a soma (diameter 24.75 µm; length 25 µm), an apical dendrite (diameter 2.5 µm; length 296 µm) on which synapses were placed, and another dendrite (diameter 5 µm; length 400 µm) that helped match passive properties. Values of specific membrane resistance, membrane capacity and cytoplasmic (axial) resistivity were within the ranges reported in previous physiological studies. The current types, equations and densities, as well as the match of single cell model and experimental data for responses to various current injections can be found in recent reports[7,15].

The interneuron model had two compartments, a soma (diameter 15 µm; length 15 µm) and a dendrite (diameter 10 µm; length 150 µm). The passive membrane properties were as follows: R_m = 20 KΩ-cm^2, C_m=1.0 µF/cm^2, R_a= 150 Ω-cm, and E_L = -70 mV.

Similar to the pyramidal cell, the interneuron model could reproduce the non-adapting repetitive firing behavior of fast spiking cells, as observed experimentally. Details including currents used have been reported separately[1].

Network structure and connectivity

It was estimated that there are 24,000 principal cells in LAd[7]. To keep computation times practical while capturing the complexity of the intra-LAd network, we modeled a scaled down (30:1) version of LAd that included 800 principal cells. Because the proportion of interneurons to principal cells is 20:80, the model included 200 interneurons. Principal cells and interneurons were distributed randomly in a realistic tri-dimensional representation of the horn-shaped LAd[7] (**Fig. 1a**).

By comparing the responses of LA cells to local applications of glutamate at various positions with respect to recorded neurons, general principles were inferred for connectivity among principal cells, as well as between local-circuit and principal neurons[16]. In particular excitatory connections between principal cells prevalently run ventrally and medially with significant rostrocaudal divergence. In contrast, inhibitory connections prevalently run mediolaterally in the horizontal plane and have no preferential directionality in the coronal plane. It was also recognized that principal LA neurons located along the external capsule (in the "shell" region of LA) form different connections than those found more medially (in the "core" region of LA; shell thickness of 100 μm)[16]. In the shell region, inhibitory neurons only affect nearby principal neurons whereas excitatory connections between principal cells are spatially less limited. To reproduce these spatially differentiated patterns of excitatory and inhibitory connections

in the model, we implemented distance–dependent gradients of connections as follows. We first converted the directional responses of principal LA neurons to local application of glutamate[8] into connectivity numbers. If a recorded site responded to x of y ejection sites in a region, then the connectivity from that region to the recorded site was taken as x/y. We then scaled the connectivity arbitrarily by a factor of three to determine the mono-synaptic connectivity needed for the model to reproduce experimental findings[16].

Activity-dependent synaptic plasticity

Model synapses could undergo activity-dependent synaptic plasticity, consistent with the experimental literature[7]. All AMPA synapses in the model were endowed with long-term postsynaptic plasticity except for those delivering shock or background inputs. Also, all GABA synapses had long-term plasticity. This form of plasticity was implemented using a learning rule that uses the concentration of a post-synaptic calcium pool at each modifiable synapse[17]. Calcium entered post-synaptic pools at excitatory synapses via NMDA receptors (and AMPA receptors for interneurons) and voltage-gated calcium channels (VGCCs). Similarly, calcium for pools at inhibitory synapses came from post-synaptic intra-cellular stores and VGCCs[7,15]. For both types of synapses, the synaptic weight decreased when the calcium concentration of the pool was below a lower threshold and increased when it exceeded an upper threshold. All model AMPA and GABA synapses also exhibited short-term presynaptic plasticity, with short-term depression at interneuron to principal cell and principal cell to interneuron connections. Further details and equations related to the learning rule can be found in a recent report[7].

Neuromodulator effects

Neuromodulators have long been implicated in fear and anxiety, and are known to regulate Pavlovian fear learning and synaptic plasticity in LA[18,19]. Conditioned aversive stimuli alter the activity of ventral tegmental area and locus coeruleus neurons, which in turn modulate fear and anxiety through their widespread forebrain projections, including to the amygdala. Therefore, the model incorporated the effects of dopamine (DA) and norepinephrine (NE) on LAd cells, based on prior experimental reports.

Inputs

Background synaptic inputs. LA projection neurons have low spontaneous firing rates in control conditions[7]. To reproduce this, Poisson-distributed, random excitatory background inputs were delivered to all model cells, resulting in average spontaneous firing rates of 0.7 Hz for principal cells and 7.2 Hz for interneurons.

Tone and shock inputs. Auditory fear conditioning is thought to depend on the convergence of inputs relaying information about the CS (tone) and US (footshock) in LA[1-3]. In the model, the CS and US inputs were represented by glutamatergic synapses acting via AMPA and NMDA receptors. The frequency of thalamic and cortical tone inputs during habituation was set to 20 Hz. The tone inputs also included noise represented by random Poisson spikes with an average frequency of 2 Hz. The following distribution of inputs was used for the simulations: uniform total tone density throughout LAd with 70% of the LAdd cells receiving thalamic and 35% receiving cortical tone projections, and the opposite for LAdv, i.e., 35% of LAdv cells receiving thalamic and 70% receiving cortical tone projections. The shock inputs were distributed uniformly to 70% of LAd cells.

Conditioning protocol used in simulations

The schedule of tone and shock inputs in the simulations was based on in vivo studies[3]. We scaled down the timing of the auditory fear conditioning protocol so that it would be suitable for computational studies (**Fig. 1b**). The protocol included three phases (habituation, conditioning and recall), comprised of 8, 16 and 4 trials, respectively. Each trial featured a 0.5 sec tone CS followed by a 3.5 sec gap. Only during conditioning, a shock was administered 100 msec prior to the end of the tone, so that they co-terminated. In light of evidence that fear conditioning leads to plasticity in CS afferent pathways[2], the frequency of thalamic and cortical tone inputs was increased to 40 Hz after the first and sixth conditioning trials, respectively.

All model runs were performed using parallel NEURON[20] running on a Beowulf supercluster with a time step of 10 μs. We have created a website at our research site from where interested parties will be able to download parts of the codes related to the model. The website is under construction but already features the single cell models. The relevant url is http://engineering.missouri.edu/neuro/research/ (under 'Software Files (NEURON) – Project Codes').

REFERENCES

15. Li, G., Nair, S.S. & Quirk, G.J. *J. Neurophysiol*. **101**, 1629-1646 (2009).

16. Samson, R.D. & Paré, D. *Neuroscience* **141**, 1599–1609 (2006).

17. Shouval, H.Z., Castellani, G.C., Blais, B.S., Yeung, L.C. & Cooper, L.N. *Biol. Cybern.* **87**, 383-391 (2002).

18. Bissière, S., Humeau, Y. & Luthi, A. *Nat. Neurosci.* **6**, 587-592 (2003).

19. Tully, K., Li, Y., Tsvetkov, E. & Bolshkov, V.Y. *Proc. Natl. Acad. Sci.* **104**, 14146-14150 (2007).

20. Carnevale, N.T. & Hines, M.L. *The NEURON book* (2006).

SUPPLEMENTARY MATERIALS

Details are provided related to additional studies to test the robustness of the model, followed by a supplemental table and two supplemental figures.

S1. Comparison with other model cases using random parameter sets

We ran three other cases with the model (cases 2-4 below), in addition to the one reported in the paper (case 1), with different random seeds for the following (each varied within the range reported earlier): (i) distribution of types of principal cells in the 3-D space, (ii) distributions of afferent tone and shock connectivity, and (iii) intra-LAd connectivity. Furthermore, we also ran the $CREB^+$ and $CREB^-$ scenarios for each of the cases.

The outputs were very similar across models for the number of plastic cells (average 189.3±6.5), the number of excitatory (average 21.3± 0.1) and inhibitory connections (average 22.2±0.1) received by principal cells, the number of excitatory (average 22.7±0.3) connection received by interneurons, and the tone responses of plastic cells. These numbers are comparable to data in Fig.1g, and table S1.

The $CREB^+$ and $CREB^-$ cases also gave similar results for the number of plastic cells across the cases. The difference across models was very small: avg. 189.3±6.5 for control, to avg. 195.3±1.4 the $CREB^+$ case, and an avg. of 183.3±4.7 for the CREB- case (similar to data in Fig. 1g). Also, in all cases, plastic cells received more monosynaptic excitatory connections (avg. 5.65±0.27) from other plastic cells, as compared to non-plastic cells (avg. 3.85±0.33; $p<0.001$). In addition, there were more disynaptic connections from plastic to non plastic cells (avg. 130.8±3.3) involving interneurons

compared to such connections from non-plastic to plastic cells (avg. 97.7±3.2). These again matched data for the main model, shown in Fig. S2 below.

S2. Alternative model (Model 2)

Considering the fact that the distribution of afferents, internal connectivity, and single cell properties were based on data from biology, the only parameters for which we did not have very definitive data were initial synaptic weights and plasticity thresholds. Although not in an exhaustive manner, we investigated whether alternative models might exist that provide output similar to that of the present model by varying these parameters. With a different set of initial weights and minor modifications to plasticity thresholds (see Kim et al., 2013 for values), we found another model (model 2) that replicated the reported findings very well. A characteristic of this model was that inhibitory transmission within amygdala decreased (i.e., the interneuron-pyramidal cell connection depressed) by about 20% after conditioning (as reported in Rea et al., 2009), compared to the present model where it increased slightly after conditioning.

Rea K, Lang Y, Finn DP. 2009. Alterations in extracellular levels of gamma-aminobutyric acid in the rat basolateral amygdala and periaqueductal gray during conditioned fear, persistent pain and fear-conditioned analgesia. *J Pain* 10(10):1088-98.

SUPPLEMENTARY TABLES & FIGURES

Table S1. Average number of afferent connections per principal cell

Cell type (total #)	Mono-syn exc	Mono-syn inh
A (n=400)	21.4±0.5	20.4±0.4
B (n=240)	21.6±0.7	20.5±0.5
C (n=160)	21.6±0.4	20.3±0.5
ANOVA	Df=2, F=0.046,p=0.955	Df=2, F=0.03, p=0.97

*afferents are from all other cells of types A, B and C

* No significant difference between A, B and C groups (p>0.05)

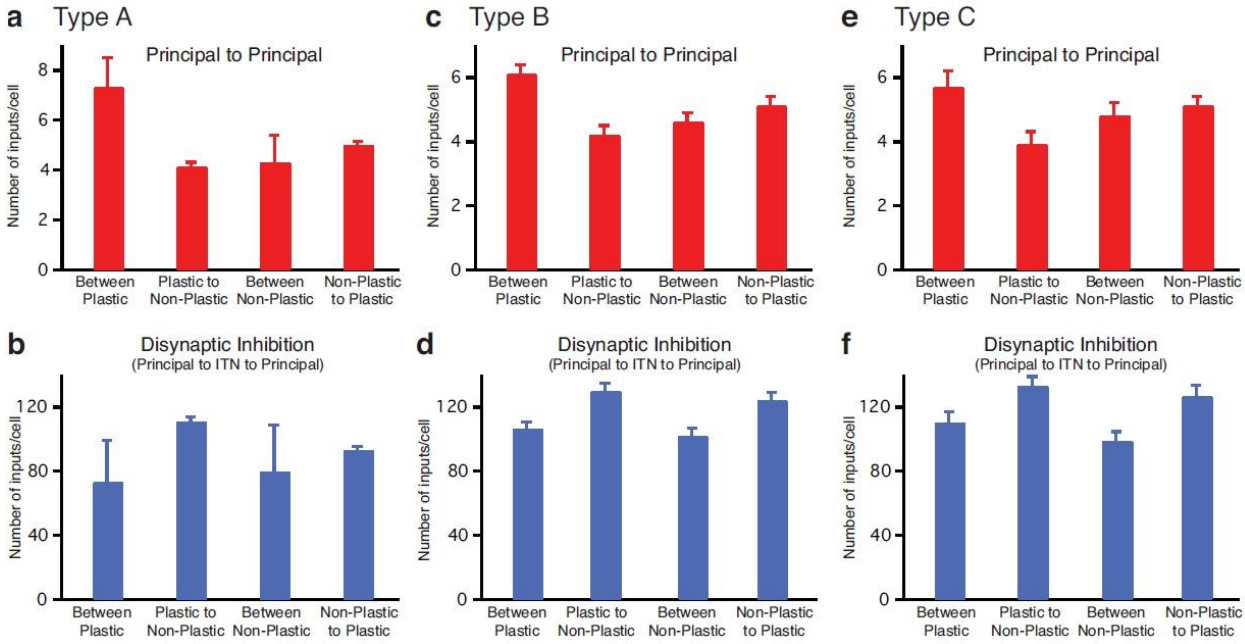

Figure S1. The differences in intrinsic connectivity between plastic and non-plastic cells in Fig. 2a,b were also reflected at a lower level among the cells types-A-C. Average number of monosynaptic excitatory (**a,c,e**) and disynaptic inhibitory (**b,d,f**) connections among as well as between plastic and non-plastic cells (x-axis) in the control case. Plastic type A cells (N=3) require more excitatory connections (7.3±1.2) and significantly less inhibitory connections (73.3±26, one-way ANOVA with post-hoc test $F=3.089$, $p<0.05$) from other plastic cells, compared to similar connections for plastic cells of types B and C. Between the cell types B and C, however, the differences were not significant, although the numbers are slightly higher for excitatory and slightly lower for inhibitory connections, as expected (one-way ANOVA with post-hoc test $F=3.089$, $p=0.63$). The other patterns were also similar as in Fig. 2a,b. Averages ± SEM. ITN-local circuit interneurons.

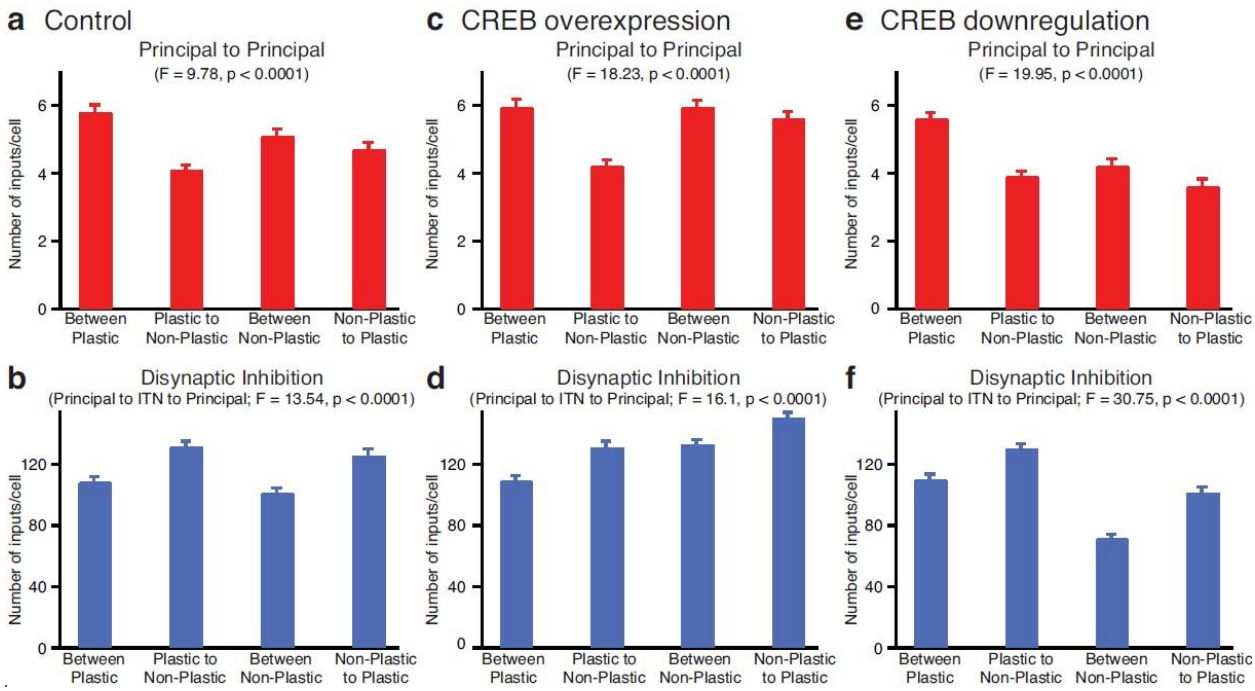

Figure S2. The differences in intrinsic connectivity between plastic and non-plastic cells in Fig. 2a,b were preserved for the CREB+ and CREB- cases also. Monosynaptic excitatory (**a, c, e**) and disynaptic inhibitory (**b, d, f**) connections among as well as between plastic and non-plastic cells (x-axis) in the control case (**a, b**), CREB+ case (**c, d**) and CREB- case (**e, f**). **(a)** plastic cells receive significantly higher excitatory connections from plastic cells, compared to non-plastic cells. **(b)** Plastic cells also receive significantly less di-synaptic inhibition from plastic cells, compared to non-plastic cells. **(c)** Plastic cells receive significantly higher excitatory connections from plastic cells, compared to non-plastic cells. **(d)** Plastic cells also receive significantly less di-synaptic inhibition from plastic cells, compared to non-plastic cells. **(e)** Plastic cells receive significantly higher excitatory connections from plastic cells, compared to non-plastic cells. **(f)** Plastic cells also receive significantly less di-synaptic inhibition from plastic cells, compared to non-plastic cells. Averages ± SEM. ITN-local circuit interneurons.

CHAPTER 4

SYNAPTIC MECHANISMS RELATED TO COMPETITION AND SPECIFICITY OF AMYGDALAR FEAR

ABSTRACT

We explored the synaptic correlates of the competition between lateral amygdala neurons underlying the formation of the Pavlovian fear memory trace, using a 1000-cell biophysical computational model. We then investigated how the memory formed by such a competition affects specificity to stimuli. The model suggested that plasticity in excitatory (PN-PN) and di-synaptic inhibitory (PN-IN and IN-PN) connections from principal cells involved in the memory were both necessary for the competition. The model also suggested that PN-PN plasticity promotes while disynaptic inhibition opposes stimulus generalization and that the plasticity configuration imprinted in the network for a particular memory by competition also ensures specificity to that memory.

INTRODUCTION

The ability to learn fear, i.e., associate fear responses to new stimuli or circumstances, is typically studied using an experimental paradigm termed Pavlovian fear conditioning, where an initially neutral stimulus (conditioned stimulus-CS) elicits conditioned fear responses after pairing with a noxious unconditioned stimulus (US). While there is evidence that fear conditioning induces widespread synaptic plasticity in the brain,

including at thalamic and cortical levels (Letzkus et al., 2011; Weinberger, 2011), there is also data indicating that the dorsal portion of the lateral amygdala (LAd) is a critical site of plasticity for the storage of CS-US associations (LeDoux, 2000; reviewed in Pape and Paré, 2010). For instance, unit recording studies have revealed that auditory fear conditioning increases the CS responsiveness of LAd neurons (Quirk et al., 1995; Collins and Paré, 2000; Repa et al., 2001; Goosens et al., 2003). In the most dorsal part of LAd, neurons display increases in CS responsiveness that last for only a few trials whereas in more ventrally located LAd neurons, CS responses are persistently increased, even resisting extinction training (Repa et al., 2001).

A recent biophysically 1000-cell model of dorsal subdivision of the rodent lateral amygdala (LAd; **Fig. 1A**; Kim et al., 2013) included conductance-based models of 800 principal cells (PN) and 200 inhibitory local circuit interneurons (IN) that reproduced the experimentally observed electroresponsive properties of these cell types, neuromodulatory inputs from brainstem dopaminergic and noradrenergic neurons, and spatially heterogeneous intrinsic connectivity (Pape and Paré, 2010). Also, all synapses in the model could undergo both short-term and long-term activity-dependent plasticity, except for those delivering shock or background inputs. The model successfully replicated the observed (Repa et al., 2001) temporal patterns of increased tone responsiveness displayed by neurons in the dorsal and ventral parts of LAd during Pavlovian fear conditioning (CS and US in **Fig. 1B**). The LAd model was used to investigate competitive mechanisms between neurons underlying formation of the 'fear memory trace' (Han et al., 2007, 2009) in LAd. Competition has been hypothesized to cause only a small subset of principal cells (25%) to be assigned to the fear memory trace

during Pavlovian fear conditioning, even though most LAd cells receive the necessary inputs. The model revealed that formation of the memory trace involved groups of principal cells with higher intrinsic excitability banding together by virtue of their excitatory interconnections, and effectively suppressing other principal cells via disynaptic inhibitory connections involving interneurons.

The excitatory and inhibitory connections among LAd cells also undergo plasticity during the training protocol. However, it is not clear what role of such intra-amygdalar plasticity (PN-PN, PN-IN and IN-PN) may play in the competition. Intra-amygdalar plasticity also affects response specificity to conditioned stimuli (CSs) but it is not clear how LAd implements such specificity. Indeed, experimental studies using lesions have shown that specificity of response to stimuli, or stimulus specificity, can be supported by plastic changes in LA alone (Armony et al., 1997). Also, a stimulus generalization gradient has been shown to exist for the fear response with the response being largest for the original CS and decreasing gradually with increasingly dissimilar stimuli (Honig and Urcuioli, 1981). We hypothesized that both competition and stimulus specificity mechanisms are related and utilize intra-amygdalar plasticity as well as differential excitatory and inhibitory connections. However, it is not presently clear how these mechanisms are implemented at the synaptic level, and how they might be related. Here we used the model to shed light on both these questions, i.e., the role of intra-amygdalar plasticity in the competition among the neurons for participation in a memory trace, and in ensuring response specificity when presented with different stimuli (e.g., **Fig. 1C**).

RESULTS

We used a previously developed biophysically-realistic model of LAd (Kim et al., 2013) to investigate the role of intra-amygdalar plasticity in the competitive process involved in the assignment of neurons to a memory trace. The simulated LAd network (**Fig. 1A**) included conductance-based models of 800 principal cells and 200 interneurons that reproduced the electroresponsive properties of these cell types, as observed experimentally, and neuromodulatory inputs from brainstem dopaminergic and noradrenergic neurons. Also, all the glutamatergic synapses in the model could undergo both short-term and long-term activity-dependent plasticity, except for those delivering shock or background inputs. The training paradigm used is shown in **Fig. 1B.** All reported values are averages ± s.e.m. expressed as percent change from control and tone responses are computed as spikes per tone within 200 ms of tone onset. The CS-evoked responses were of two distinct types as reported previously (Kim et al., 2013), plastic cells (**e.g., Fig. 2B1-control**) which showed a significant increase in their firing rates from habituation levels, and non-plastic cells that were unchanged from habituation levels.

Competition among cells holds over a large range of intrinsic excitability levels.

We first extended the competition studies in Kim et al. (2013) where we had considered only a 25% CREB over-expression case, by considering two other CREB over-expression cases, 50% and 70%, by converting 200 and 280, respectively, of type A cells to type C cells. Remarkably, competition continued to restrict the size of the fear memory trace to 25% (N=199/800) and 26% (N=211/800), respectively, further supporting the findings in

Kim et al. (2013). The underlying causes enabling this in the 50% and 70% CREB over-expression cases were again found to be the differences in extrinsic and intrinsic connections, as in 25% case. In the following, we provide numbers in parenthesis for the 50% and 70% CREB over-expression cases considered. With respect to extrinsic connections, a higher proportion of plastic cells received tone inputs from the thalamus and/or cortex (98%; 99%) than non-plastic type-B or C cells (76%; 71%). Shock inputs were also more prevalent to plastic (99%; 99%) than non-plastic type-B or C cells (66%; 58%). Intrinsic connections also differed between the two cell types: plastic cells formed more monosynaptic excitatory connections (2.53±0.17; 3.24±0.19) with other plastic cells, as compared to non-plastic cells (1.53±0.16; 2.3±0.15). In addition, there were more disynaptic connections involving interneurons from plastic to non-plastic cells (35±2.7; 45±1.9) compared to such connections between plastic cells (23.8±2.1; 34.4±2.6). The model thus demonstrates that competition is a viable hypothesis for restricting the memory size, as hypothesized by Han et al. (2009) by showing that it holds over a large range of excitability levels. Furthermore, the various model runs implicate the differences in extrinsic and intrinsic connections as being the underlying mechanisms.

Role of intra-amygdalar plasticity in competition.

The control case for competition studies had the following distribution of principal cell types: 120 type A, 240 type B, and 440 type C (see methods). This case was selected because competition is accentuated with 680 principal cells with higher intrinsic excitability (types B and C). Of these 680 cells, only 211 were recruited into the memory trace, i.e., became plastic, consistent with the fraction seen in experiments (Han et al.,

2007, 2009), and also shown recently in a model as being due to competition (Kim et al., 2013). **Fig. 2A** shows the spike histograms for plastic and non-plastic cells before and after conditioning for the control case, providing a snap shot of the competition. It clearly shows the significant increase in tone responses of plastic cells due to plasticity accrued during conditioning, and how plastic cell may suppress non-plastic cells. We then investigated the role of intra-amygdalar plasticity in this competition, via a series of model inactivation experiments. The tone responses resulting from these inactivation experiments are shown in **Fig. 2B**, and the specifics related cell numbers are provided below.

Inactivation of all intra-amygdalar plasticity. We first disabled all intra-amygdalar plasticity, i.e., in PN-PN, IN-PN, and PN-IN synapses, to study their combined effect. Instead of remaining constant at 26% (N=211/800), inactivation of all intra-amygdalar plasticity caused the size of the number of plastic cells to increase by 83% (to N=386/800). Further analysis revealed that while 47% (0.002% A, 18%B, and 29%C) of the principal cells that received both tone and shock became plastic in the control case, a much larger number, 85% (1% A, 30%B, and 54%C), became plastic when intra-amygdalar plasticity was disabled, and their tone responses were also higher (Table1; **Fig.2B1**). This implicates intra-amygdalar plasticity as the mechanism limiting the number of plastic cells to 26%. Then we asked what the contribution of plasticity in the individual synapses might be towards this overall effect. To investigate this, we disabled plasticity individually in the connections.

Inactivation of only PN-PN plasticity. This resulted in a 25% decrease in both the number of plastic cells (from 211 to 158), and in the tone responses (**Fig. 2B1**). Of the 53 that

became non-plastic, 77% (41) were type A (1) and B (40) cells, and 23% (12) were type C cells, indicating that higher intrinsic excitability (together with both tone and shock afferents) confers cells with the ability to retain plasticity. The loser cells of type B and C (N=52) had less mono-synaptic excitatory (5.7±0.51; t-test p=0.4) and more di-synaptic inhibitory (109±2.5, t-test $p<0.05$) inputs from other plastic cells, compared to the cells that retained their plasticity (exc:6.12±0.24; inh:100.5±2.3).

Inactivation of only IN-PN plasticity. This caused an 80% increase in the number of plastic cells (to N=380/800). Of the 169 new plastic cells, 166 were from the group that received both tone and shock, indicating that this inhibitory plasticity was important in implementing competition among the principal cells. Also, only 3 type C cells that received both tone and shock were non-plastic, compared to 5 of type B and 66 of type A, highlighting that competition favors cells with higher intrinsic excitability.

Inactivation of only PN-IN plasticity. This resulted in a 60% increase in the number of plastic cells (to N=338/800). This change was comparable to that of the IN-PN only case suggesting that both components of the disynaptic inhibition pathway had approximately similar contributions towards the resultant inhibition on the principal cell.

Inactivation of IN-PN and PN-IN, but not PN-PN plasticity. With only PN-PN plasticity, there was a 117% increase in the number of plastic cells (to N=458/800). All type B and C cells that received tone and shock became plastic, an increase of 169 from the control case, and 72 such cells became plastic even when they received only one of these afferents.

Plasticity in synapses of representative cells

To investigate the role of plasticity in competition at the individual cell level, we considered the change in synaptic weights of five representative cells among plastic and non-plastic cell groups. Of the five in each group we picked two of type B and three of type C. Since they were rare we omitted type A plastic cells (<1%) from this particular analysis.

For this group of representative cells, each plastic cell received 5.85±0.2 mono-synaptic excitatory connection from other plastic cells, while each non-plastic cell received only 4.2±0.15 connections from plastic cells. Also, each interneuron typically received 5.6±0.3 connections from plastic cells. Then we considered all disynaptic inhibitory connections from plastic cells to cells of each of the two groups. As cited earlier, plastic cells had significantly fewer (107.4±4) connections of this type, as compared to non-plastic cells (132±4.5). Since the excitability of a cell depends on these connections as well as on plasticity in these connections, we next investigated the role of plasticity.

For each group we investigated the effect of fear conditioning on the various synapses, on a per cell basis (average ±SEM). This analysis revealed that tone-PN synapses increased by 54±5 % for a plastic cell but only by 4±2% for a non-plastic cell. Also, PN-PN synapses from all plastic cells to a plastic cell increased by 80±2%, but such synapses from plastic cells to a non-plastic cell grew only by 10±1%. Plasticity in IN-PN connections was considered by taking all connections from interneurons to the specific principal cell. Among the interneuron population, there were six that did not receive any projections from principal cells, and these were excluded to ensure that we considered only inhibitory disynaptic pathways from plastic cells. Interestingly, IN-PN plasticity was

found to be similar for both plastic and non-plastic post-synaptic cell types: plasticity in IN-PN connections to non-plastic cells increased by 66±7% and they increased by 69±7% in such connections to plastic cells. For completion, we also considered plasticity in the PN-IN connections for both plastic and non-plastic pre-synaptic cells, and these were 80±2%, and 10±1%, respectively.

Role of intra-amygdalar plasticity in maintaining stimulus specificity.

We used five CSs for the stimulus specificity studies, with the cells targeted by CS2-CS5 overlapping in a graded manner with those targeted by CS1/+. Specifically, CS2 targeted 75% of the cells targeted by CS1; CS3 targeted 50%; CS4 targeted 25%; and CS5 targeted 0% (**Fig. 1C**). The network was conditioned to CS+ (paired CS and US) and to CS- (unpaired CS and US), with the other CSs only used for testing. We also used same (e.g., auditory tones with overlapping frequencies) and different (e.g., auditory and olfactory) stimuli types that converged onto the same LAd cells. To implement the different stimuli types, we used different synapses for the CSs, but with the same mapping (**Fig. 1C**) when connecting the stimuli to the principal cells. We then investigated how intra-amygdalar plasticity might contribute to stimulus specificity using model experiments.

Same stimuli types. After training with CS1/+ and CS5/-, the model was tested with the five CSs of the same stimuli type. Since CS1-CS5 were gradually decreasing in similarity, the CS-evoked responses correspondingly decreased (**Fig. 3A1,A2**), as expected (Lissek et al., 2010). Specifically, the responses to CS2 showed the most potentiation and responses to CS5 depressed. Thus, the stimulus generalization gradient

expanded to include stimuli that were more similar to CS+. As a next step, motivated by behavioral experiments that reported differences in stimulus generalization gradients between healthy subjects and those exhibiting anxiety disorders (Lissek et al., 2010), we explored the role of intrinsic plasticity in stimulus generalization. We varied the learning factors of LTP induction in PN-PN synapses after removing plasticity in PN-IN and IN-PN connections. **Fig. 3 B1** shows that the decrease in CS-evoked responses paralleled the impairment in PN-PN plasticity.

To explore the effect of plasticity in each intrinsic connection (PN-PN, PN-IN or IN-PN) individually on the CS-evoked responses with same stimuli type, we disabled plasticity in each connection prior to conditioning. After training with CS1/+ and CS5/-, the model was tested with the five CSs and exhibited the responses shown in **Fig. 3B2**. With no PN-PN synaptic plasticity, CS1/+ evoked responses decreased by 14% and CS2 responses decreased by 47%, while the other CSs-evoked responses were not different from habituation levels (t-test, $p>0.05$), suggesting that PN-PN plasticity was important for stimulus generalization. When either PN-IN or IN-PN synaptic plasticity was removed, the responses to CS2 showed the most potentiation and responses to CS5 depressed, as in the control case (full PN-PN plasticity). With no PN-IN synaptic plasticity, all CSs-evoked responses increased by 10%, and with no IN-PN synaptic plasticity, all CSs-evoked responses increased by 24%.

Distinct stimuli types. To explore the role of intrinsic plasticity within LAd on the CS-evoked responses with distinct stimuli (e.g., auditory and olfactory), we assumed that CS2-CS4 used different synapses to project to the same set of cells, i.e., same configuration as in **Fig. 1C** but with different afferent synapses. As shown in **Fig. 4 A1,A2**, the specificity to the trained

stimulus CS1/+ was maintained very well, with responses evoked by CS2-CS5 being at habituation levels. **Fig. 4 B1** shows that the decrease in CS-evoked responses paralleled the impairment in PN-PN plasticity.

Similar to the previous case, we explored the effect of plasticity in each intrinsic connection (PN-PN, PN-IN and IN-PN) individually on the CS-evoked responses with distinct stimuli type. For this we disabled plasticity in each connection prior to conditioning. After training with CS1/+ and CS5/-, the model was tested with the five CSs and exhibited the responses shown in **Fig. 4B2**. With no PN-PN synaptic plasticity, CS1/+ evoked responses decreased by 33% and other CSs-evoked responses were not significantly different from control (t-test, $p>0.05$). When PN-IN synaptic plasticity was removed, the responses to all CSs showed potentiation. With no PN-IN synaptic plasticity, all CSs-evoked responses increased by 27% and CS2 evoked response potentiated from habituation levels (t-test, $p<0.05$). And with no IN-PN synaptic plasticity, all CSs-evoked responses increased by 45% and CS2-3 evoked responses potentiated compared to habituation levels (t-test, $p<0.05$).

The model showed that conditioning to a particular stimulus causes several PN-PN synapses to potentiate, in addition to tone-PN synapses. As discussed earlier, plasticity of PN-PN synapses causes stimulus generalization, but how exactly is this implemented at the circuit level? To investigate this, we considered two typical configuration motifs for the different stimuli types case.

Motif 1: The synapse linking cell #223 (receiving CS1 and US; plastic cell) to cell #633 (receiving US, but not CS1; non-plastic cell) is representative of the case in which removal of inhibitory LTP (inactivation of PN-IN and IN-PN plasticity; e.g., **Fig. 4A1**) facilitated potentiation of conditioned responses to cells that did not receive direct CS1

input. The response of cell #633 to CS1/+ was unchanged by conditioning in the control case (producing <1 spike both before and after conditioning). However, with no inhibitory LTP (impaired case), its response to CS1/+ potentiated considerably after conditioning (from <1 spike to 4 spikes). Two pathways connect these two cells: A direct excitatory synapse, and feed-forward inhibition through five local interneurons. In both the control and no inhibitory LTP cases, the excitatory PN-PN connection potentiated strongly (+60% control; +110% no inhibitory LTP). However, in the control case, the feed-forward inhibitory pathway also potentiated strongly. This effect was seen both in PN-IN synapses from cell #223 to these five local interneurons (+100% LTP control), as well as the IN-PN synapses from the five local interneurons to cell #633 (+140% LTP control). The synapse from CS1/+ to cell #223 potentiated similarly in both cases (+130% control, +140% no inhibitory LTP case). Thus, biasing local synaptic plasticity toward excitation (by disabling LTP in the inhibitory pathway) contributed to the spread of conditioned responses to cell #633. It is noted that cell #633 received 8 connections similar to those from cell #223.

Motif 2. The synapse linking cell #574 (receiving CS3 and US; plastic cell) to cell #157 (receiving CS1 and US, but not CS3; plastic cell) is representative of the case in which removal of inhibitory LTP facilitated generalization of conditioning by CS1+/US pairing to other CSs. As expected, the response of cell #157 to CS1/+ potentiated in both cases. In contrast, the response of cell #157 to CS3 potentiated only in the no inhibitory LTP case (pre-conditioning: <1 spike; post-conditioning: <1 spike in control, but 3 spikes with no inhibitory LTP). Again, the excitatory connection from cell #574 to cell #157 potentiated strongly and similarly in both cases (+80% control; +90% no inhibitory LTP);

but the feed-forward inhibitory pathway through local interneurons (N=7) potentiated considerably in control (PN-IN: +60% LTP control; IN-PN: +110% LTP control). The synapse from CS3 to cell #574 did not potentiate in either case (<10% change), indicating that these generalization mechanisms operated independently of stimulus afferents to LA. This shows how removal of inhibitory LTP contributed to the generalization of conditioned responses to unconditioned stimuli. It is noted that cell #157 received a total of four connections similar to those from cell #574.

DISCUSSION

Competition has been hypothesized to cause only a small subset of cells (25%) to be assigned to the fear memory trace, even though most LAd cells receive the necessary inputs (Han et al., 2007, 2009). This was validated recently using a biologically-realistic model of LAd (Kim et al., 2013) that compared the intrinsic connectivity of plastic vs. non-plastic cells and identified a major substrate of this competition as being the distribution of excitatory connections between principal cells and the amount of disynaptic inhibition they generate in other projection cells. These two factors conspired to enhance the likelihood that some principal cells will fire more strongly to the CS and US at the expense of others. Effectively, this suggests that subsets of intrinsically more excitable projection cells band together by virtue of their excitatory interconnections to suppress plasticity in other projection cells via the recruitment of inhibitory interneurons. The present study focused on the role of intra-amygdalar plasticity played in this competitive process, and also on how it affected response specificity to a stimulus.

Distinct roles of the different components of intra-amygdalar plasticity

All intra-amygdalar synapses, PN-PN, PN-IN, and IN-PN participated in the competition in different ways as evident from the analysis in Results. Even though 56% of all principal cells received both tone and shock inputs, intra-amygdalar plasticity limited the number of plastic cells to 26% of the total. This was demonstrated by inactivating intra-amygdalar plasticity which caused almost all type B and C cells receiving tone and shock to become plastic (374/377). It is noted that type A cells played a marginal role in the competition (**Table 1**). PN-PN plasticity helped cells band together and make other cells plastic in the absence of plasticity in the disynaptic inhibitory pathways (PN-IN and IN-PN plasticity disabled) since this increased the number of plastic cells to 458 (a 117% increase), even recruiting 72 cells that did not receive both tone and shock. However, when only PN-PN plasticity was disabled, inhibitory plasticity reduced the number of plastic cells by 27% from the control case, indicating that inhibitory plasticity effectively counters plasticity in the afferent tone-PN synapses. But would PN-PN plasticity or inhibitory plasticity by themselves be enough for competition? To address this, we performed two additional model runs. In one we retained only inhibitory plasticity, i.e., inactivated PN-PN plasticity alone (N=158 plastic cells), and then simulated the 25% CREB down-regulation experiment. This showed that the number of plastic cells was not maintained, and dropped from 158 to 116, indicating that PN-PN plasticity was important to stabilize the size of the memory trace. In the second model run we simulated the 'No IN-PN & PN-IN plasticity' case (i.e., only PN-PN plasticity) and found that the number of plastic cells were again not maintained, dropping from 458 to

363. These two model experiments showed that plasticity in excitatory connections between principal cells and disynaptic inhibitory plasticity from plastic cells were both necessary for stabilizing the size of the fear memory trace, i.e., competition thus requires both forms of intra-amygdalar plasticity. Considering the components of inhibitory plasticity, we found that PN-IN and IN-PN plasticity had similar contributions. In all cases, cells with higher intrinsic excitability (types B and C) were consistently represented in disproportionately larger numbers in the plastic cell group (**Table 1**), while type A cells were ineffective in the competition, as hypothesized in Kim et al. (2013). This was also highlighted by the fact that none of the type A cells that received only one or none of the tone and shock afferents became plastic even when inhibitory plasticity was disabled.

Analysis at the single cell level revealed that the dominant plasticity mechanisms separating plastic and non-plastic cells were tone-PN plasticity and PN-PN plasticity, but not IN-PN plasticity. In addition, the numbers of such connections were also significantly different for the two cell types as cited in results. Also, for PN-PN connections to a principal cell, both the number of such connections and plasticity in the connections are relevant, but for the disynaptic inhibitory connections from plastic cells, only the number of connections is relevant.

PN-PN plasticity promotes while disynaptic inhibition opposes stimulus generalization

For the control case, intra-amygdalar plasticity maintained stimulus specificity very well for both similar and distinct stimuli types (**Figs. 3A1** and **4A1**). For stimuli of the

same type, e.g., tones with over-lapping frequencies, since CS2 to CS5 declined in similarity from CS1 in a graded manner, the trend in **Fig. 3A1** which parallels this decline is as expected. In contrast, for distinct stimuli, specificity is tightly maintained (**Fig. 4A1**) indicating that inhibitory plasticity effectively overcomes PN-PN plasticity. Indeed, a slight decrease, compared to control, was noted in stimulus-evoked responses for CS2-CS5 in this case, similar to that reported in experiments (Collins and Pare, 2000). That it is plasticity in the PN-PN synapses that causes generalization is evident particularly from **Fig. 4A1** where the 'no PN-IN and IN-PN plasticity' case (i.e., only PN-PN plasticity) shows that the PN-PN synapses potentiated by conditioning with CS1 cause the subsequent CS2-CS5 evoked responses to be considerably higher than control. As expected, they continue to decline in a graded manner from CS2 to CS5. Considering individual components of inhibition, plasticity in PN-IN and IN-PN seem to contribute equally (**Figs. 3B2, 4B2**). Finally, the changes in non-plastic cells was negligible, suggesting that non-plastic have negligible contribution to stimulus generalization.

Competition and specificity to stimulus - two sides of the same coin

LAd receives input from multiple stimuli and is a key site of memory formation in fear conditioning. As hypothesized in Han et al. (2007), model experiments showed that competition plays a key role in keeping the size of the fear memory trace constant even if the proportion of cells with high intrinsic excitability is increased or decreased (Kim et al., NN). Competition potentiates both the PN-PN synapses linking the plastic cells, and the disynaptic inhibitory connections from plastic cells involving interneurons. It is plasticity in the disynaptic inhibitory connections from plastic cells that effectively limits

responses of non-plastic cells, and these disynaptic inhibitory pathways are effectively used in maintaining specificity to a stimulus. Indeed, CS2 evoked responses were at habituation levels in the distinct stimuli case in **Fig. 4A1**, even when CS2 shared 75% of the cells with CS1. This was due to two reasons. First, CS1 and CS2 shared different synapses, and so the conditioning-inducted potentiation of the afferents to CS1 was not utilized by CS2. Secondly, conditioning induced potentiation of the PN-PN synapses was countered by potentiation along the disynaptic inhibitory pathways from the plastic cells involving interneurons. This kept CS2-evoked responses at habituation levels, and inactivation of PN-IN and IN-PN plasticity resulted in an increase in the same responses (**Fig. 4A1**). In the specific example of motif 2 discussed in results, cell #157 receiving only CS1 and US, in the disabled inhibitory plasticity (PN-IN and IN-PN) case, could show conditioned responses to CS3 solely by a connection to cell #574 that received CS3 and US, but not CS1. This was because conditioning to CS1 induced potentiation of the PN-PN synapse linking the two cells, since both received shock inputs. However, the disynaptic inhibitory pathway linking the cells also potentiated, and this prevented cell #157 from responding to CS3 in the control case.

To summarize, competition forms a specific memory. It appears that the plasticity configuration imprinted in the network by this competition automatically ensures specificity to that memory. This is done by potentiating all inhibitory pathways emanating from the principal cells that code that memory, effectively ensuring that the principal cells that receive these potentiated inhibitory projections are suppressed unless they receive direct afferents related to that memory. For instance, if the memory for CS1 is imprinted in the network, i.e., plastic cells are formed by CS1/US pairings, the

disynaptic inhibitory pathways from these plastic cells to all the other plastic cells are potentiated. This means that if afferents related to another memory, say CS3, use some of the plastic cells related to CS1 (via different synapses), this will not generate sufficient responses in other plastic cells unless those cells directly receive CS3 afferents themselves, i.e., are directly involved in the CS3 memory.

CONCLUSIONS

Competition has been hypothesized to play a role in memory formation in the lateral amygdala in auditory fear conditioning (Han et al., 2007, 2009), and a recent biologically-realistic model of LAd (Kim et al., 2013) showed that excitatory connections between principal cells and the amount of disynaptic inhibition they generate in other projection cells were the two factors that controlled the formation of such a memory. We extended the study to the role played by plasticity in these two connections in this competitive process, and how that, in turn, affected specificity to a stimulus. The model suggests that plasticity in excitatory (PN-PN) and di-synaptic inhibitory (PN-IN and IN-PN) connections from plastic cells were both necessary for the competition. The model also suggested that PN-PN plasticity promotes while disynaptic inhibition opposes stimulus generalization. We also found that the plasticity configuration imprinted in the network for a particular memory by competition also automatically ensures specificity to that memory.

METHODS

Single cell models

To reproduce to diversity of spike frequency adaptation seen in principal LA neurons (Faber et al., 2001, Faber and Sah, 2003; Power et al., 2011), we modeled three types of regular spiking principal cells, with high (type-A), intermediate (type-B), or low (type-C) spike frequency adaptation, due to the differential expression of a Ca^{2+}-dependent K^+ current. LA also contains local GABAergic interneurons that exhibit various firing patterns, even among neurochemically-homogeneous subgroups (Pape and Pare´, 2010). However, the majority displays a fast-spiking pattern, which was reproduced in the model.

The principal cell model had three compartments representing a soma (diameter 24.75 µm; length 25 µm), an apical dendrite (diameter 2.5 µm; length 296 µm) on which synapses were placed, and another dendrite (diameter 5 µm; length 400 µm) that helped match passive properties. Values of specific membrane resistance, membrane capacity and cytoplasmic (axial) resistivity were within the ranges reported in previous physiological studies. The current types, equations and densities, as well as the match of single cell model and experimental data for responses to various current injections can be found in recent reports (Li et al., 2009; Kim et al., 2013).

The interneuron model had two compartments, a soma (diameter 15 µm; length 15 µm) and a dendrite (diameter 10 µm; length 150 µm). The passive membrane properties were as follows: R_m = 20 KΩ-cm^2, C_m=1.0 µF/cm^2, R_a= 150 Ω-cm, and E_L = -70 mV. Similar to the pyramidal cell, the interneuron model could reproduce the non-adapting

repetitive firing behavior of fast spiking cells, as observed experimentally. Details including currents used have been reported separately (Kim et al., 2013).

Network structure and connectivity

It was estimated that there are 24,000 principal cells in LAd. To keep computation times practical while capturing the complexity of the intra-LAd network, we modeled a scaled down (30:1) version of LAd that included 800 principal cells. Because the proportion of interneurons to principal cells is 20:80, the model included 200 interneurons. Principal cells and interneurons were distributed randomly in a realistic tri-dimensional representation of the horn-shaped LAd (Kim et al., 2013) (**Fig. 1A**).

By comparing the responses of LA cells to local applications of glutamate at various positions with respect to recorded neurons, general principles were inferred for connectivity among principal cells, as well as between local-circuit and principal neurons[16]. In particular excitatory connections between principal cells prevalently run ventrally and medially with significant rostrocaudal divergence. In contrast, inhibitory connections prevalently run mediolaterally in the horizontal plane and have no preferential directionality in the coronal plane. It was also recognized that principal LA neurons located along the external capsule (in the "shell" region of LA) form different connections than those found more medially (in the "core" region of LA; shell thickness of 100 μm) (Samson and Pare´, 2006). In the shell region, inhibitory neurons only affect nearby principal neurons whereas excitatory connections between principal cells are spatially less limited. To reproduce these spatially differentiated patterns of excitatory and inhibitory connections in the model, we implemented distance–dependent gradients

of connections as follows. We first converted the directional responses of principal LA neurons to local application of glutamate into connectivity numbers. If a recorded site responded to x of y ejection sites in a region, then the connectivity from that region to the recorded site was taken as x/y. We then scaled the connectivity arbitrarily by a factor of three to determine the mono-synaptic connectivity needed for the model to reproduce experimental findings (Samson and Pare´, 2006). With this connectivity, a principal cell had an average of 21.4±0.35 excitatory inputs from other cells and 22.2±0.28 inhibitory inputs from interneurons, and an interneuron had an average of 22.4±0.37 excitatory inputs from principal cells.

Activity-dependent synaptic plasticity

Model synapses could undergo activity-dependent synaptic plasticity, consistent with the experimental literature (details in Kim et al., 2013). All AMPA synapses in the model were endowed with long-term postsynaptic plasticity except for those delivering shock or background inputs. Also, all GABA synapses had long-term plasticity. This form of plasticity was implemented using a learning rule that uses the concentration of a post-synaptic calcium pool at each modifiable synapse (Shouval et al., 2002). Calcium entered post-synaptic pools at excitatory synapses via NMDA receptors (and AMPA receptors for interneurons) and voltage-gated calcium channels (VGCCs). Similarly, calcium for pools at inhibitory synapses came from post-synaptic intra-cellular stores and VGCCs (Li et al., 2009; Kim et al., 2013). For both types of synapses, the synaptic weight decreased when the calcium concentration of the pool was below a lower threshold and increased when it exceeded an upper threshold. All model AMPA and GABA synapses also exhibited

short-term presynaptic plasticity, with short-term depression at interneuron to principal cell and principal cell to interneuron connections. Further details and equations related to the implementation of these plasticity mechanisms can be found in Kim et al. (2013).

Neuromodulator effects

Neuromodulators have long been implicated in fear and anxiety, and are known to regulate Pavlovian fear learning and synaptic plasticity in LA (Bissiere et al., 2003; Tully et al., 2007). Conditioned aversive stimuli alter the activity of ventral tegmental area and locus coeruleus neurons, which in turn modulate fear and anxiety through their widespread forebrain projections, including to the amygdala. Therefore, the model incorporated the effects of dopamine (DA) and norepinephrine (NE) on LAd cells, based on prior experimental reports.

Inputs

Background synaptic inputs. LA projection neurons have low spontaneous firing rates in control conditions. To reproduce this, Poisson-distributed, random excitatory background inputs were delivered to all model cells, resulting in average spontaneous firing rates of 0.7 Hz for principal cells and 7.2 Hz for interneurons.

Tone and shock inputs. Auditory fear conditioning is thought to depend on the convergence of inputs relaying information about the CS (tone) and US (footshock) in LA (LeDoux, 2000; Pape and Paré, 2010; Quirk et al., 1995). In the model, the CS and US inputs were represented by glutamatergic synapses acting via AMPA and NMDA receptors. The frequency of thalamic and cortical tone inputs during habituation was set to 20 Hz. The tone inputs also included noise represented by random Poisson spikes with

an average frequency of 2 Hz. The following distribution of inputs was used for the simulations: uniform total tone density throughout LAd with 70% of the LAdd cells receiving thalamic and 35% receiving cortical tone projections, and the opposite for LAdv, i.e., 35% of LAdv cells receiving thalamic and 70% receiving cortical tone projections. The shock inputs were distributed uniformly to 70% of LAd cells.

Conditioning protocol used in simulations

The schedule of tone and shock inputs in the simulations was based on in vivo studies (Quirk et al., 1995). We scaled down the timing of the auditory fear conditioning protocol so that it would be suitable for computational studies (**Fig. 1B**). The protocol included three phases (habituation, conditioning and recall), comprised of 8, 16 and 4 trials, respectively. Each trial featured a 0.5 sec tone CS followed by a 3.5 sec gap. Only during conditioning, a shock was administered 100 msec prior to the end of the tone, so that they co-terminated. In light of evidence that fear conditioning leads to plasticity in CS afferent pathways (Pape and Paré, 2010), the frequency of thalamic and cortical tone inputs was increased to 40 Hz after the first and sixth conditioning trials, respectively.

Competition and Stimulus specificity studies

We used the 70% CREB over-expression scenario of the model described above as the control case for the competition studies since that highlighted competition the most among the various scenarios considered (Kim et al., 2013).

For stimulus specificity studies, we reduced the tone and shock density from 70% to 50% in the control case of Kim et al. (2013) to accommodate five different CSs (Ball et

al., 2012), with varying degrees of overlap (**Fig. 1C**). All five CSs and the US targeted 50% of the pyramidal cells (**Fig. 1C**) and 70% of the interneurons. CS1 was co-presented with the US, and so is termed CS+. For this experimental design, the CSs and US were connected in a pattern that satisfied two criteria: First, the cells targeted by CS2-CS5 overlapped in a graded manner with those targeted by CS1/+. Specifically, CS2 targeted 75% of the cells targeted by CS1; CS3 targeted 50%; CS4 targeted 25%; and CS5 targeted 0%. Because of the complete lack of overlap between CS1 and CS5, CS5 is also termed CS5/- or just CS-. Second, each CS randomly targeted cells of each type (pyramidal cells of types A, B, C). This choice ensured that no CS preferentially targeted a disproportionate number of highly excitable cells. We followed the protocol in Lissek et al. (2008) and Repa et al. (2001) and conditioned the network to CS+ (paired CS and US) and to CS- (unpaired CS and US). As cited, the other CSs were used only for testing. Two types of CSs were used to represent same stimuli types but with differing characteristics (e.g., auditory tones with overlapping frequencies), and different stimuli types (e.g., auditory and olfactory) that may converge on the same LA cells. To implement the different stimuli types, we used different synapses for the CSs, but with the same mapping (**Fig. 1C**) when connecting the stimuli to the principal cells.

The training protocol also had minor modifications. For the pre-conditioning test (to obtain baseline responses), we presented the stimuli as follows: CS1, CS2, CS3, CS4, CS5, CS1, CS2, CS3, etc, 10x each, 3.5 sec interval, no shock. Plasticity is turned off during this phase. The presentations during the other phases were as follows. During habituation: CS1, random shock during interval (no overlap), CS5, random shock (no overlap), CS1, random shock, etc., 10x each, 4 sec interval. Plasticity is turned

on. During conditioning: Identical to habituation, except shock is only co-presented with CS1, and there is no shock during intervals. Plasticity is turned on. For post-conditioning test: Identical to pre-conditioning test. Plasticity is turned off during this phase. It is noted that CS1 and CS5 are presented with shock, but only the former one is paired. CS2 targets 75% of the cells that CS1 targets, CS3 targets 50% of those cells targeted by CS1, CS4 targets 25%, and CS5 targets 0%. Also, CS1-5 targeted randomly selected 70% of the interneurons.

All model runs were performed using parallel NEURON (Carnevale and Hines, 2006) running on a Beowulf supercluster with a time step of 10 μs.

REFERENCES

COMPETITION

Benito, E., & Barco, A. CREB's control of intrinsic and synaptic plasticity: implications for CREB dependent memory models. *Cell* **33**, 230-240 (2010).

Collins, D.R. & Paré, D. Differential fear conditioning induces reciprocal changes in the sensory responses of lateral amygdala neurons to the CS(+) and CS(-). *Learn. Mem*. **7**, 97-103 (2000).

Faber, E.S., Callister, R.J. & Sah, P. Morphological and electrophysiological properties of principal neurons in the rat lateral amygdala in vitro. *J. Neurophysiol.* **85**, 714-723 (2001).

Faber, E.S. & Sah, P. Ca^{2+}-activated K^{+} (BK) channel inactivation contributes to spike broadening during repetitive firing in the rat lateral amygdala. *J. Physiol.* **552**, 483-497 (2003).

Goosens, K.A., Hobin, J.A. & Maren S. Auditory-evoked spike firing in the lateral amygdala and Pavlovian fear conditioning: mnemonic code or fear bias? *Neuron* **40**,1013-1022 (2003).

Han, J.H. *et al.* Neuronal competition and selection during memory formation. *Science* **316**, 457-460 (2007).

Han, J.H. *et al.* Selective erasure of a fear memory. *Science* **323**, 1492-1496 (2009).

Kim, D., Pare, D. & Nair S.S. Mechanisms contributing to the induction and storage of pavlovian fear memories in the lateral amygdala. *Learn. Mem.*(2013).

LeDoux, J.E. Emotional circuits in the brain. *Annu. Rev. Neurosci.* **23**, 155-184 (2000).

Letzkus, J. J. *et al.,* A disinhibitory microcircuit for associative fear learning in the auditory cortex. *Nature* **480**, 331-335 (2011).

Li, G., Nair, S. S. & Quirk, G.J. A biologically realistic network model of acquisition and extinction of conditioned fear associations in lateral amygdala neurons. *J. Neurophysiol.* **101**, 1629-1646 (2009).

McGaugh, J.L. Memory consolidation and the amygdala: a systems perspective. *Trends Neurosci.* **25**, 456-461 (2002).

Pape, H.C. & Paré, D. Plastic synaptic networks of the amygdala for the acquisition, expression, and extinction of conditioned fear. *Physiol. Rev.* **90**, 419-463 (2010).

Power, J.M *et al.* Location and function of the slow afterhyperpolarization channels in the basolateral amygdala. *J. Neurosci*. **31**: 526-537 (2011).

Quirk, G.J., Repa, J.C. & LeDoux, J.E. Fear conditioning enhances short latency auditory responses of lateral amygdala neurons: parallel recordings in the freely behaving rat. *Neuron* **15**, 1029-1039 (1995).

Repa, J.C. *et al.* Two different lateral amygdala cell populations contribute to the initiation and storage of memory. *Nat. Neurosci* **4**, 724-731 (2001).

Rumpel, S. et al. Postsynaptic receptor trafficking underlying a form of associative learning. *Science* **308**, 83–88 (2005).

Viosca, J. *et al.* Enhanced CREB-dependent gene expression increases the excitability of neurons in the basal amygdala and primes the consolidation of contextual and cued fear memory. *Learn Mem* **16**, 193-197 (2009).

Weinberger, N.M. The medial geniculate, not the amygdala, as the root of auditory fear conditioning. *Hear Res* **274**, 61-74 (2011).

Zhou, Y. et al. CREB regulates excitability and the allocation of memory to subsets of neurons in the amygdala. *Nat. Neurosci* **12**, 1438-1443 (2009).

STIMULUS SPECIFICITY

Antunes R, Moita MA (2010) Discriminative auditory fear learning requires both tuned and non-tuned auditory pathways to the amygdala. J Neurosci 30:9782–9787.

Armony JL et al. (1997) Stimulus generalization of fear responses: effects of auditory cortex lesions in a computational model and in rats. Cereb Cortex 7(2):157-65.

Ball JM, Hummos AM, Nair SS (2012) Role of sensory input distribution and intrinsic connectivity in lateral amygdala during auditory fear conditioning: A computational study. Neurosci 224: 249-267.

Collins DR, Pare D (2000) Differential fear conditioning induces reciprocal changes in the sensory responses of lateral amygdala neurons to the CS+ and CS-. Learn Mem 7: 97-103.

Doyere V. *et al. (*2003) Long-term potentiation in freely moving rats reveals asymmetries in thalamic and cortical inputs to the lateral amygdala. Eur J Neurosci 17: 2703–2715.

Doyere, V. *et al. (*2007) Synapse-specific reconsolidation of distinct fear memories in the lateral amygdala. Nat. Neurosci 10:414–416.

Duvel AD, Smith DM, Talk A, Gabriel M (2001) Medial geniculate, amygdalar and cingulate cortical training-induced neuronal activity during discriminative avoidance learning in rabbits with auditory cortical lesions. J Neurosci 21:3271–3281.

Honig WK, Urcuioli PJ (1981) The legacy of Guttman and Kalish (1956): 25 years of research on stimulus generalization. J Exp Anal Behav 36:405–445.

Izumi T et al. (2011) Retrieval of conditioned fear activates the basolateral and intercalated nucleus of amygdala. J. Neurosci Res 89:773–790.

Jarrell TW *et al.* (1987) Involvement of cortical and thalamic auditory regions in retention of differential bradycardiac conditioning to acoustic conditioned stimuli in rabbits. Brain Res 412: 285–294.

Lin HC, Mao SC, Su CL, Gean PW (2010) Alterations of excitatory transmission in the lateral amygdala during expression and extinction of fear memory. Int J Neuropsychopharmacol 13, 335–345

Lissek S, Biggs AL, Rabin SJ, Cornwell BR, Alvarez RP, Pine DS, Grillon C (2008) Generalization of conditioned fear-potentiated startle in humans: experimental validation and clinical relevance. Behav Res Ther 46:678–687.

Lissek S, Rabin S, Heller RE, Lukenbaugh D, Geraci M, Pine DS, Grillon C (2010) Overgeneralization of conditioned fear as a pathogenic marker of panic disorder. Am J Psychiatry 167:47–55.

Shaban H, et al. (2006) Generalization of amygdala LTP and conditioned fear in the absence of presynaptic inhibition. Nat Neurosci 9(8):1028-35.

Mahan AL, Ressler KJ (2012) Fear conditioning, synaptic plasticity and the amygdala: implications for posttraumatic stress disorder. Trends Neurosci 35(1):24-35).

Siberberg G, Markram H (2007) Disynaptic inhibition between neocortical pyramidal cells mediated by Martinotti cells. Neuron 53(5):735-746.

TABLES

Table 1. Plastic cell numbers and types when intra-amygdala plasticity components are disabled.

Model Run (Cells: A-120; B-240; C-440)	Cells receiving both tone & shock		Cells receiving only tone or only shock or neither		Total number of plastic cells
	Plastic A/B/C cells	Non-Plastic A/B/C cells	Plastic A/B/C cells	Non-Plastic A/B/C cells	
Control case	1/80/128	71/57/112	0/0/2	48/103/198	211
No intrinsic plasticity	6/135/239	66/2/1	0/2/4	48/101/196	386
No PN-PN plasticity	0/40/116	72/97/124	0/0/2	48/103/198	158
No IN-PN plasticity	6/132/237	66/5/3	0/2/3	48/101/197	380
No PN-IN plasticity	4/121/210	68/16/30	0/1/2	48/102/198	338
No IN-PN & PN-IN plasticity	9/137/240	63/0/0	0/25/47	48/78/153	458

FIGURES

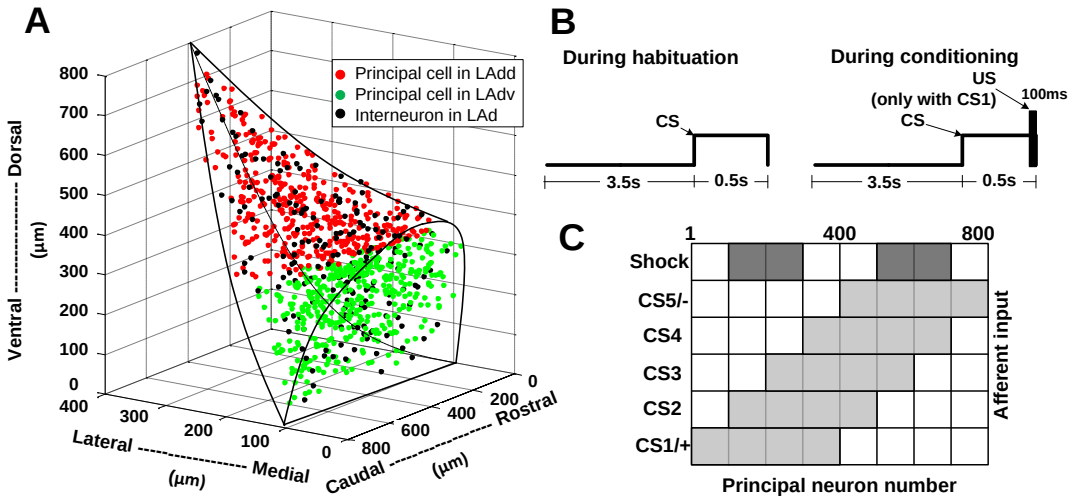

Figure1. **(A)** Schematic of the LAd network model with 800 principal cells (red and green dots, 400 each, represent principal cells in LAdd and LAdv, respectively) and 200 interneurons (black dots). The principal cells in the model were populated randomly in the horn shaped tridimensional structure with dimensions of 800 μm in the rostral-caudal, 800 μm in the ventral-dorsal, and 400 μm in the medial-lateral directions. **(B)** fear conditioning protocol for the model. **(C)** 50% of the principal cells received CS tone and shock inputs. Five different tones, CS1–5, were used, and the cells they targeted are indicated on the X-axis in black. For instance, CS1/+ was paired with the US (shock) during conditioning, and it targeted cells principal cells 1-400. CS2–5 exhibit a graded decline in similarity compared to CS1. CS2-4 were used for testing purposes only. CS5/- was also presented during conditioning with US, but they were not paired, and targeted precisely the 50% of pyramidal cells not targeted by CS1/+. Tone and shock inputs were distributed randomly and independently to 70% of the interneurons.

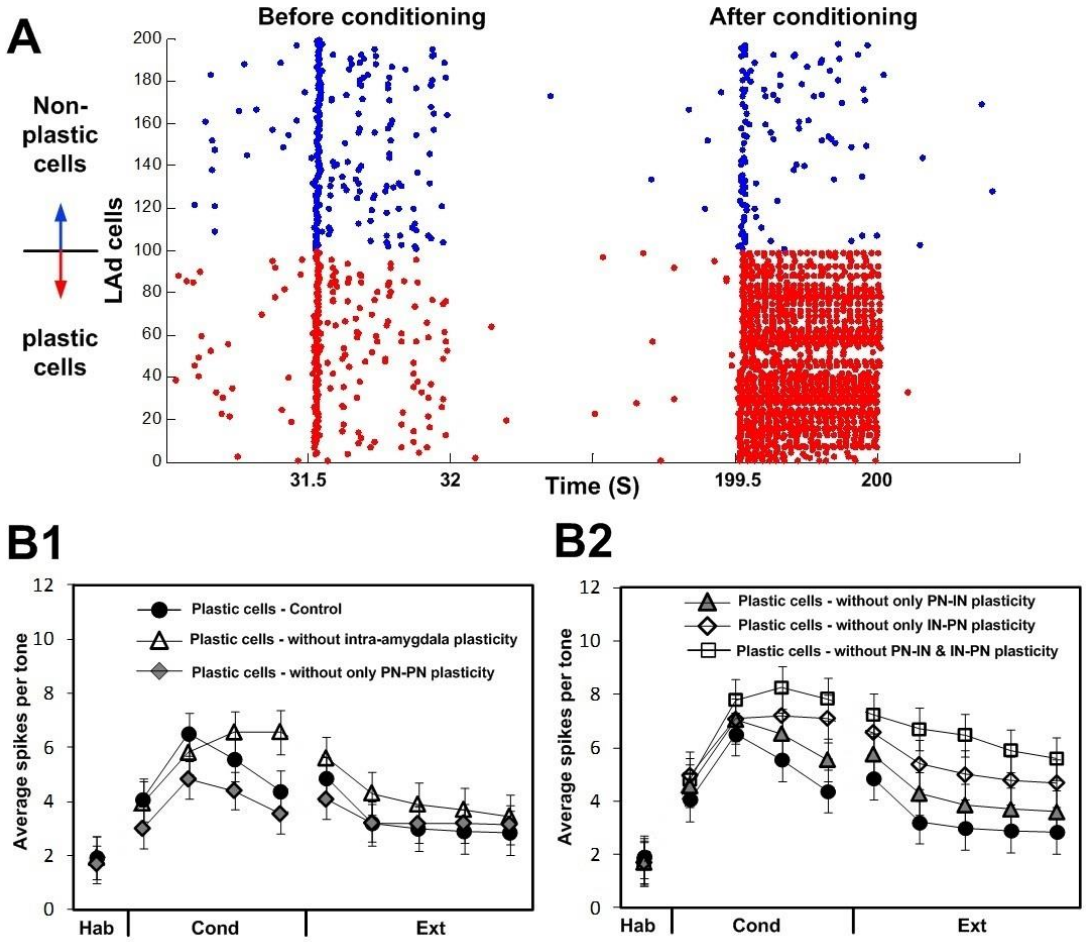

Figure 2. (A) Spike histogram for non-plastic cells (blue) and plastic (red) cells before and after conditioning, one tone trial each. The tone starts at 31.5s and 199.5s, respectively in the tone trials shown. Both plastic and non-plastic cells start with similar CS-evoked responses before conditioning. However, after conditioning, plasticity (due to competition) causes much higher CS-evoked responses in plastic cells, and these in turn suppress non-plastic cell effectively preventing plasticity in their synapses. **(B)** Intra-amygdala plasticity is required to generate competition in LAd. Without all intra-amygdala plasticity (B1, empty triangles), the proportion of plastic cells (386 of 800) and the amplitude of their conditioned tone responses were higher than seen in control case with intra-amygdala plasticity (black circles, N=211/800). But without only PN-PN plasticity (B1, grey diamonds), the proportion of plastic cells (158 of 800) and the amplitude of their conditioned tone responses decrease. Without PN-IN plasticity (B2, grey triangles), the proportion of plastic cells (307 of 800) and the amplitude of their conditioned tone responses were higher than seen in control case with intra-amygdala plasticity. Also without IN-PN plasticity (empty diamonds), the proportion of plastic cells (380 of 800) and the amplitude of their conditioned tone responses increase. In addition, without IN-PN & PN-IN plasticity (empty squares), the proportion of plastic cells (458 of 800) and the amplitude of their conditioned tone responses of 70% CREB+ case were highest.

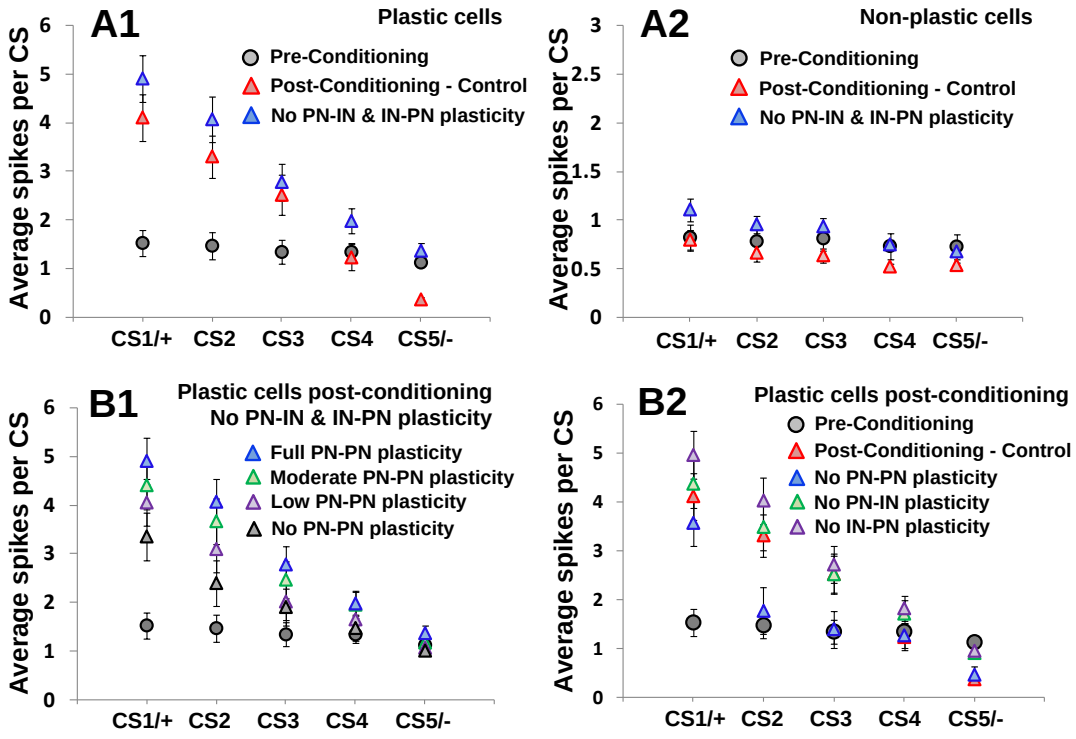

Figure 3. Intrinsic plasticity in LAd modulates stimulus generalization in two different 1000-cell LAd network model for the same stimuli type case. Average responses of plastic **(A1)** and non-plastic **(A2)** pyramidal cells in response to the indicated CS before conditioning (circles) and after conditioning (triangles): **(A1)** At base levels of intrinsic plasticity, no stimulus generalization was observed (red triangles). With impaired plasticity of IN–PN and PN–IN synapses, high generalization was observed with normal plasticity of PN–PN synapses (blue triangles) **(B1)** moderate (green triangles; 2/3 of the scaling factor) and low levels (purple triangle; 1/3 of the scaling factor) of plasticity in PN–PN synapses reduced generalization and sharpened the observed gradient. **(B2)** Each of intrinsic plasticity in LAd modulates stimulus generalization in LAd network. Average tone responses of plastic pyramidal cells to the indicated CS before conditioning (circles) and after conditioning (triangles). At base levels of PN-PN plasticity, no stimulus generalization was observed (blue triangles). With no plasticity of PN–IN (green triangles) or IN-PN (purple triangles) synapses, high generalization was observed.

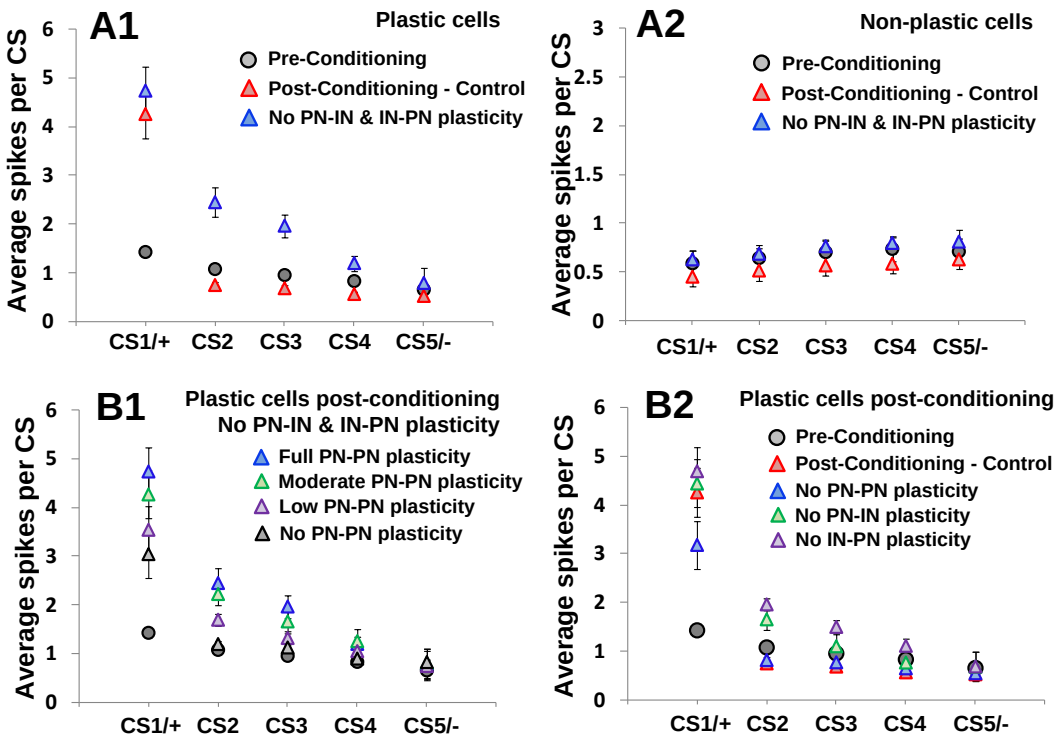

Figure 4. Intrinsic plasticity in LAd modulates stimulus generalization in two 1000-cell LAd network for the distinct stimuli type case. Average responses of plastic **(A1,B1)** and non-plastic **(A2)** pyramidal cells in response to the indicated CS before conditioning (circles) and after conditioning (triangles). **(A1)** At base levels of intrinsic plasticity, no stimulus generalization was observed (red triangles). With impaired plasticity of IN–PN and PN–IN synapses, high generalization was observed with normal plasticity of PN–PN synapses (blue triangles) **(B1)** moderate (green triangles; 2/3 of the scaling factor) and low levels (purple triangles; 1/3 of the scaling factor) of plasticity in PN–PN synapses reduced generalization and sharpened the observed gradient. **(B2)** Each of intrinsic plasticity in LAd modulates stimulus generalization in LAd network. Average tone responses of plastic pyramidal cells to the indicated CS before conditioning (circles) and after conditioning (triangles). At base levels of PN-PN plasticity, no stimulus generalization was observed (blue triangles). With no plasticity of PN–IN (green triangles) or IN-PN (purple triangles) synapses, high generalization was observed.

SUPPLEMENTARY MATERIALS

S1. DETAILS RELATED TO METHODS

S1.1 Mathematical Equations for voltage-dependent ionic currents

The equation for each compartment (soma or dendrite) followed the Hodgkin-Huxley formulations (Byrne and Roberts, 2004) in eqn. S1,

$$C_m dV_s/dt = -g_L(V_s - E_L) - g_c(V_s - V_d) - \sum I_{cur,s}^{int} - \sum I_{cur,s}^{syn} + I_{inj} \quad \text{(S1)}$$

where V_s/V_d are the somatic/dendritic membrane potential (mV), $I_{cur,s}^{int}$ and $I_{cur,s}^{syn}$ are the intrinsic and synaptic currents in the soma, I_{inj} is the electrode current applied to the soma, C_m is the membrane capacitance, g_L is the is the conductance of leak channel, and g_c is the coupling conductance between the soma and the dendrite (similar term added for other dendrites connected to the soma). The intrinsic current $I_{cur,s}^{int}$, was modeled as $I_{cur,s}^{int} = g_{cur} m^p h^q (V_s - E_{cur})$, where g_{cur} is its maximal conductance, *m* its activation variable (with exponent *p*), *h* its inactivation variable (with exponent *q*), and E_{cur} its reversal potential (a similar equation is used for the synaptic current $I_{cur,s}^{syn}$ but without *m* and *h*). The kinetic equation for each of the gating variables *x* (*m* or *h*) takes the form

$$\frac{dx}{dt} = \frac{x_\infty\left(V,[Ca^{2+}]_i\right) - x}{\tau_x(V,[Ca^{2+}]_i)} \quad \text{(S2)}$$

where x_∞ is the steady state gating voltage- and/or Ca^{2+}- dependent gating variable and τ_x is the voltage- and/or Ca^{2+}- dependent time constant. The equation for the dendrite

follows the same format with '*s*' and '*d*' switching positions in eqn. S1. Details related to the model, including types of channels and parameter values are provided in **Tables S1-2**.

S1.2 Mathematical Equations for Synaptic Currents

Excitatory transmission was mediated by AMPA/NMDA receptors, and inhibitory transmission by $GABA_A$ receptors. The corresponding synaptic currents (shown in dendrites below) were modeled by dual exponential functions (Durstewitz et al., 2000), as shown in Eqns. S3-5,

$$I_{AMPA} = \bar{A}w(t)g_{AMPA,max}\frac{\tau_1\tau_2}{\tau_2-\tau_1}[\exp(-t/\tau_2) - \exp(-t/\tau_1)](V - E_{AMPA}) \quad \text{(S3)}$$

$$I_{NMDA} = \bar{A}wg_{NMDA,max}s(V)\frac{\tau_1\tau_2}{\tau_2-\tau_1}[\exp(-t/\tau_2) - \exp(-t/\tau_1)](V - E_{NMDA}) \quad \text{(S4)}$$

$$I_{GABA} = \bar{A}w(t)g_{GABAA,max}\frac{\tau_1\tau_2}{\tau_2-\tau_1}[\exp(-t/\tau_2) - \exp(-t/\tau_1)](V - E_{GABA}) \quad \text{(S5)}$$

where V is the membrane potential (mV) of the compartment (dendrite or soma) where the synapse is located, $w(t)$is the adjustable synaptic weight for AMPA synapses (see section S1.7; w was held fixed for all NMDA synapses); $\bar{A}$ is a normalization constant chosen so $g_{AMPA,max}$ $g_{NMDA,max}$ and $g_{GABA,max}$ assume maximum values of the conductances; τ_1 and τ_2 are the rise and decay time constants respectively. For AMPA receptor channels, τ_1 = 0.25 ms and τ_2 = 7 ms; for NMDA receptor channels, τ_1 = 3.65 ms and τ_2 = 125.0 ms, and for $GABA_A$ receptors, τ_1 = 0.13ms and τ_2 = 3.75 ms. The voltage-dependent variable $s(V)$ which implements the Mg^{2+} block was defined as: $s(V) = [1 + 0.33 \exp(-0.06\ V)]^{-1}$ (Zador et al., 1990). The maximal conductances were chosen as: $g_{AMPA,max}$= 1 nS, $g_{NMDA,max}$ = 0.5 nS and $g_{GABA,max}$= 0.6 nS. Synaptic reversal potentials were set as follows: $E_{AMPA} = E_{NMDA}$ = 0 mV and E_{GABAA} = -75 mV (Durstewitz

et al., 2000).

S1.3 Calcium dynamics and Hebbian learning

Intracellular calcium was regulated by a simple first-order differential equation shown in Eqn. S6 (Warman et al., 1994),

$$\frac{d[Ca^{2+}]_i}{dt} = -f\frac{I'_{Ca}}{zFA} + \frac{[Ca^{2+}]_{rest} - [Ca^{2+}]_i}{\tau_{Ca}} \quad \text{(S6)}$$

where f is the fraction of the Ca^{2+} influx (f =0.024), $V = wA$ with w being the shell thickness (1μm) and A the dendritic/soma surface area, z=2 is the valance of the Ca^{2+} ion, F is the Faraday constant, and τ_{Ca} is the time constant associated with Ca^{2+} removal. The resting Ca^{2+} concentration was $[Ca^{2+}]_{rest}$ =50 nmol/l (Durstewitz et al., 2000).

The biophysical Hebbian rule was implemented by adjusting the synaptic weight w(t) in synaptic conductances (Eqns. S3 and S5) using equation S7,

$$\Delta w_j = \eta([Ca^{2+}]_j)\Delta t(\lambda_1\Omega([Ca^{2+}]_j) - \lambda_2\omega_j) \quad \text{(S7)}$$

where η is the Ca^{2+}-dependent learning rate and Ω is a Ca^{2+}-dependent function with two thresholds (θ_d and θ_p; $\theta_d \leq \theta_p$) (for details see Li et al., 2009); λ_1 and λ_2 represent scaling and decay factors respectively; the local calcium level at synapse j is denoted by $[Ca^{2+}]_j$ and Δt is the simulation time step. With this learning rule, the synaptic weight decreases when $\theta_d < [Ca^{2+}]_j < \theta_p$, and increases when $[Ca^{2+}]_j > \theta_p$, with modulation by the decay term $\lambda_2 w_j$.

Concentration of calcium pools: The concentration of the calcium pool at synapse j followed the dynamics in Eq. S6, with f_j= 0.024 (Warman et al. 1994), τ_j = 50 ms

(Shouval et al. 2002b), *V* is the volume of a spine head with a diameter of 2 μm (Kitajima and Hara 1997). All the synaptic weights were constrained by upper (W_{max}) and lower (W_{min}) limits (Li et al., 2009). Maximum (f_{max}) and minimum (f_{min}) folds were specified for each modifiable synapse so that $W_{max}= f_{max}*w(0)$ and $W_{min} = f_{min}*w(0)$.

Excitatory synapses onto principal cells. For tone-principal cell, and principal cell-principal cell connections, the calcium influx which determines learning was calculated by using the NMDA current, $I_{Ca}^{N} = P_0 w^{-1} G_{NMDA}(V - E_{Ca})$ (Shouval et al., 2002b), where $G_{NMDA} = \bar{A} w(t) g_{NMDA,max} s(V) \frac{\tau_1 \tau_2}{\tau_2 - \tau_1} \left[\exp\left(-\frac{t}{\tau_2}\right) - \exp\left(-\frac{t}{\tau_1}\right)\right]$ from eqn. S4, the term w^{-1} ensures that it is calculated per synapse, and $P_0 = 0.015$.

Excitatory synapses onto interneurons. For tone-interneuron, and principal cell-interneuron connections, the calcium influx (used for learning) at the excitatory synapses on interneurons occurs through both NMDA and AMPA receptors (details in Li et al., 2009). In addition to calcium influx through NMDA current I_{Ca}^{N}, the calcium influx through AMPA receptors was calculated as $I_{Ca}^{A} = P_0 w^{-1}(0) G_{AMPA}(V - E_{Ca})$ where G_{AMPA} is the AMPA conductance in eqn. S4 (as described in the earlier para for G_{NMDA}), and $w(0)$ is the initial AMPA synaptic weight, $P_0 = 0.001$. The Ca^{2+} current through the AMPA/NMDA receptors was separated from the total AMPA/NMDA current in this manner and used for implementation of the learning rule (Kitajima and Hara, 1997; Shouval et al., 2002a; Li et al., 2009).

Inhibitory synapses onto principal cells. Several different mechanisms have been reported for potentiation at GABAergic synapses in other brain regions (e.g., Gaiarsa et al., 2002). A rise in postsynaptic intracellular Ca^{2+} concentration seems to be required in most mechanisms to trigger long-term plasticity. In the neonatal rat hippocampus, potentiation could be induced by Ca^{2+} influx through the voltage-dependent Ca^{2+} channels (VDCCs), whereas in the cortex and cerebellum, this process requires Ca^{2+} release from postsynaptic internal stores that is dependent on stimulation of GABA receptors (Gaiarsa et al., 2002). Thus, both presynaptic activity (GABA receptor stimulation or interneuron firing) and postsynaptic activity (activation of VDCCs by membrane depolarization) contribute to the potentiation of GABA synapses. The process from GABA receptor stimulation to internal Ca^{2+} release involves activating a cascade of complex intracellular reactions (Komatsu 1996). Such a complex process can be simplified by assuming that the Ca^{2+} release is proportional to the stimulation frequency or $GABA_A$ conductance (Li et al., 2009). Hence we modeled this simplified process by considering Ca^{2+} release from the internal stores into a separate Ca^{2+} pool, using an equation similar to that for the AMPA/NMDA case cited above:

$I_{Ca}^{G} = P_0 w^{-1}(t) G_{GABA}(V - E_{Ca})$ with P_0 = 0.01, and G_{GABA} as the $GABA_A$ conductance in Eq. S5 (as described earlier for G_{NMDA}). Note that the current I_{Ca}^{G}, models the dependence of Ca^{2+} release on $GABA_A$ stimulation frequency but not Ca^{2+} influx through the $GABA_A$ channel. The current I_{Ca}^{G}, together with post-synaptic voltage dependent calcium current (I_{Ca}), contributed towards plasticity. Hence, $I'_{Ca} = I_{Ca}^{G} + 0.01 I_{Ca}$ was used to calculate calcium influx for learning at such synapses. (Li et al., 2009)

S1.4 Short-term presynaptic plasticity

Short term plasticity was implemented as follows: (Varela et. al 1997): For facilitation, the factor F was calculated using the equation: $\tau_F * \frac{dF}{dt} = 1 - F$ and was constrained to be ≥ 1. After each stimulus, F was multiplied by a constant, f (≥ 1) representing the amount of facilitation per pre-synaptic action potential, and updated as $F \rightarrow F * f$. Between stimuli, *F* recovered exponentially back toward 1. A similar scheme was used to calculate the factor D for depression: $\tau_D * \frac{dD}{dt} = 1 - D$ and *D* constrained to be ≤ 1. After each stimulus, *D* was multiplied by a constant *d* (≤ 1) representing the amount of depression per pre-synaptic action potential, and updated as $D \rightarrow D * d$. Between stimuli, *D* recovered exponentially back toward 1. We modeled depression using two factors d_1 and d_2 with $d1$ being fast and d_2 being slow subtypes, and $d = d1 * d2$. The parameters for the short-term plasticity models, the initial weights and other learning parameters for the synapses are listed in **Table S4**.

S.2 ADDITIONAL RESULTS

S2.1 50% of tone and shock input distribution

To test specificity to CS, 50% of LAd neurons have CS1/+ input (Fig 1). Although 50% of LAd neurons and interneurons have tone and shock input, it can make the same tone response of Repa et al. (2001)

S2.1 Additional specificity test

We tested specificity in LAd with blockage of intra-LA plasticity (Fig S2) or blockage of only di-synaptic inhibitory plasticity in PN-IN and IN-PN synapses (Fig S3). And also the model took the recall test which is set to habituation levels during post-conditioning test (Fig S4 and Fig S5).

S2.2 Supplementary figures and tables

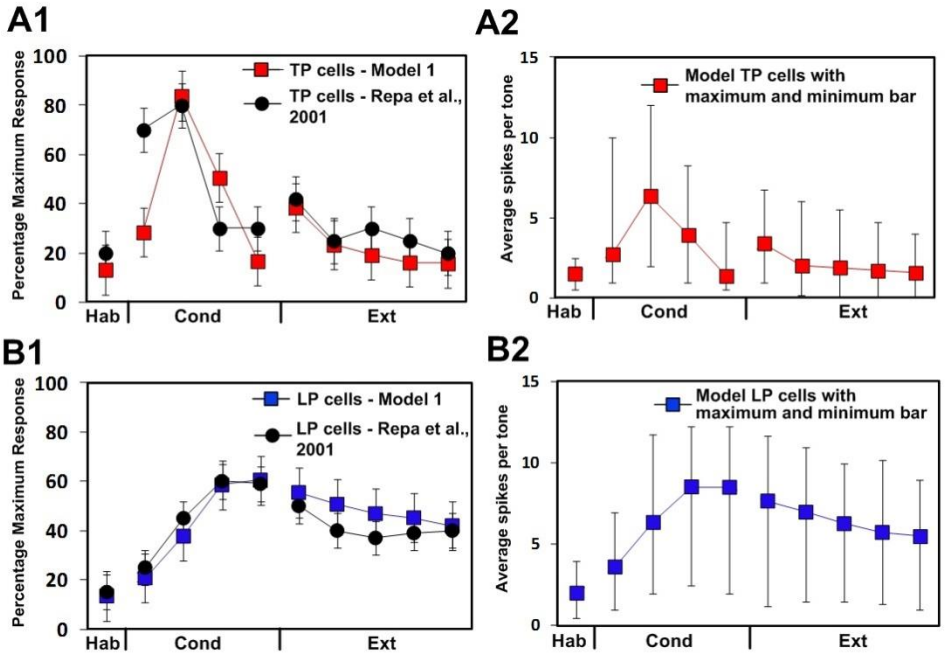

Figure S1. Tone responses of LAd cells in Model1 during the different phases of the behavioral protocol. (**A**) Model (red, N=198/800) and experimental (black; N=24/100; from Repa et al., 2001) tone responses of plastic cells. (**B**) Vertical bars on each block indicate maximum response (upper) and minimum response (lower).

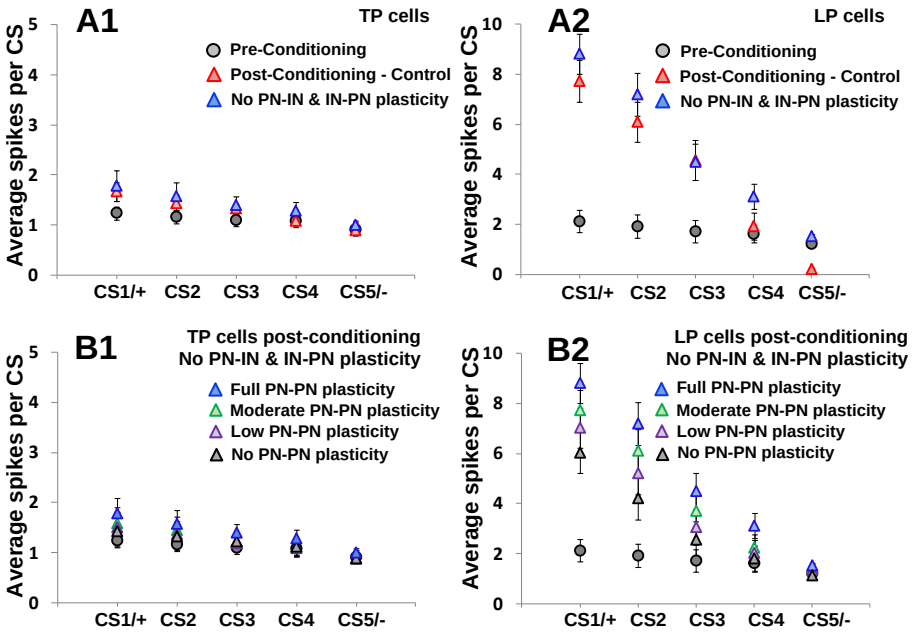

Figure S2. Intrinsic plasticity in LAd modulates stimulus generalization with *same stimuli type* in two different 1000-cell LAd network model1. Average responses of TP **(A)** and LP **(B)** cells in response to the indicated CS before conditioning (circles) and after conditioning (triangles): **(1)** At base levels of intrinsic plasticity, no stimulus generalization was observed (red triangles). With impaired plasticity of IN–PN and PN–IN synapses, high generalization was observed with normal plasticity of PN–PN synapses (blue triangles) **(2)** moderate (green triangles; 2/3 of the scaling factor) and low levels (purple triangle; 1/3 of the scaling factor) of plasticity in PN–PN synapses reduced generalization and sharpened the observed gradient.

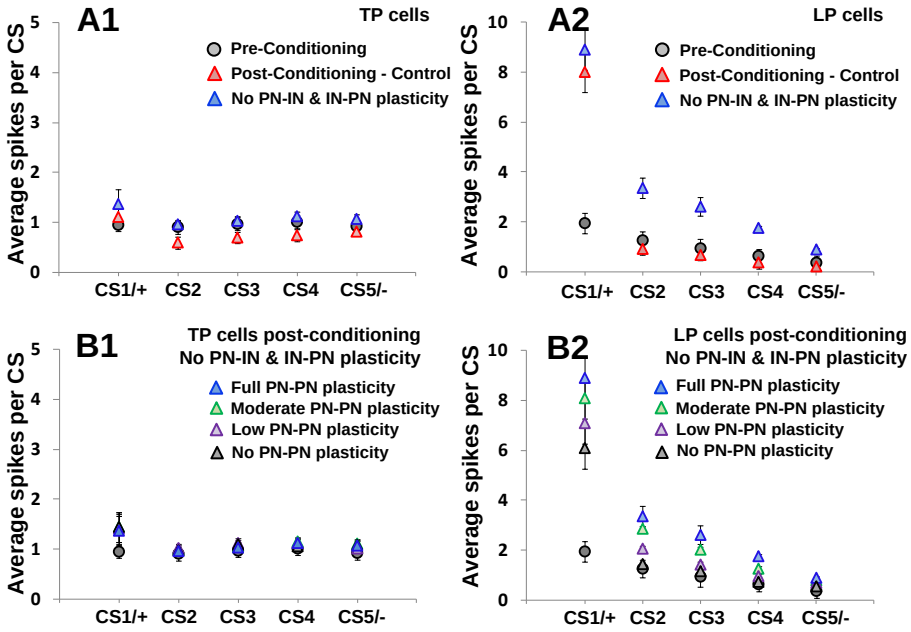

Figure S3. Intrinsic plasticity in LAd modulates stimulus generalization with *distinct stimuli* in two 1000-cell LAd networks – Model 1 and Model 2. Average responses of TP **(A)** and LP **(B)** cells in response to the indicated CS before conditioning (circles) and after conditioning (triangles). **(1)** At base levels of intrinsic plasticity, no stimulus generalization was observed (red triangles). With impaired plasticity of IN–PN and PN–IN synapses, high generalization was observed with normal plasticity of PN–PN synapses (blue triangles) **(2)** moderate (green triangles; 2/3 of the scaling factor) and low levels (purple triangles; 1/3 of the scaling factor) of plasticity in PN–PN synapses reduced generalization and sharpened the observed gradient.

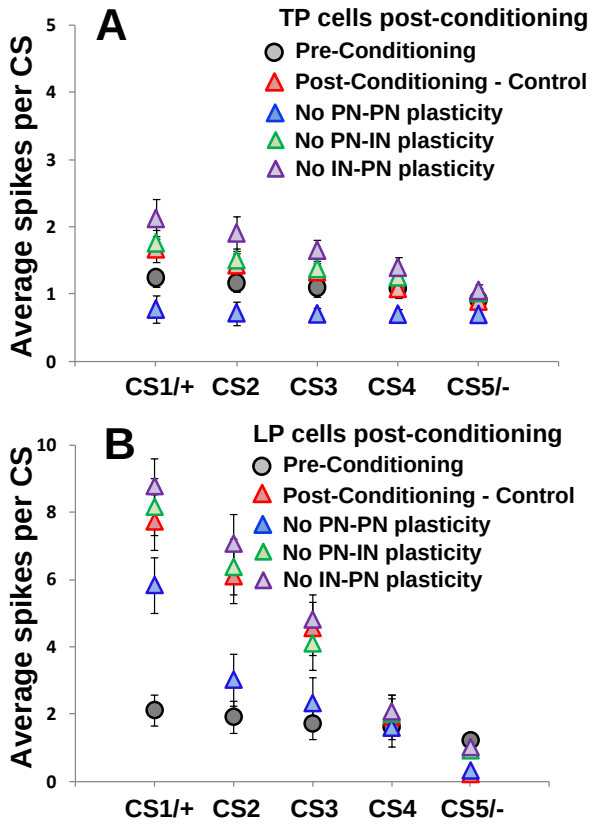

Figure S4. Each of intrinsic plasticity in LAd modulates stimulus generalization with *same stimuli type* in two types of 1000-cell LAd network. Average tone responses of TP **(A)** and LP **(B)** cells to the indicated CS before conditioning (circles) and after conditioning (triangles). At base levels of PN-PN plasticity, no stimulus generalization was observed (blue triangles). With no plasticity of PN–IN (green triangles) or IN-PN (purple triangles) synapses, high generalization was observed.

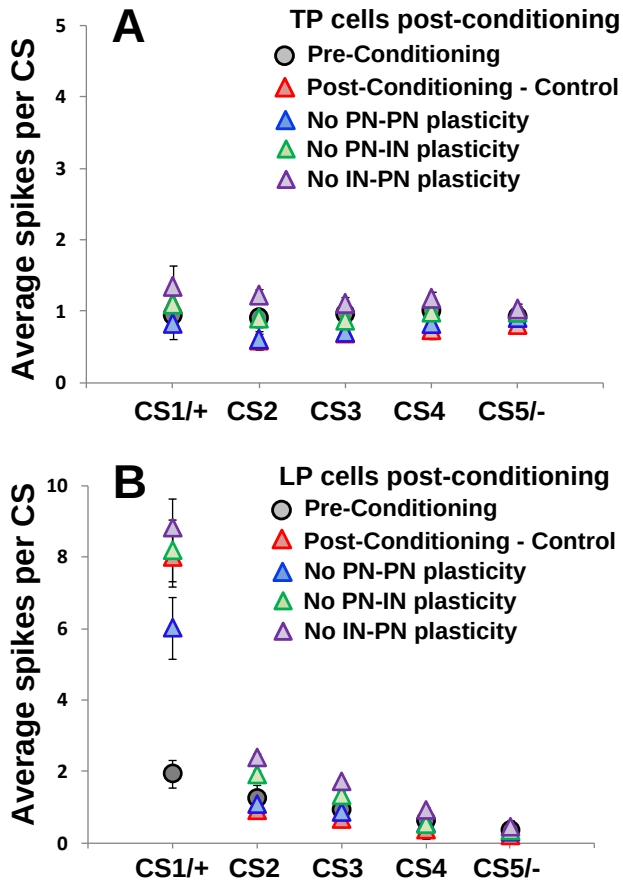

Figure S5. Each of intrinsic plasticity in LAd modulates stimulus generalization with *distinct stimuli* in two types of 1000-cell LAd network. Average tone responses of TP **(A)** and LP **(B)** cells to the indicated CS before conditioning (circles) and after conditioning (triangles). At base levels of PN-PN plasticity, no stimulus generalization was observed (blue triangles). With no plasticity of PN–IN (green triangles) or IN-PN (purple triangles) synapses, high generalization was observed.

S3. STUDIES WITH MODEL 2.

We used another version of a 1000-cell LAd model (Model 2) to test for the robustness of the reported findings. Model 2 differed from model 1 in that it had different intra-amygdala initial weights (for numbers and details see Kim et al., 2013) which resulted in a drop in inhibitory transmission (IN-PN synapses depressed) after conditioning, as reported in some experiments. Interestingly, post-conditioning the synaptic weights in both the models were of similar magnitudes. We simulated the model exactly as we did for model 1.

S3.1. CASE I RESULTS

CASE I-1. After training with CS1/+ and CS5/-, the model was tested with the five CSs for Case I (same stimuli type) and exhibited the responses shown in Fig. S7. As in the case of model 1, the stimulus generalization gradient expanded to include stimuli that were more similar to CS+. Motivated by behavioral experiments that reported differences in stimulus generalization gradients between healthy subjects and those exhibiting anxiety disorders (Lissek et al., 2010), we explored the role of intrinsic plasticity in stimulus generalization, and found that the decrease in CS-evoked responses paralleled the impairment in PN-PN plasticity (Fig. S7).

CASE I-2. In model2, as expected, disabling PN-IN synaptic plasticity again eliminated stimulus generalization as in the case of model 1. However, the responses were different from those of model 1 in the other cases. Although no PN-PN synaptic plasticity

decreased CS1/+ responses by 20%, CS2-responses by 34% and CS3-responses by 43%, it didn't completely eliminate the stimulus generalization in CS2 and CS3 responses (Fig.S8). Because IN-PN synapses have LTD during conditioning, CSs-evoked responses still showed a small potentiation without PN-PN plasticity. Disabling IN-PN synaptic plasticity decreased all CS-evoked responses by 9% unlike in model 1, and with no PN-IN plasticity, all CSs-evoked responses increased by 25% (Fig.S8).

CASE I-3.

Because there are two types of plastic cells, TP and LP cells, we checked how intrinsic plasticity modulated stimulus generalization in two different types of plastic cells. After fear conditioning, response of TP cells to CS turned back to habituation level, while response of LP cells to CS kept higher level than habituation level (Repa et al. 2001). So intrinsic plasticity didn't affect much on stimulus generalization in TP cells (Figure3 C1, D1), but LP cells showed almost same results as plastic cells in CASE1-1 (Fig. 7 C2, D2).

S3.2. CASE II RESULTS

CASE II-1. To explore the role of intrinsic plasticity within LAd on the CS-evoked responses with distinct stimuli (e.g., auditory and olfactory; Case II), we assumed that CS2-CS4 used different synapses to project to the same set of cells, i.e., same configuration as in Fig. 1C but with different afferent synapses. As shown in Fig. 8A, the specificity to the trained stimulus CS1/+ was maintained very well, with responses evoked by CS2-CS5 being at habituation levels. Fig. 8B shows that the decrease in CS-evoked responses paralleled the impairment in PN-PN plasticity.

CASE II-2. To explore the effect of plasticity in each intrinsic connection (PN-PN, PN-IN and IN-PN) individually on the CS-evoked responses with distinct stimuli type, similar to Case I-2, we disabled plasticity in each connection prior to conditioning. After training with CS1/+ and CS5/-, the model was tested with the five CSs and exhibited the responses shown in Fig. 8 for both the models. In model 2, disabling PN-PN synaptic plasticity decreased CS1/+ responses by 20% and other CSs-evoked responses were not significantly different from control (t-test, $p>0.05$). Disabling IN-PN synaptic plasticity decreased all CS-evoked responses by 6% unlike for model 1. With no PN-IN synaptic plasticity, all CSs-evoked responses increased by 70% and all CSs evoked response potentiated compared to habituation levels (t-test, $p<0.05$).

CASE II-3.

Because there are two types of plastic cells, TP and LP cells, we checked how intrinsic plasticity modulated stimulus generalization in two different types of plastic cells. After fear conditioning, response of TP cells to CS turned back to habituation level, while response of LP cells to CS kept higher level than habituation level (Repa et al. 2001). So intrinsic plasticity didn't affect much on stimulus generalization in TP cells (Fig.8 C1, D1), but LP cells showed almost same results as plastic cells in CASE2-1 (Figure 8 C2, D2).

All other observations found in model 1 were reproduced in model 2 except for one. Plasticity in IN-PN synapse has a different role depending on type of model. In model1, because IN-PN synapses have LTP during conditioning, it has significant role to suppress stimuli generalization, even more than plasticity in PN-IN synapse, whereas it has similar role with plasticity in PN-PN synapse due to LTD in IN-PN synapse.

In model2, results of recall test are similar to model1 except IN-PN recall. PN-PN recall test didn't decrease response of plastic cells to CS1/+ much (by 9%, t-test $p>0.05$) while it significantly decrease response to CS2 and CS3 (27% and 23%, t-test both $p<0.05$). PN-IN recall test increased response of plastic cells to CSs by 13% while IN-PN recall decrease response of plastic cells to CSs by 6%. Therefore, stimulus generalization decrease at PN-PN and IN-PN recall test and specificity decrease at PN-IN recall test (Figure S11).

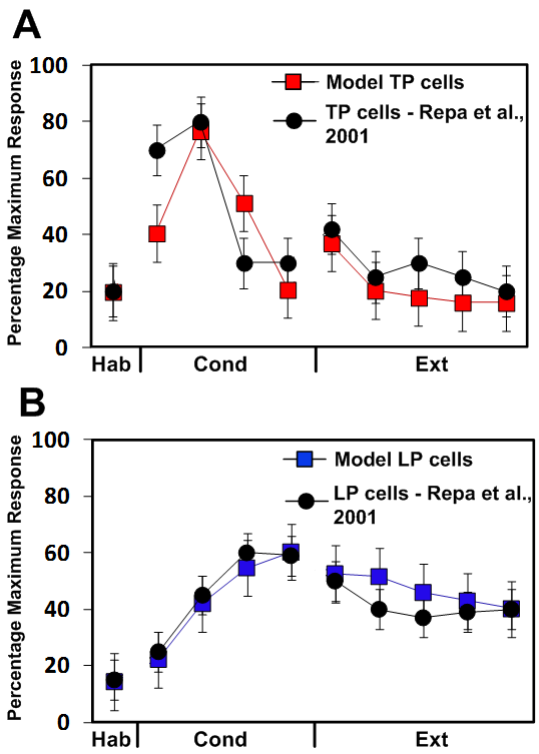

Figure S6. Tone responses of LAd cells in model 2 during the different phases of the behavioral protocol. (**A**) Model (red, N=98/800) and experimental (black; N=12/100; from Repa et al., 2001) tone responses of TP cells show a sudden increase during early conditioning, and then drop to habituation levels during late conditioning. (**B**) Model (blue; N=90/800) and experimental (black; N=12/100) tone responses of LP cells increase gradually with conditioning and persist during extinction.

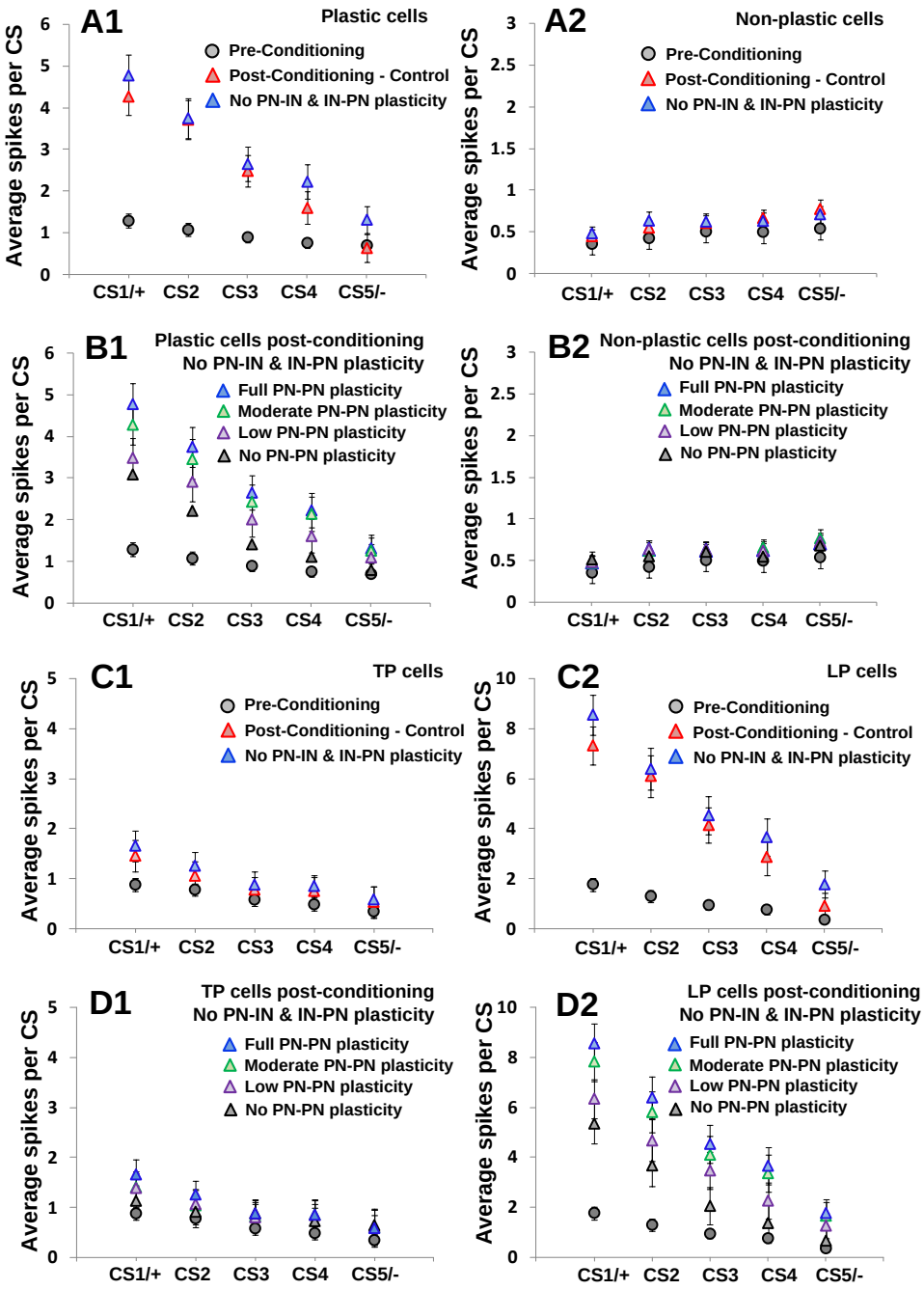

Figure S7. Intrinsic plasticity in LAd modulates stimulus generalization with *same stimuli type* in two different 1000-cell LAd network model. Average responses of plastic **(A),** non-plastic **(B)** pyramidal cells, TP **(C)** and LP cells **(D)** in response to the indicated CS before conditioning (circles) and after conditioning (triangles): **(1)** At base levels of intrinsic plasticity, no stimulus generalization was observed (red triangles). With impaired plasticity of IN–PN and PN–IN synapses, high generalization was observed with normal plasticity of PN–PN synapses (blue triangles) **(2)** moderate (green triangles; 2/3 of the scaling factor) and low levels (purple triangle; 1/3 of the scaling factor) of plasticity in PN–PN synapses reduced generalization and sharpened the observed gradient.

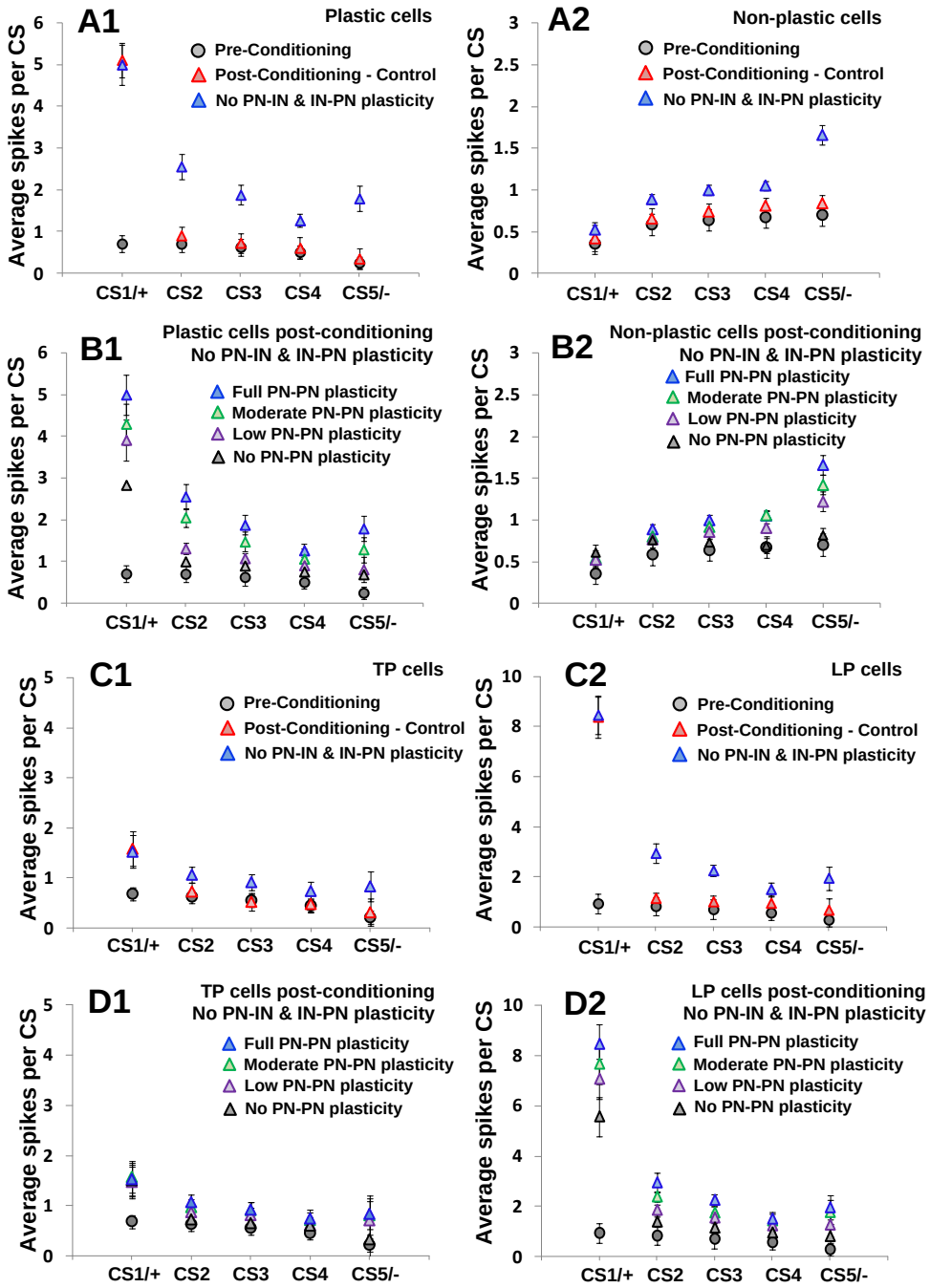

Figure S8. Intrinsic plasticity in LAd modulates stimulus generalization with *distinct stimuli* in two 1000-cell LAd network. Average responses of plastic **(A),** non-plastic **(B)** pyramidal cells, TP **(C)** and LP **(D)** cells in response to the indicated CS before conditioning (circles) and after conditioning (triangles). **(1)** At base levels of intrinsic plasticity, no stimulus generalization was observed (red triangles). With impaired plasticity of IN–PN and PN–IN synapses, high generalization was observed with normal plasticity of PN–PN synapses (blue triangles) **(2)** moderate (green triangles; 2/3 of the scaling factor) and low levels (purple triangles; 1/3 of the scaling factor) of plasticity in PN–PN synapses reduced generalization and sharpened the observed gradient.

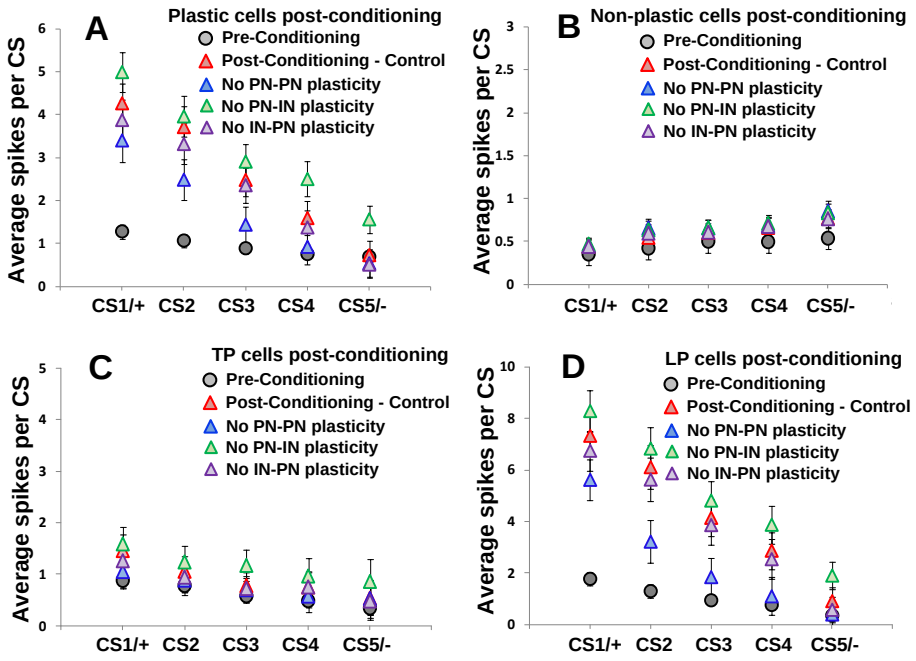

Figure S9. Each of intrinsic plasticity in LAd modulates stimulus generalization with *same stimuli type* in two types of 1000-cell LAd networks. Average tone responses of plastic **(A),** non-plastic **(B),** TP **(C)** and LP **(D)** pyramidal cells to the indicated CS before conditioning (circles) and after conditioning (triangles). At base levels of PN-PN plasticity, no stimulus generalization was observed (blue triangles). With no plasticity of PN–IN (green triangles) or IN-PN (purple triangles) synapses, high generalization was observed.

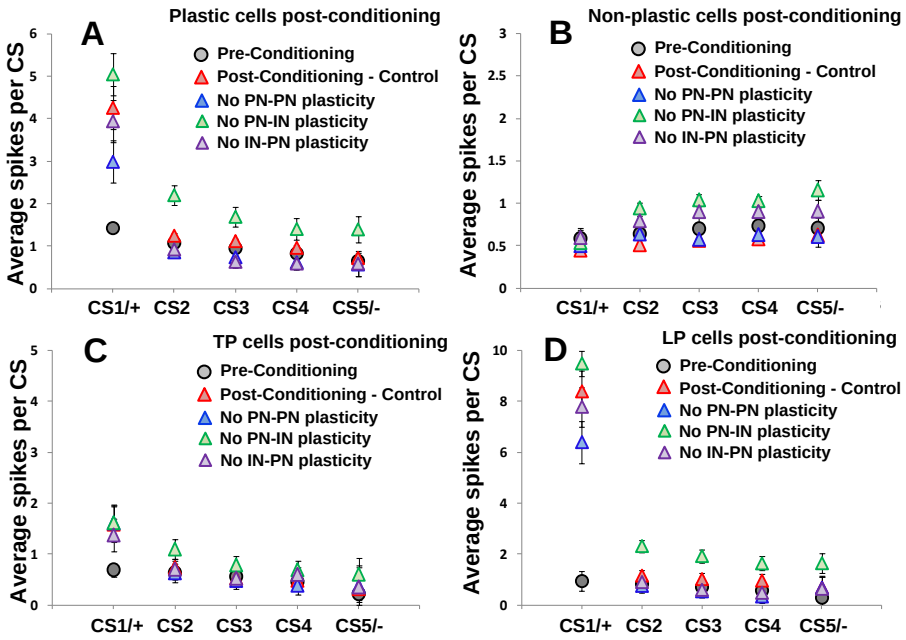

Figure S10. Each of intrinsic plasticity in LAd modulates stimulus generalization with *distinct stimuli* in two types of 1000-cell LAd network. Average tone responses of plastic **(A),** non-plastic **(B),** TP **(C)** and LP **(D)** pyramidal cells to the indicated CS before conditioning (circles) and after conditioning (triangles). At base levels of PN-PN plasticity, no stimulus generalization was observed (blue triangles). With no plasticity of PN–IN (green triangles) or IN-PN (purple triangles) synapses, high generalization was observed.

Model_1

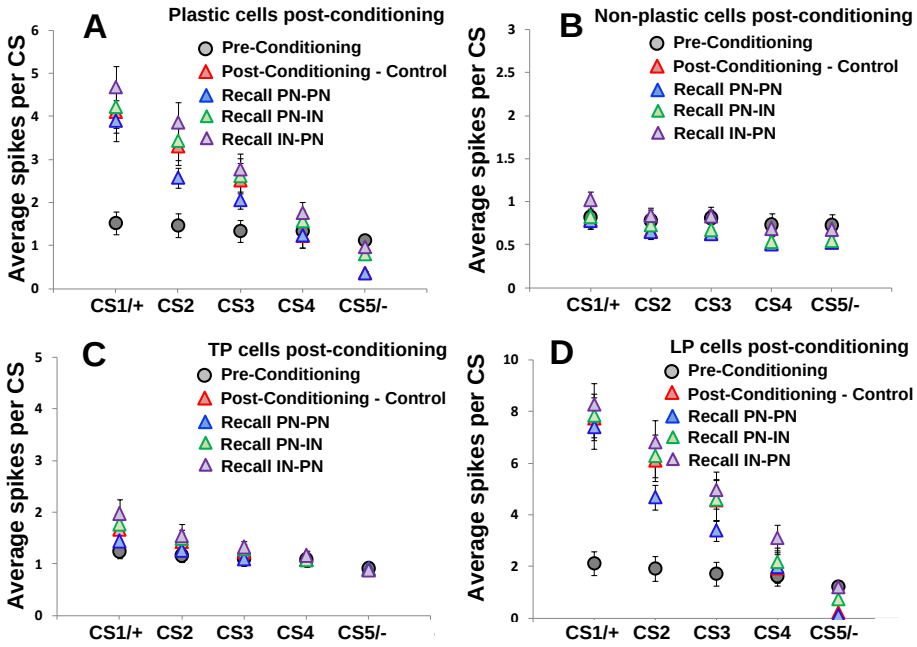

Model_2

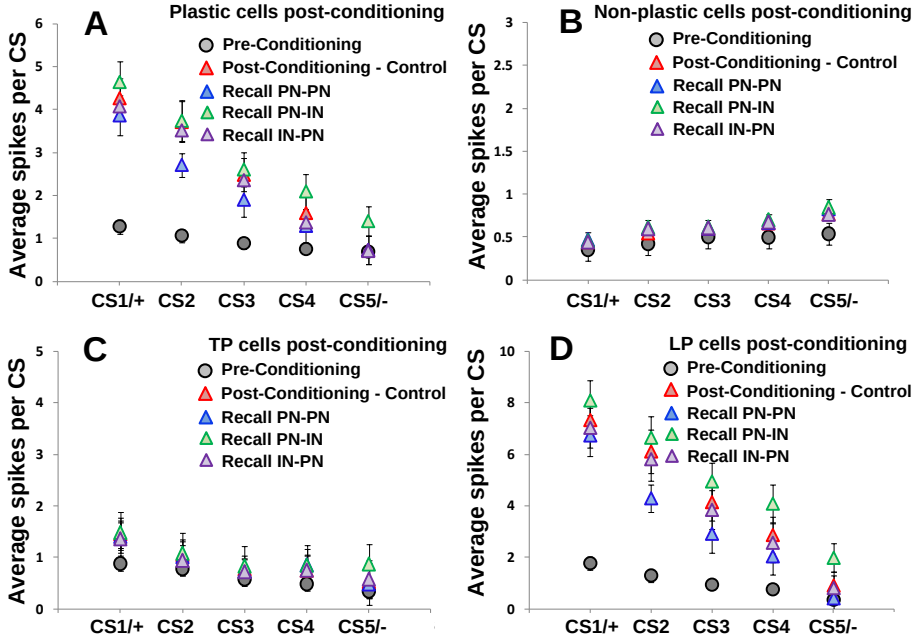

Figure S11. Recall test of intrinsic plasticity in LAd to habituation level with *same stimuli type* in two types of 1000-cell LAd networks, Model 1 and Model 2. Average tone responses of plastic **(A),** non-plastic **(B),** TP **(C)** and LP **(D)** pyramidal cells to the indicated CS before conditioning (circles) and after conditioning (triangles). At base levels of PN-PN plasticity, no stimulus generalization was observed (blue triangles). With no plasticity of PN–IN (green triangles) or IN-PN (purple triangles) synapses, high generalization was observed.

Model_1

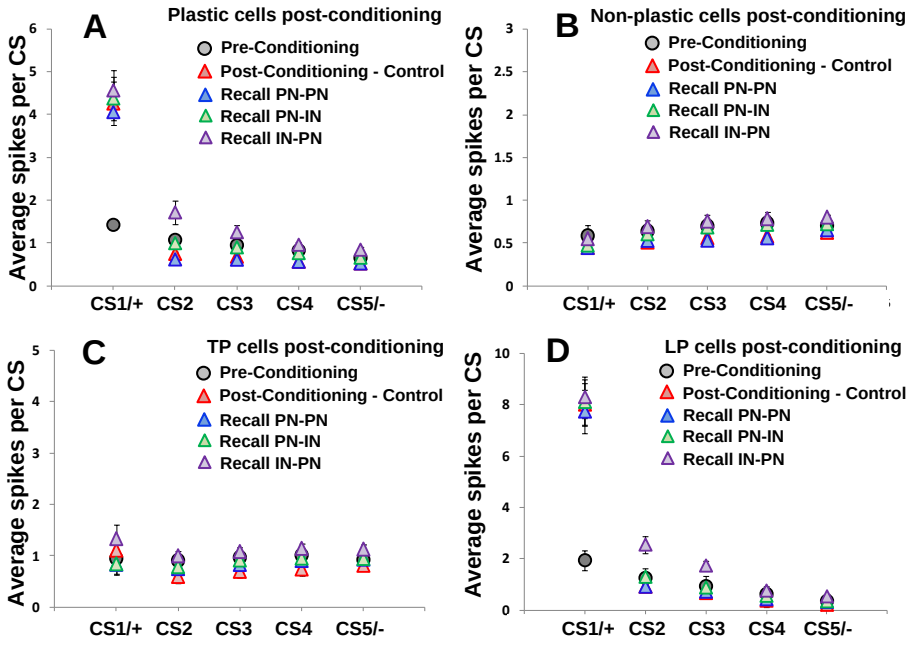

Model_2

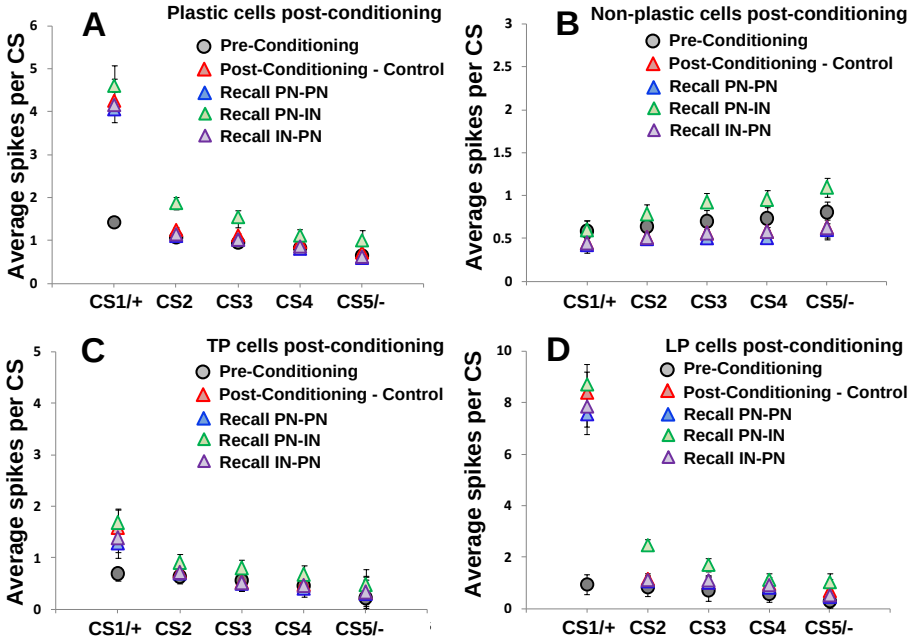

Figure S12. Recall test of intrinsic plasticity in LAd to habituation level with *distinct stimuli* in two types of 1000-cell LAd networks, Model 1 and Model 2. Average tone responses of plastic **(A),** non-plastic **(B),** TP **(C)** and LP **(D)** pyramidal cells to the indicated CS before conditioning (circles) and after conditioning (triangles). At base levels of PN-PN plasticity, no stimulus generalization was observed (blue triangles). With no plasticity of PN–IN (green triangles) or IN-PN (purple triangles) synapses, high generalization was observed.

Tables

Table S1. Average synaptic weights* pre- and post-conditioning for Model 2.

Models 2	Tone-PN		Tone-IN		PN-PN	PN-IN	IN-PN
	Thalamic pathway	Cortical pathway	Thalamic pathway	Cortical pathway			
Pre-conditioning	5.5	6.5	4.5	4.5	0.7	1	22
Post-conditioning	9	14	13	6	2.5	2	18

* with 50 randomly selected principal cells

Table S2. Variations in maximal conductances to model neuromodulator effects.

NM	Receptor	Channel	Low level of NM (during trials 2-10 of conditioning)	High level of NM (during trials 11-16 of conditioning and trails 1-4 of extinction)	Highest level of NM (during shock)
Dopamine	D_1Rs (Low affinity)	I_{Kdr}	-	Decrease *gKdr* by 10%	Decrease *gKdr* by 20%
		AP threshold	-	Change activation of Na^+ channel by -0.5mV	Change activation of Na^+ channel by -1.5mV
		NMDA (pyr-pyr)	-	Decrease *gNMDA* by 5% Decrease *gNMDA* by 20%	Decrease *gNMDA* by 20% Decrease *gNMDA* by 30%
		GABA (interneuron-pyr)	-	Increase *gGABA* by 40% Increase *gGABA* by 30%	Increase *gGABA* by 60% Increase *gGABA* by 40%
	D_2Rs (High affinity)	Input Resistance	Decrease *gleak* by 5%	Decrease *gleak* by 10%	Decrease *gleak* by 20%
		GABA (interneuron-pyr)	Decrease *gGABA* by 20%	Decrease *gGABA* by 20%	Decrease *gGABA*,by 30%
Norepinephrine	NE-α (High affinity)	NMDA (thalamic input to interneuron)	Increase *gNMDA* by 5%	Increase *gNMDA* by 10%	Increase *gNMDA* by 30%
		NMDA (Cortical input to principal cells)	Decrease *gNMDA* by 10%	Decrease *gNMDA* by 30%	Decrease *gNMDA* by 30%
		NMDA (Thalamic input to principal cells)	Decrease *gNMDA* by 5%	Decrease *gNMDA* by 10%	Decrease *gNMDA* by 20%
	NE-β (Low affinity)	I_{sAHP}		Reduce *gK,sAHP* by 20%	Reduce *gK,sAHP* by 30%
		NMDA (Cortical input to principal cells)	-	Increase *gNMDA* by 20%	Increase *gNMDA* by 50%
		NMDA (Cortical input to interneurons)	-	Decrease *gNMDA* by 20%	Decrease *gNMDA* by 30%

Table S3. Model synaptic strengths and learning parameters.

Long-term postsynaptic plasticity						
Connection	**Initial Weight**	**f_max** (f_min=0.8 for all)	**Learning factor**		**Ca^{2+} Threshold**	
			scaling	**Decay**	**Low**	**High**
Tone to Pyr (Thalamic)	6 5.5	3.5 3	80 100	0.04	0.30 0.30	0.40 0.45
Tone to Pyr (Cortical)	5.5 6.5	3.5	10	0.04	0.30 0.30	0.40 0.45
Tone to Inter (Thalamic)	3.8 4.5	4	5 4.5	0.01	0.45	0.5
Tone to Inter (Cortical)	3.5 4.5	4	20	0.01	0.45	0.5
PyrD to PyrD	1 0.7	4	80	0.03 0.04	0.3 0.25	0.55 0.5
PyrD to PyrV	1 0.7	4	10	0.03	0.3 0.25	0.55 0.5
PyrV to PyrD	1 0.7	4	80	0.03 0.04	0.3 0.25	0.55 0.5
PyrV to PyrV	1 0.7	4	10	0.03	0.3 0.25	0.55 0.5
InterD to PyrD	4.5 22	4	4	0.01 0.04	0.47 0.6	0.52 0.7
InterD to PyrV	4.5 22	4	2	0.01 0.04	0.47 0.6	0.52 0.7
InterV to PyrD	4.5 22	4	4	0.01 0.04	0.47 0.6	0.52 0.7
InterV to PyrV	4.5 22	4	2	0.01 0.04	0.47 0.6	0.52 0.7
PyrD to InterD	1.5 1.0	3	3	0.01	0.4 0.3	0.45 0.35
PyrD to InterV	1.5 1.0	2	2	0.01	0.4 0.3	0.45 0.35
PyrV to InterD	1.5 1.0	3	3	0.01	0.4 0.3	0.45 0.35
PyrV to InterV	1.5 1.0	3	2	0.01	0.4 0.3	0.45 0.35

Short-term presynaptic plasticity				
Connection	**Short-term dynamics**	**Parameters**		
		D (Maximum limit)	**d_1/d_2**	**τ_{D1} / τ_{D2} (ms)**
Inter-Pyr	depression	0.6	0.9 / 0.95	40 / 70
Pyr-Pyr	depression	0.5	0.9 / 0.95	40 / 70
Pyr-Inter	depression	0.7	0.9 / 0.95	40 / 70

- Shock synapses do not potentiate (weight =10 for synapses onto both principal cells and interneurons, in thalamic and cortical pathways).

Table S4. Comparison of synaptic weight changes with three groups of cells: winners, losers and five random cells from cells that were high firing during habituation but did not fall in either of the groups.

LOSER CELLS (N=5)												
cell ID	Type	Tone		Shock	Tone-PN		PLST-Loser		Loser-IN		IN-Loser	
		Thlm	Crtx		before	after	before	after	before	after	before	after
116	C	O	X	O	5.5	5.4	1	1±0.01	1	1.1±0.01	4.5	7±0.03
181	C	O	X	O	5.5	5.7	1	1±0.01	1	1.2±0.01	4.5	8±0.04
275	B	O	O	O	5.5	6	1	1±0.01	1	1.1±0.01	4.5	8±0.04
504	C	O	X	O	5.5	5.9	1	1±0.01	1	1.0±0.01	4.5	7±0.03
509	B	O	O	O	5.5	5.5	1	1±0.01	1	1.1±0.01	4.5	7.5±0.03
Avg.						5.7±0.1		1±0.02		1.1±0.01		7.5±0.03
WINNER CELLS (N=5)												
cell ID	Type	Tone		Shock	Tone-PN		PLST-Winner		Winner-IN		IN-Winner	
		Thlm	Crtx		before	after	before	after	before	after	before	after
116	C	O	X	O	5.5	8	1	2±0.02	1	1.5±0.01	4.5	7±0.03
181	C	O	X	O	5.5	9	1	1.5±0.01	1	2±0.02	4.5	8±0.04
275	B	O	O	O	5.5	8	1	1.4±0.01	1	1.6±0.01	4.5	9±0.04
504	C	O	X	O	5.5	8	1	2±0.02	1	1.8±0.02	4.5	7±0.03
509	B	O	O	O	5.5	9	1	1.9±0.02	1	1.5±0.01	4.5	7±0.03
Avg.						8.5±0.3		1.8±0.02		1.7±0.01		7.6±0.03
NON-PLASTIC CELLS (N=5)												
cell ID	Type	Tone		Shock	Tone-PN		PLST-nonP		nonP-IN		IN-nonP	
		Thlm	Crtx		before	after	before	after	before	after	before	after
116	C	O	O	X	5.5	5.2	1	1±0.01	1	1±0.01	4.5	5.5±0.02
181	C	O	X	O	5.5	5.3	1	1±0.01	1	1±0.01	4.5	5.5±0.03
275	B	O	O	X	5.5	5.4	1	1±0.01	1	1±0.01	4.5	5±0.02
504	C	O	X	O	5.5	5.3	1	1±0.01	1	1±0.01	4.5	6±0.03
509	B	O	O	X	5.5	5.3	1	1±0.01	1	1±0.01	4.5	5±0.02
Avg.						5.3±0.3		1±0.001		1±0.001		5.4±0.03

Connection type	Mono-syn exc	Di-syn inh
Plastic→Winner	6.2±0.5	110±5
Plastic→Loser	5.4±0.4	121±6
Plastic→Non-Pl.	3.8±0.4	128±4

S4. SUPPLEMENTARY REFERENCES

Byrne JH, Roberts JL. 2004. *From Molecules to Networks – An introduction to cellular and molecular neuroscience.* Elsevier Academic Press.

Farb C, Chang W, LeDoux JE. 2010. Ultrastructural characterization of noradrenergic axons and beta-adrenergic receptors in the lateral nucleus of the amygdale. *Front Behav Neurosci* **4**:162.

Hu H, Real E, Takamiya K, Kang M, LeDoux J, Huganir R, Malinow R. 2007. Emotion enhances learning via norepinephrine regulation of AMPA receptor trafficking. *Cell* **131**: 160-173.

Johnson LR, Hou M, Prager EM, LeDoux JE. 2011. Regulation of the fear network by mediators of stress: norepinephrine alters the balance between cortical and subcortical afferent excitation of the lateral amygdala. *Front Behav Neurosci* **5**: 23.

Kroner S, Rosenkranz JA, Grace AA Barrionuevo G. 2004. Dopamine modulates excitability of basolateral amygdala neurons in vitro. *J Neurophysiol* **93**: 1598-1610.

Loretan K, Bissiere S, Luthi A 2004. Dopaminergic modulation of spontaneous inhibitory network activity in the lateral amygdale. *Neuropharmacology* **47**: 631-639.

Martina M, Bergeron R. 2008. D1 and D4 dopaminergic receptor interplay mediates coincident G protein-independent and dependent regulation of glutamate NMDA receptors in the lateral amygdala. *J Neurochemi* **106**: 2421-2435.

Muller JF, Mascagni F, McDonald AJ. 2009. Dopaminergic innervation of pyramidal cells in the rat basolateral amygdala. *Brain Struct Funct* **213**: 275-288.

Rainbow TC, Parsons B, Wolfe BB. 1984. Quantitative autoradiography of β1- and β2-adrenergic receptors in rat brain. *Proc Natl Acad Sci* **81**: 1585-1589.

Rosenkranz JA, Grace AA. 2002. Cellular Mechanisms of infralimbic and prelimbic prefrontal cortical inhibition and dopaminergic modulation of basolateral amygdala neurons in vivo. *J Neurosci* **22**: 324-337.

Sara SJ. 2009. The Locus coeruleus and noradrenergic modulation of cognition. *Nat Neurosci Rev* **10**: 211-223.

Shouval HZ, Bear MF, Cooper LN. 2002b. A unified model of NMDA receptor-dependent bidirectional synaptic plasticity. *Proc Natl Aca Sci* **99**: 10831-10836.

Zador A, Koch C, Brown TH. 1990. Biophysical model of a Hebbian synapse. Proc Natl Acad Sci **87**: 6718-6722.

CHAPTER 5

SINGLE CELL MODEL SELECTION FOR NETWORK SIMULATION

ABSTRACT

Biophysical conductance based models of neurons incorporate physiological information including morphology, individual channels, and synapses. Such single cell models are of different complexities ranging from simple one-compartment models for network studies, to cells with over 500 compartments for detailed studies of single cell properties. We report a methodology to develop a three-compartmental single cell model that retains the important biological characteristics, and is suitable for incorporation into network models. The performance of this three-compartment neuronal single cell model is compared with those of 1-, 2- and 69-compartmental single cell models, by considering electrophysiological characteristics as well as network behavior. For comparing network behavior, the single cell model types are inserted into a 100-cell network that is then trained using the Pavlovian fear conditioning paradigm (Quirk et al., 1995, 1997) to investigate how single cell properties might affect network behavior. The models also incorporate effects of neuromodulation, and short- and long- term plasticity.

INTRODUCTION

Neuronal network models typically use simplified single cells models with either one or two compartments presently. This is largely due to the fact that computational times

become prohibitive with cells containing multiple compartments. Although other model such as Izhikevich model (Izhikevich, 2009) that preserves neuro-computational properties do provide an attractive alternative, they may not be suited for studies require characterization of individual channel currents, effects of blockers and of neuromodulation. We report a procedure to develop a reduced order biophysical single cell model which provides a good compromise between biological realism and ease of computation.

To create such reduced order neuron models, we start with biological data about the neuron, including its morphology. In some cases such information has already been utilized to developed multi-compartmental models and so such detailed models can be used as the starting point (e.g., Power et al., 2011). In either case, the data required to constrain the model includes passive properties of the cell (e.g., input resistance, time constant, resting potential), known current channel types and their maximal conductance densities, and responses to current injections (e.g., Bar-Ilan et al., 2013). The reduced order neuron model is developed in a series of steps. We consider reasons why two-compartment models including (soma+axon and dendrite) generally do not satisfy all the key cellular properties. A three-compartment model, on the other hand, may be adequate but may not be able to integrate synaptic inputs on multiple dendrites, particularly from different afferents. Other issues are also considered, including the effect of dendritic v/s somatic inhibition.

A detailed 69compartment model of a lateral amygdala was reduced to both 3-compartmental models to illustrate the proposed methodology. Examples of principal cells and interneurons from other areas such as the prefrontal cortex are also considered.

METHODS

Biological data.

A diversity of spike frequency adaptation is seen in principal LA neurons (reviewed in Sah et al., 2003), with three types of regular spiking principal cells, with high (type-A), intermediate (type-B), or low (type-C) spike frequency adaptation, due to the differential expression of a Ca^{2+}-dependent K^+ current. LA also contains local GABAergic interneurons that exhibit various firing patterns, even among neurochemically-homogeneous subgroups (Lang and Paré, 1998; Rainnie et al., 2006; Sosulina et al., 2006; Woodruff and Sah, 2007; Jasnow et al., 2009). However, the majority of interneurons displays a fast-spiking pattern, which was reproduced in the model.

The principal cells in LA are found to be in the ratio of 50:30:20, and the principal cell to interneuron ratio is 80:20 (McDonald and Augustine, 1993). Principal cells and interneurons were distributed randomly in a realistic tri-dimensional representation of the horn-shaped LAd (**Fig. 2A**; Kim et al., 2013).

Single cell and network models.

We modeled three types of regular spiking principal cells in LA, with high (type-A), intermediate (type-B), or low (type-C) spike frequency adaptation, due to the differential expression of a Ca^{2+}-dependent K^+ current (Sah et al., 2003). LA also contains local GABAergic interneurons that exhibit various firing patterns, with the majority displaying a fast-spiking pattern, and we modeled this interneuron type in our study.

Membrane properties and currents: For the principal cells, the values of specific membrane resistance, membrane capacity and cytoplasmic (axial) resistivity were, respectively, R_m = 55 KΩ-cm^2, C_m= 1.2-2.4 μF/cm^2, and R_a= 150-200 Ω-cm. Leakage reversal potential (E_L) was set to -67 mV. The resulting V_{rest} was – 69.5± 0.5mV, input resistance (R_{IN}) was 150±10 MΩ, and τ_m was 30±1 ms, all of which were within the ranges reported in previous physiological studies (Washburn and Moises, 1992; Faber et al., 2001). The following currents were common to the soma and the main dendrite compartments: leak (I_L), voltage-gated persistent muscarinic (I_M), high-voltage activated Ca^{2+} (I_{Ca}), spike-generating sodium (I_{Na}), potassium delayed rectifier (I_{DR}) and A-type potassium (I_A) (Li et al., 2009; Power et al., 2011). In addition, the dendrites had a hyperpolarization-activated nonspecific cation (I_h) currents and a slow apamin-insensitive, voltage-independent afterhyperpolarization current (I_{sAHP}) (Power et al., 2011). See sections S1.5 and S1.6 of the supplementary materials as well as Tables S1-2 for current equations and densities.

For the interneuron model, the passive membrane properties were as follows: R_m = 20 KΩ-cm^2, C_m=1.0 μF/cm^2, R_a= 150 Ω-cm, and E_L = -70 mV. Each compartment contained a fast Na^+ (I_{Na}) and a delayed rectifier K^+ (I_{DR}) currents with kinetics (Durstewitz et al., 2000) that reproduced the much shorter spike duration that is characteristic of fast-spiking cells.

Morphology: We propose a 3-compartment model that is a good compromise between biological realism and computational tractability, starting with the morphological

structure of . Each is described below briefly, starting with the proposed 3-compartment model.

3-compartment model. The 3-compartment principal cell had a soma (dia 24.75 μm; length 25 μm), an apical dendrite (dia 2.5 μm; length 296 μm) on which synapses were placed, and another dendrite (dia 5 μm; length 400 μm) that helped match passive properties. The soma and dendrites had the current cited earlier. We propose a methodology to add a third compartment to match the passive properties and current injection properties as explained in the Results section. This additional dendrite had has same ionic channels as apical dendrite (Table S5).

1-compartment model. For this case, an effective compartment was modeled that represented the soma and dendrites with diameter and length of 24.75 μm and 25 μm, respectively. It had all the current channels as the 3-compartment model soma and apical dendrite.

2-compartment model. This model had a soma (dia 2.5 μm; length 101.3 μm), and one dendrite (dia 5 μm; length 400 μm) that had the synapses. The distribution of channels between the soma and dendrite were different from the 3-compartmental model (Table S3).

69-compartment model. The dimensions of the 69-compartmental model are provided in the supplementary materials. In this model, I_{Kdr} was uniformly distributed with a maximum conductance of 30 pSμm^2. The maximum conductance of I_{Na} was 180 pSμm^2 in the soma and dendrite and was 360 pSμm^2 in the axon. A calcium current (I_{Ca}) was used to represent the various types of voltage-dependent calcium channels. The maximum conductance of I_{Ca} was set at 20 pSμm^2. The peak conductances for I_A and I_H

were linearly increased with distance from the soma (Hoffman et al., 1997; Magee, 1999) up to 500µm. The peak conductance for I_A was 132 pSµm^{2}in the soma increasing with distance at 13.2 pSµm^2 every 10 µm. The peak conductance density for I_H was 0.3 pSµm^2 in the soma, increasing by 0.9 pSµm^2 every 10µm.

Network structure and connectivity.

A 100-cell network was developed with principal cells A, B, and C in the ratio 50:30:20 and a principal cell (PN) to interneuron (IN) ratio of 80:20. The network had 80 PN and 20 IN that reproduced the experimentally observed electroresponsive properties of these cell types, neuromodulatory inputs from brainstem dopaminergic and noradrenergic neurons, and spatially heterogeneous intrinsic connectivity (Pape and Paré, 2010).

Activity-dependent synaptic plasticity

Model AMPA and GABA synapses could undergo activity-dependent short-term and long-term synaptic plasticity, consistent with the experimental literature (see section S1.1 of supplementary materials). The tone to pyramidal cell and tone to interneuron AMPA synapses were endowed with long-term plasticity. For this form of plasticity we used a Ca^{2+}-dependent Hebbian learning algorithm (Gerstner and Kistler, 2002; Shouval et al., 2002a,b; Li et al., 2009) for these synapses, where synaptic activation caused a postsynaptic rise in intracellular Ca^{2+} concentration, the magnitude of which determined how the synaptic strength was altered, as described next. Calcium entered post-synaptic pools at excitatory synapses via NMDA receptors (and includes Ca^{2+}-permeable AMPA

receptors for interneurons) and voltage-gated calcium channels. The synaptic weight decreased when the calcium concentration was below a lower threshold and increased when it exceeded an upper threshold. Equations and details related to the learning rule are listed in section S1.7 of the supplementary materials. Model GABA synapses did not have any long-term plasticity.

Short term plasticity was modeled in AMPA and GABA synapses for all the intra-LAd connections, with short-term presynaptic facilitation in the principal-principal cell and interneuron-principal cell connections, and short-term depression in the principal cell-interneuron connections (Markram et al., 2004; Woodruff and Sah, 2007). For convenience in modeling, these were implemented by multiplying the synaptic conductances of the relevant AMPA and GABA synapses after each spike with appropriate factors that were frequency dependent (Varela et. al, 1997). Details are provided in section S1.7 of the supplementary materials.

Model NMDA synapses did not have any form of plasticity, and neither did the excitatory synapses connecting afferents delivering shock or background inputs.

Neuromodulator effects

Neuromodulators have long been implicated in fear and anxiety, and are known to regulate Pavlovian fear learning and synaptic plasticity in LA (Bissiere, 2003; Tully and Bolshakov, 2001). Conditioned aversive stimuli alter the activity of ventral tegmental area and locus coeruleus neurons (Feenstra et al., 2001), which in turn modulate fear and anxiety through their widespread forebrain projections, including to the amygdala (Guarraci and Kapp, 1999). Therefore, the model incorporated the effects of dopamine

(DA) and norepinephrine (NE) on LAd cells, based on prior experimental reports (see section S1.2 of the supplementary materials)**.**

Inputs

Background synaptic inputs. LA projection neurons have low spontaneous firing rates in control conditions (Gaudreau and Paré, 1996). To reproduce this, Poisson-distributed, random excitatory background inputs were delivered to all model cells, resulting in average spontaneous firing rates of 0.7 Hz for principal cells and 7.2 Hz for interneurons.

Tone and shock inputs. Auditory fear conditioning is commonly thought to depend on the convergence of inputs relaying information about the CS (tone) and US (footshock) in LA (reviewed in Pape and Paré 2010). In the model, the CS and US inputs were represented by glutamatergic synapses acting via AMPA and NMDA receptors. The frequency of thalamic and cortical tone inputs during habituation was set to 20 Hz (Quirk et al., 1997). The tone inputs also included noise represented by random Poisson spikes with an average frequency of 2 Hz. The density of both cortical and thalamic tone inputs to LAd was determined iteratively (see S1.3 of supplementary materials). The following distribution of inputs was used for the simulations described in the Results section: uniform total tone density throughout LAd with 70% of the LAdd cells receiving thalamic and 35% receiving cortical tone projections, and the opposite for LAdv, i.e., 35% of LAdv cells receiving thalamic and 70% receiving cortical tone projections. The shock inputs continued to be distributed uniformly to 70% of LAd cells.

Conditioning protocol used in simulations

The schedule of tone and shock inputs in the simulations was based on in vivo studies (Repa et al., 2001; Quirk et al. 1995). We scaled down the timing of the auditory fear conditioning protocol so that it would be suitable for computational studies . The protocol included three phases (habituation, conditioning and extinction), comprised of 8, 16 and 20 trials, respectively. Each trial featured a 0.5 sec tone CS followed by a 3.5 sec gap. Only during conditioning, a shock was administered 100 msec prior to the end of the tone, so that they co-terminated. In light of evidence that fear conditioning leads to plasticity in CS afferent pathways (reviewed in Weinberger, 2011), the frequency of thalamic and cortical tone inputs was increased to 40 Hz after the first and sixth conditioning trials, respectively. Simulations were performed using the NEURON modeling package (Carnevale and Hines, 2006).

RESULTS

Insights into developing multi-compartmental models

Proposed procedure for developing a 3-compartment model. For the neuron considered, the dominant dendrite is selected as one of the compartments, the axon and soma are merged into one compartment (henceforth termed 'soma'), and another passive compartment is added to account for the other dendrites not considered. The morphology of the dominant dendrite (termed apical here) and soma are kept approximately the same as in the biological cell to ensure that the synaptic transmission properties, and the integration properties, respectively, are retained. The morphology of the third dendrite (termed basal here) is adjusted to account for all the other dendrites. Figure 2 show the procedure to develop a 3-compartment order single cell model to match these properties of the multi-compartmental model.

Passive properties of the cell. The capacitance (C_m) and membrane resistance (R_m) of the compartments the typical values of 2.0-4.0 μF/cm2 and 45KΩ-cm2, respectively. Axial resistivity, R_a, was in the range of 150-200 Ω-cm. The values of input resistance R_{in} and time constant τ_m are obtained from in vitro recordings (e.g., Faber et al. 2001). The time constant can be calculated as $\tau_m = C_m * R_m \quad where\ R_m = 1/G_{leak}$ and its value was matched to value recoded in vitro. R_{in} is measured as $\Delta V/I$ where I = the negative current injected and ΔV the resultant change in voltage. Despite their small volume, surface area of the spines effectively doubles the surface area of thin dendrites (Power et al., 2011; Migliore et al., 1995; Gasparini et al., 2004). Changing the area also increases the total conductance of the intrinsic channels. Because the dendrites had

spines, C_m and G_{leak} increased appropriately to account for the spines. Matching the passive electrophysiological properties of the model to data from in vitro cells (which have more complex morphological structure), required the addition of a third dendrite which contained enough leak channels and capacitance to replace the morphology not modeled.

Ionic channel conductance and density. Because channel distribution and densities in BLA projection neurons have not been fully worked out, we started with channel densities and distributions from models of hippocampal pyramidal neurons (Gasparini et al., 2004) and adjusted the densities to match electrophysiological recordings (Faber et al.,2001).

Current flow between soma and dendrites. The reduced order model should be checked with the current from a compartment to other compartment, between soma and dendrites. To obtain similar current flows to the appropriate dendrite in the 3-compartmental model, we changed the dimensions of the apical dendrite and the additional dendrite.

In vitro firing properties

Three-compartmental model: As shown in figure 1, single cell models could reproduce the voltage responses of three types of principal cell (A-C) to depolarizing (two left panels) and hyperpolarizing (right panel) current injection, matching biological data from in vitro studies (Faber et al., 2001). With a 400 pA depolarizing current step for 600 ms, the type A cell fired only two spikes, and type B cell fired 12 spikes due to frequency adaptation while type C cell fired repetitively. A slow depolarizing sag was

observed with a hyperpolarizing current injection (right panel in figure 1), due to the activation of the I_H current (Womble and Moises 1993).

Figure 1A shows the voltage response of the three principal cell models to depolarizing (two left panels) and hyperpolarizing (right panel) current injection. The three model cells could reproduce previous experimental observations (Sah et al., 2003) including the temporal dynamics of repetitive firing produced by membrane depolarization as well as their responses to membrane hyperpolarization. The interneuron model had two compartments, a soma (diameter 15 μm; length 15 μm) and a dendrite (diameter 10 μm; length 150 μm). As shown in figure 1B, the interneuron model could reproduce the non-adapting repetitive firing behavior of fast spiking cells, as observed experimentally (Lang and Paré, 1998; Woodruff and Sah, 2007).

Comparison of performance of network models: We developed a 100-cell model of the LAd network with the 3-compartment single cell model, and used that as the control case for the comparisons with other single cell models. For this comparison the same 100-cell structure was used, and the single cell models were replaced with 1-compartment, 2-compartment and 69-compartment neurons.

Network with 3-compartment neuron. The 100-cell network was able to reproduce the key results with the 1000-cell model in Kim et al. (2013). These included (i) the numbers of plastic cells, which were 11 TP and 9 LP cells; (ii) their tone responses as shown in Fig. 3, (iii) the cell types preferentially recruited in to the fear memory trace (type C – 9, type B – 11, and type A – 0), (iv) number of mono-synaptic excitatory and disynaptic

inhibitory connection involving interneurons from plastic cells (exc:1.8±0.2; inh:5.7±0.8), (v) the effect of thalamic plasticity and cortical afferents on tone responses (tone responses dropped considerably with fixed tone response, and without cortical afferents) , (v) the effect of blockade of DA and NE receptors (tone responses again dropped to very low levels), (vi) growth patterns for the various synapses, tone-PN, tone-IN, PN-PN, PN-IN and IN-PN, and (vii) competition and specificity characteristics. These characteristics are used as control cases for the comparisons with the other single cell model types.

Network with 1-compartment neuron

The 1-compartment neuron model did not have enough degrees of freedom to reproduce both the passive and current injection properties of the biological LA cells. For instance, with the type C cells reproducing the passive and current injection properties, conversion to types B and C could not be achieved with only changes to the sAHP channel properties as was done for the 3-compartmental model. For instance, matching the current injection traces for the three cells using the same logic resulted in the the input resistance and resting membrane potential values for cell types A and B exceeding the biological bounds (see suppl matls). The current injection traces did, however, match very well. Further studies related to other ‘solutions’ will be performed.

In the network, the 1-compartment models showed very different behavior compared to the 3-compartmental model. One was the need to have much higher tone-PN initial weights (with all other initial weights unchanged; Fig.4-5). The other was the observation that more of type A cells were being recruited into the fear memory trace compared to

type C cells, an idea that runs counter to the results found with the 3-compartmental model.

We are presently in the process of adding results from networks with 2-compartment and 69-compartment neurons to this.

DISCUSSION

We proposed a structure for a reduced order single cell model with 3-compartments that was a good compromise between biological realism and ease of computation. We then compared 1-, 2- and 60-compartmental cell models with the 3-compartmental model to investigate the role of single cell model structure on network properties.

Selection of single cell model for network studies

Single cell electrophysiology properties that are typically reported include the resting membrane potential, input resistance, and current injection characteristics. Models with single and two compartmental models were unsuccessful in reproducing all these three properties, and we proposed a model with three compartments and a procedure to develop the model so as to satisfy all passive and current injection properties, and thus retain biological realism to the extent possible.

Need to provide details and explain why the other cells did not work.

Control of neuronal excitability by neuromodulation

One of the observations while developing the single cell models was that the intrinsic excitability of the principal cells was affected by the sAHP channel that is present only in

the dendrites. Power et al. (2011) state that changes in the levels of this sAHP channel is what differentiates the principal cell types A, B and C. Using this 'requirement' in the model resulted in the single compartment model having a very large sAHP conductance for type A and B cells, which resulted in the cell increasing its excitability considerably with neuromodulation.

Network behavior is influenced by single cell characteristics

As cited in results, the 1-compartmental model required much higher tone-PN weights in the network. This was due to several reasons.....

An analysis of the reasons for more of type A cells being recruited into the fear memory trace, compared to the type C cells revealed the cause to be the channel density distributions of the calcium activated potassium channel sAHP being very different between cells types of A, B and C in the single compartmental model, compared to the 3-compartmental models. It was found that insertion of the 1-compartmental principal cells into the network and subsequent training led to very different results in the types of cells recruited in the fear memory trace. Indeed it was found that instead of type C cells being recruited preferentially into the fear memory trace, there was a preponderance of type A cells in the trace, when in reality type A cells compete very poorly during the memory allocation process. This was a significant short coming of the single compartmental model. Both 2- and 69-compartmental models will be analyzed in a similar manner and the results compiled here.

CONCLUSIONS

We report a systematic procedure to develop a 3-compartmental biophysical model of a neuron that preserves the in vitro passive and current injection properties, and is suitable for use in network models. Comparatives studies with single cell models with 1-, 2- and 69-compartmental models reveal that the 3-compartmental model had some key characteristics that were essential for completion, which the 1- and 2-compartmental models did not possess. This was the fact that intrinsic excitability levels were controlled by the sAHP channel, which has been reported to be controlled by neuromodulatory effects.

REFERENCES

Bar-Ilan L, Gidon A and Segev I (2013) The role of dendritic inhibition in shaping the plasticity of excitatory synapses. Front. Neural Circuits **6**:118. doi: 10.3389/fncir.2012.00118

Carnevale, N.T., and Hines, M.L. (2006). The NEURON book (Cambridge, UK: Cambridge University Press).

Collins, D.R., and Paré, D. (2000). Differential fear conditioning induces reciprocal changes in the sensory responses of lateral amygdala neurons to the CS(+) and CS(-). Learn. Mem. 7, 97-103.

Durstewitz, D., Seamans, J.K., and Sejnowski, T.J. (2000). Dopamine-mediated stabilization of delay-period activity in a network model of prefrontal cortex. J. Neurophysiol. 83, 1733-1750.

Dyhrfjeld-Johnsen, J., Santhakumar, V., Morgan, R.J., Huerta, R., Tsimring, L., and Soltesz, I. (2007). Topological determinants of epileptogenesis in large-scale structural and functional models of the dentate gyrus derived from experimental data. J. Neurophysiol. 97, 1566-1587.

Faber, E.S., Callister, R.J., and Sah, P. (2001). Morphological and electrophysiological properties of principal neurons in the rat lateral amygdala in vitro. J. Neurophysiol. 85, 714-723.

Faber, E.S., and Sah, P. (2002). Physiological role of calcium-activated potassium currents in the rat lateral amygdala. J Neurosci 22, 1618–1628.

Faber, E.S. and Sah, P. (2003). Ca2+-activated K+ (BK) channel inactivation contributes to spike broadening during repetitive firing in the rat lateral amygdala. J. Physiol. 552, 483-497.

Feenstra, M.G., Vogel, M., Botterblom, M.H., Joosten, R.N., and de Bruin, J.P. (2001). Dopamine and noradrenaline efflux in the rat prefrontal cortex after classical aversive conditioning to an auditory cue. Eur. J. Neurosci. 13, 1051–1054.

Gaudreau, H., and Paré, D. (1996). Projection neurons of the lateral amygdaloid nucleus are virtually silent throughout the sleep-walking cycle. J. Neurophysiol. 75, 1301–1305.

Gerstner, W., and Kistler, W. (2002). Spiking neuron models: Single neurons, populations, plasticity. (Cambridge , UK: Cambridge University Press).

Goosens, K.A., Hobin, J.A., and Maren, S. (2003). Auditory-evoked spike firing in the lateral amygdala and Pavlovian fear conditioning: mnemonic code or fear bias? Neuron 40,1013-1022.

Guarraci, F.A., and Kapp, B.S. (1999). An electrophysiological characterization of ventral tegmental area dopaminergic neurons during differential Pavlovian fear conditioning in the awake rabbit. Behav. Brain Res. 99, 169-179.

Han, J.H., Kushner, S.A., Yiu, A.P., Cole, C.J., Matynia, A., Brown, R.A., Neve, R.L., Guzowshi, J.F., Silva, A.J., and Josselyn, S.A. (2007). Neuronal competition and selection during memory formation. Science 316, 457-460.

Han, J.H., Kushner, S.A., Yiu, A.P., Hsiang, H.L., Buch, T., Waisman, A., Bontempi, B., Neve, R.L., Frankland, P.W., and Josselyn, S.A. (2009). Selective erasure of a fear memory. Science 323, 1492-1496.

Hennevin, E., and Maho, C. (2005). Fear conditioning-induced plasticity in auditory thalamus and cortex: to what extent is it expressed during slow-wave sleep? Behav. Neurosci. 110,1277-1289.

Johnson, L.R., Hou. M., Prager, E.M. and LeDoux, J.E. (2011). Regulation of the fear network by mediators of stress: norepinephrine alters the balance between cortical and subcortical afferent excitation of the lateral amygdala. Front, Behav. Neurosci. 5, 23.

Kroner, S., Rosenkranz, J.A., Grace, A.A. and Barrionuevo, G. (2004). Dopamine modulates excitability of basolateral amygdala neurons in vitro. J. Neurophysiol. 93, 1598-1610.

LeDoux, J.E. (2000). Emotional circuits in the brain. Annu. Rev. Neurosci. 23, 155-184.

Letzkus, J.J., Wolff, S.B., Meyer, E.M., Tovote, P., Courtin, J., Herry, C., and Lüthi, A. (2011). A disinhibitory microcircuit for associative fear learning in the auditory cortex. Nature 480, 331-335.

Li, G., Nair, S., and Quirk, G.J. (2009). A biologically realistic network model of acquisition and extinction of conditioned fear associations in lateral amygdala neurons. J. Neurophysiol. 101, 1629-1646.

Loretan, K., Bissiere, S., and Luthi, A. (2004). Dopaminergic modulation of spontaneous inhibitory network activity in the lateral amygdale. Neuropharmacology 47, 631-639.

Pape, H.C., and Paré, D. (2010). Plastic synaptic networks of the amygdala for the acquisition, expression, and extinction of conditioned fear. Physiol. Rev. 90, 419-463.

Paré, D. (2002). Mechanisms of Pavlovian fear conditioning: Has the engram been located? Trends Neurosci. 25:436-437.

Paré, D. (2003). Role of the basolateral amygdala in memory consolidation. Prog. Neurobiol. 70, 409-420.

Pezze, M.A., and Feldon, J. (2004). Mesolimbic dopaminergic pathways in fear conditioning. Prog. Neurobiol. 74,301-320.

Power, J.M., Bocklisch, C., Curby, P., and Sah, P. (2011). Location and function of the slow afterhyperpolarization channels in the basolateral amygdala. J. Neurosci. 31, 526-537.

Quirk, G.J., Repa, J.C., and LeDoux, J.E. (1995). Fear conditioning enhances short latency auditory responses of lateral amygdala neurons: parallel recordings in the freely behaving rat. Neuron 15,1029-1039.

Quirk, G.J., Armorny, J.L., and LeDoux, J.E. (1997). Fear conditioning enhance different temporal component of tone-evoked spike trains in auditory cortex and lateral amygdala. Neuron 19, 613-624.

Repa, J.C., Muller, J., Apergis, J., Desrochers, T.M., Zhou, Y., and LeDoux, J.E. (2001). Two different lateral amygdala cell populations contribute to the initiation and storage of memory. Nat. Neurosci. 4, 724-731.

Rumpel, S., LeDoux, J., Zador, A., and Malinow, R. (2005). Postsynaptic receptor trafficking underlying a form of associative learning. Science 308, 83–88.

Sah, P., Faber, E.S., Lopez de Armentia, M., and Power, J. (2003). The amygdaloid complex : anatomy and physiology. Phsiol. Rev. 83, 803-834.

Shouval, H.Z., Castellani, G.C., Blais, B.S., Yeung, L.C., and Cooper, L.N. (2002a). Converging evidence for a simplified biophysical model of synaptic plasticity. Biol. Cybern. 87, 383-391.

Shouval, H.Z., Bear, M.F., and Cooper, L.N. (2002b). A unified model of NMDA receptor-dependent bidirectional synaptic plasticity. Proc. Natl. Aca. Sci. 99, 10831-10836.

Tully, K., and Bolshkov, V.Y. (2001). Emotional enhancement of memory: how norepinephrine enables synaptic plasticity. Mol. Brain 3, 15.

Tuunanen, J., and Pitkänen, A. (2000). Do seizures cause neuronal damage in rat amygdala kindling? Epilepsy Res. 39, 171-176.

Varela, J., Sen, K., Gibson, J., Fost, J., Abbott, L., Nelson, S. (1997). A quantitative description of short-term plasticity at excitatory synapses in layer 2/3 of rat primary visual cortex. J Neurosci. 17(20):7926–7940.

Washburn, M.S., Moises, and H.C. (1992). Electrophysiological and morphological properties of rat basolateral amygdaloid neurons in vitro. J. Neurosci. 12, 4066-4079.

Woodruff, A.R., and Sah, P. (2007). Networks of parvalbumin-positive interneurons in the basolateral amygdala. J. Neurosci. 27, 553–563.

Zhou, Y., Won, J., Karlsson, M.G., Zhou, M., Rogerson, T., Balaji, J., Neve, R., Poirazi, R., and Silva, A.J. (2009). CREB regulates excitability and the allocation of memory to subsets of neurons in the amygdala. Nat. Neurosci. 12, 1438-1443.

FIGURES

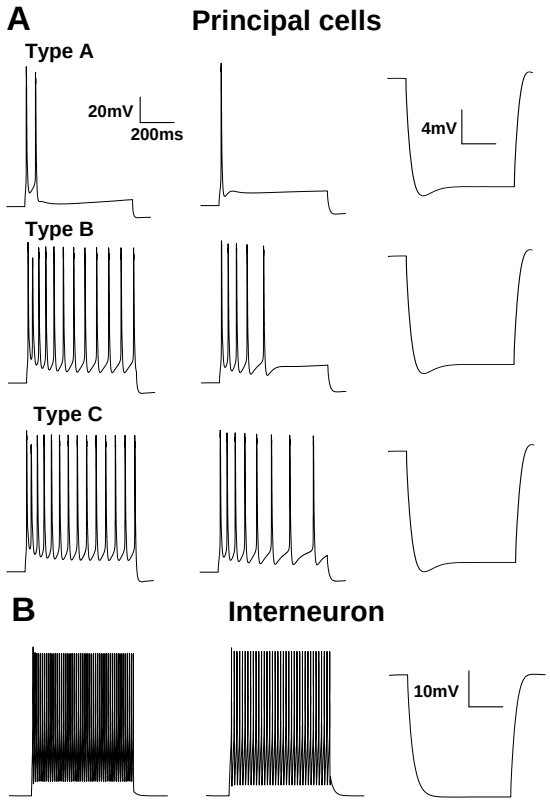

Figure 1. Electroresponsive properties of model LA neurons.Voltage responses of model cells to intracellular current injection. (**A**) The responses of the three types of principal cells (types A, B and C) to current injections (left: 400 pA; middle: 300 pA; right: -100 pA; duration 600 ms) are similar to those reported in Faber et al. (2001). (**B**) Voltage responses of the interneuron model to 200-ms current injections of the same magnitude as in A.

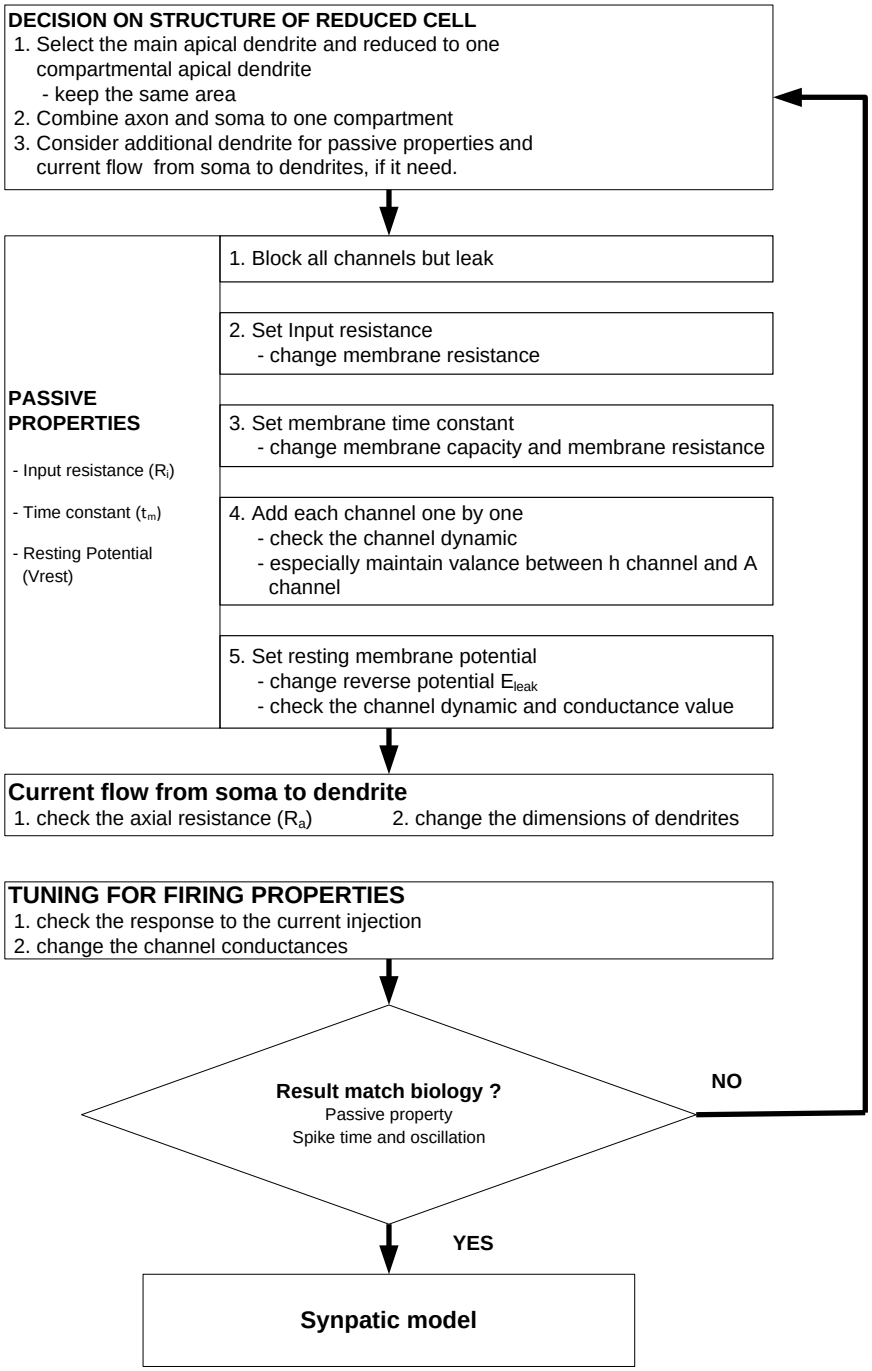

Figure 2. Flowchart of the development of a 3-compartmental cell model.

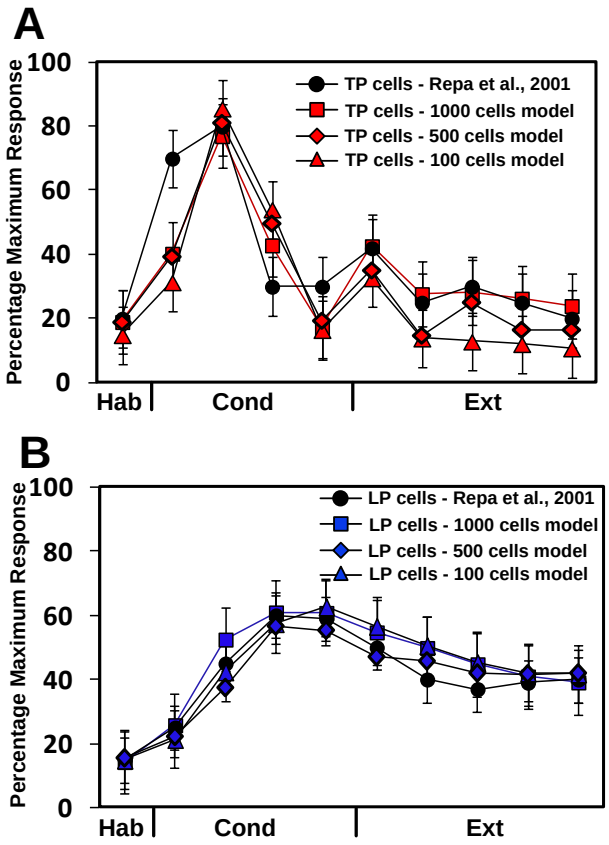

Figure 3. The tone responses of TP (**A**) and LP (B) cells in 1000 cells (squares), 500 cells (triangles) and 100 cells (diamonds) LAd model. (**A**) Tone responses of LAd cells during the different phases of the behavioral protocol. (**A**) 1000 cells Model (red squares, N=98/800), 500 cells Model (red triangles, N=50/400) , 100 cells Model (red diamonds, N=10/80) and experimental (black; N=12/100; from Repa et al., 2001) tone responses of TP cells show a sudden increase during early conditioning, and then drop to habituation levels during late conditioning. (**A2**) 1000 cells Model (blue; N=90/800), 500 cells Model (blue; N=50/400), 100 cells Model (blue; N=9/80) and experimental (black; N=12/100) tone responses of LP cells increase gradually with conditioning and persist during extinction.

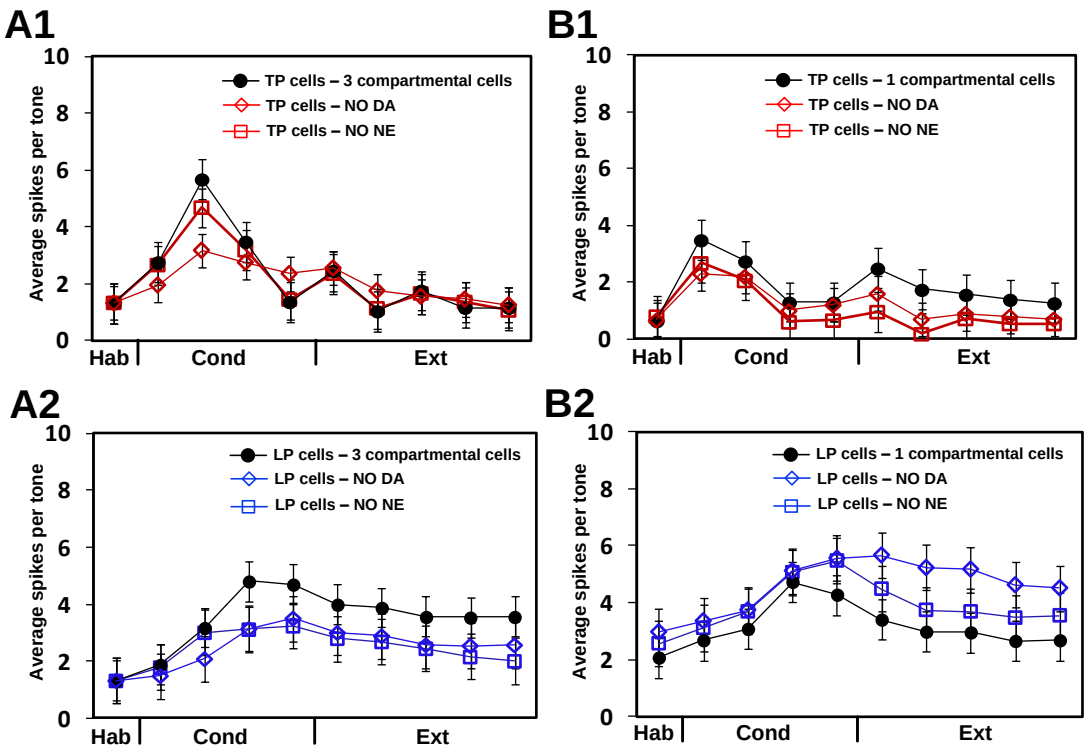

Figure 4. Contributions of neuromodulators to learning-induced changes in the tone responses of LAd cells. Tone responses of TP cells (top, **panels 1 of A-B**) and LP neurons (bottom, **panels 2 of A-B**) during the different phases of the behavioral protocol (x-axis) in the following conditions: (**A**) when the increased release of DA (diamonds) of NE (squares) was blocked in 100 cells model with 3-compartment cell or (**B**) one-compartment cell with doubled tone-PN synaptic weight. In **A-B**, black circles represent each of control condition with normal neuromodulation. (**A1**) Tone responses of TP cells decreased when the DA (N=6; 50±3%, p<0.01) but not the NE (N=9; 11±0.8%, p=0.54) concentrations were kept at habituation levels; (**A2**) Tone responses of LP cells decreased when DA (N=7; 56±6%, p < 0.05 during conditioning; 55±5%, p < 0.01 during extinction) or NE (N=6; 34±3%, p < 0.05 during conditioning; 58±7%, p < 0.001 during extinction) concentrations were kept at habituation levels; (**B1**) Tone responses of TP cells decreased when the DA (N=3; 28±4%, p=0.28) or the NE (N=5; 27±4%, p=0.26) concentrations were kept at habituation levels during conditioning. (**B2**) Unlike as three-compartment model, tone responses of LP cells increased when DA (N=5; 17±2%, p = 0.18 during conditioning; 63±7%, p < 0.01 during extinction) or NE (N=10; 16±2%, p = 0.13 during conditioning; 37±4%, p < 0.05 during extinction) concentrations were kept at habituation levels.

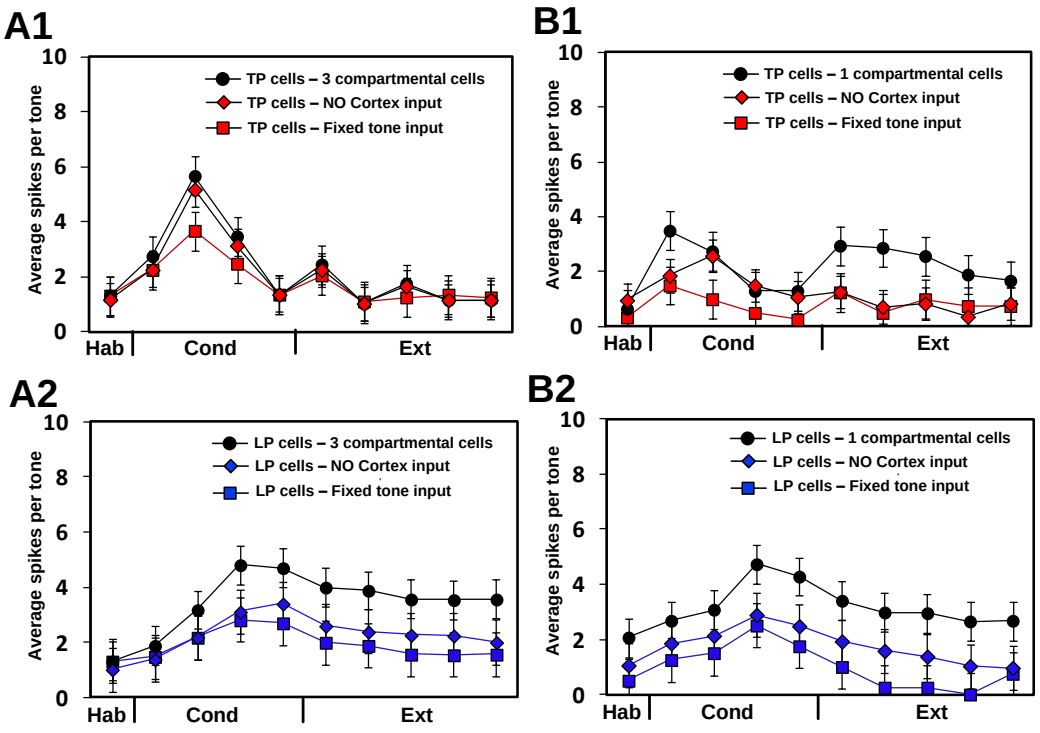

Figure 5. **(A)** Cortical inputs and plasticity of tone inputs are required to generate plastic cells in LAd. Spikes per tone (mean ±s.e.m.) of plastic LAd model cells. TP (red) and LP cells (blue), for the following cases: control (square), no cortical input (diamond) and no plasticity in thalamic and cortical inputs, i.e., frequency fixed to 20 Hz in model with 3-compartment cells **(A)** or one-compartment cells with doubled tone-PN synaptic weight **(B). (A1)** Tone responses of TP cells decreased without cortex input (N=9; 3±0.2%, p=0.89) and with fixed tone input (N=7; 31±3%, p<0.05); **(A2)** Tone responses of LP cells decreased without cortex input (N=5; 43±4%, p<0.001) and with fixed tone input (N=6; 51±5%, p<0.001). **(B1)** Tone responses of TP cells decreased without cortex input (N=5; 15±2%, p=0.12) and with fixed tone input (N=1; 72±8%). **(B2)** Tone responses of LP cells increase without cortex input (N=4; 41±5%, p<0.005) and with fixed tone input (N=1; 81±2%).

SUPPLEMENTARY MATERIALS

Mathematical Details

The equation for each compartment (soma or dendrite) followed the Hodgkin-Huxley formulations (Byrne and Roberts, 2004) in eqn. S1,

$$C_m dV_s/dt = -g_L(V_s - E_L) - g_c(V_s - V_d) - \sum I_{cur,s}^{int} - \sum I_{cur,s}^{syn} + I_{inj} \quad \text{(S1)}$$

where V_s/V_d are the somatic/dendritic membrane potential (mV), $I_{cur,s}^{int}$ and $I_{cur,s}^{syn}$ are the intrinsic and synaptic currents in the soma, I_{inj} is the electrode current applied to the soma, C_m is the membrane capacitance, g_L is the is the conductance of leak channel, and g_c is the coupling conductance between the soma and the dendrite (similar term added for other dendrites connected to the soma). The intrinsic current $I_{cur,s}^{int}$, was modeled as $I_{cur,s}^{int} = g_{cur} m^p h^q (V_s - E_{cur})$, where g_{cur} is its maximal conductance, *m* its activation variable (with exponent *p*), *h* its inactivation variable (with exponent *q*), and E_{cur} its reversal potential (a similar equation is used for the synaptic current $I_{cur,s}^{syn}$ but without *m* and *h*). The kinetic equation for each of the gating variables *x* (*m* or *h*) takes the form

$$\frac{dx}{dt} = \frac{x_\infty\left(V,[Ca^{2+}]_i\right) - x}{\tau_x(V,[Ca^{2+}]_i)} \quad \text{(S2)}$$

where x_∞ is the steady state gating voltage- and/or Ca^{2+}- dependent gating variable and τ_x is the voltage- and/or Ca^{2+}- dependent time constant. The equation for the dendrite follows the same format with '*s*' and '*d*' switching positions in eqn. S1. Details related to the model, including types of channels and parameter values are provided in **Tables S1-2**.

Synaptic Currents

Excitatory transmission was mediated by AMPA/NMDA receptors, and inhibitory transmission by $GABA_A$ receptors. The corresponding synaptic currents (shown in dendrites below) were modeled by dual exponential functions (Durstewitz et al., 2000), as shown in Eqns. S3-5,

$$I_{AMPA} = \bar{A}w(t)g_{AMPA,max}\frac{\tau_1\tau_2}{\tau_2-\tau_1}[\exp(-t/\tau_2) - \exp(-t/\tau_1)](V - E_{AMPA}) \quad \text{(S3)}$$

$$I_{NMDA} = \bar{A}w(t)g_{NMDA,max}s(V)\frac{\tau_1\tau_2}{\tau_2-\tau_1}[\exp(-t/\tau_2) - \exp(-t/\tau_1)](V - E_{NMDA}) \quad \text{(S4)}$$

$$I_{CABA} = \bar{A}w(t)g_{GABAA,max}\frac{\tau_1\tau_2}{\tau_2-\tau_1}[\exp(-t/\tau_2) - \exp(-t/\tau_1)](V - E_{GABA}) \quad \text{(S5)}$$

where V is the membrane potential (mV) of the compartment (dendrite or soma) where the synapse is located, $w(t)$is the adjustable synaptic weight for AMPA synapses (see section S1.7; w was held fixed for all NMDA synapses); $\bar{A}$ is a normalization constant chosen so $g_{AMPA,max}$ $g_{NMDA,max}$ and $g_{GABA,max}$ assume maximum values of the conductances; τ_1 and τ_2 are the rise and decay time constants respectively. For AMPA receptor channels, τ_1 = 0.25 ms and τ_2 = 7 ms; for NMDA receptor channels, τ_1 = 3.65 ms and τ_2 = 125.0 ms, and for $GABA_A$ receptors, τ_1 = 0.13ms and τ_2 = 3.75 ms. The voltage-dependent variable $s(V)$ which implements the Mg^{2+} block was defined as: $s(V) = [1 + 0.33 \exp(-0.06\ V)]^{-1}$ (Zador et al., 1990). The maximal conductances were chosen as: $g_{AMPA,max}$= 1 nS, $g_{NMDA,max}$ = 0.5 nS and $g_{GABA,max}$= 0.6 nS. Synaptic reversal potentials were set as follows: $E_{AMPA} = E_{NMDA}$ = 0 mV and E_{GABAA} = -75 mV (Durstewitz et al., 2000).

Calcium dynamics and Hebbian learning

Intracellular calcium was regulated by a simple first-order differential equation shown in Eqn. S6 (Warman et al., 1994),

$$\frac{d[Ca^{2+}]_i}{dt} = -f\frac{I'_{Ca}}{zFA} + \frac{[Ca^{2+}]_{rest} - [Ca^{2+}]_i}{\tau_{Ca}} \quad \text{(S6)}$$

where f is the fraction of the Ca^{2+} influx (f =0.024), $V = wA$ with w being the shell thickness (1μm) and A the dendritic/soma surface area, z=2 is the valance of the Ca^{2+} ion, F is the Faraday constant, and τ_{Ca} is the time constant associated with Ca^{2+} removal. The resting Ca^{2+} concentration was $[Ca^{2+}]_{rest}$ =50 nmol/l (Durstewitz et al., 2000).

The biophysical Hebbian rule was implemented by adjusting the synaptic weight w(t) in synaptic conductances (Eqns. S3 and S5) using equation S7,

$$\Delta w_j = \eta([Ca^{2+}]_j)\Delta t(\lambda_1\Omega([Ca^{2+}]_j) - \lambda_2\omega_j) \quad \text{(S7)}$$

where η is the Ca^{2+}-dependent learning rate and Ω is a Ca^{2+}-dependent function with two thresholds (θ_d and θ_p; $\theta_d \leq \theta_p$) (for details see Li et al., 2009); λ_1 and λ_2 represent scaling and decay factors respectively; the local calcium level at synapse j is denoted by $[Ca^{2+}]_j$ and Δt is the simulation time step. With this learning rule, the synaptic weight decreases when $\theta_d < [Ca^{2+}]_j < \theta_p$, and increases when $[Ca^{2+}]_j > \theta_p$, with modulation by the decay term $\lambda_2 w_j$.

Concentration of calcium pools: The concentration of the calcium pool at synapse j followed the dynamics in Eq. S6, with f_j= 0.024 (Warman et al. 1994), τ_j = 50 ms (Shouval et al. 2002b), V is the volume of a spine head with a diameter of 2 μm (Kitajima and Hara 1997). All the synaptic weights were constrained by upper (W_{max}) and lower

(W_{min}) limits (Li et al., 2009). Maximum (f_{max}) and minimum (f_{min}) folds were specified for each modifiable synapse so that $W_{max}= f_{max}*w(0)$ and $W_{min} = f_{min}*w(0)$.

Excitatory synapses onto principal cells. For tone-principal cell, and principal cell-principal cell connections, the calcium influx which determines learning was calculated by using the NMDA current, $I_{Ca}^{N} = P_0 w^{-1} G_{NMDA}(V - E_{Ca})$ (Shouval et al., 2002b), where $G_{NMDA} = \bar{A}w(t)g_{NMDA,max}s(V)\frac{\tau_1\tau_2}{\tau_2-\tau_1}\left[\exp\left(-\frac{t}{\tau_2}\right) - \exp\left(-\frac{t}{\tau_1}\right)\right]$ from eqn. S4, the term w^{-1} ensures that it is calculated per synapse, and $P_0 = 0.015$.

Excitatory synapses onto interneurons. For tone-interneuron, and principal cell-interneuron connections, the calcium influx (used for learning) at the excitatory synapses on interneurons occurs through both NMDA and AMPA receptors (details in Li et al., 2009). In addition to calcium influx through NMDA current I_{Ca}^{N}, the calcium influx through AMPA receptors was calculated as $I_{Ca}^{A} = P_0 w^{-1}(0) G_{AMPA}(V - E_{Ca})$ where G_{AMPA} is the AMPA conductance in eqn. S4 (as described in the earlier para for G_{NMDA}), and $w(0)$ is the initial AMPA synaptic weight, $P_0 = 0.001$. The Ca^{2+} current through the AMPA/NMDA receptors was separated from the total AMPA/NMDA current in this manner and used for implementation of the learning rule (Kitajima and Hara, 1997; Shouval et al., 2002a; Li et al., 2009).

Inhibitory synapses onto principal cells. Several different mechanisms have been reported for potentiation at GABAergic synapses in other brain regions (e.g., Gaiarsa et al., 2002). A rise in postsynaptic intracellular Ca^{2+} concentration seems to be required in most mechanisms to trigger long-term plasticity. In the neonatal rat hippocampus,

potentiation could be induced by Ca^{2+} influx through the voltage-dependent Ca^{2+} channels (VDCCs), whereas in the cortex and cerebellum, this process requires Ca^{2+} release from postsynaptic internal stores that is dependent on stimulation of GABA receptors (Gaiarsa et al., 2002). Thus, both presynaptic activity (GABA receptor stimulation or interneuron firing) and postsynaptic activity (activation of VDCCs by membrane depolarization) contribute to the potentiation of GABA synapses. The process from GABA receptor stimulation to internal Ca^{2+} release involves activating a cascade of complex intracellular reactions (Komatsu 1996). Such a complex process can be simplified by assuming that the Ca^{2+} release is proportional to the stimulation frequency or $GABA_A$ conductance (Li et al., 2009). Hence we modeled this simplified process by considering Ca^{2+} release from the internal stores into a separate Ca^{2+} pool, using an equation similar to that for the AMPA/NMDA case cited above:
$I_{Ca}^{G} = P_0 w^{-1}(t) G_{GABA}(V - E_{Ca})$ with P_0 = 0.01, and G_{GABA} as the $GABA_A$ conductance in Eq. S5 (as described earlier for G_{NMDA}). Note that the current I_{Ca}^{G}, models the dependence of Ca^{2+} release on $GABA_A$ stimulation frequency but not Ca^{2+} influx through the $GABA_A$ channel. The current I_{Ca}^{G}, together with post-synaptic voltage dependent calcium current (I_{Ca}), contributed towards plasticity. Hence, $I'_{Ca} = I_{Ca}^{G} + 0.01 I_{Ca}$ was used to calculate calcium influx for learning at such synapses. (Li et al., 2009)

The initial weights and other learning parameters for the synapses are listed in **Table S4**.

Table S1. Gating variables for ion channels used in the single cell models.

Current Type		Gating Variable	α	β	x_∞	τ_x (ms)
I_{Na}		*p=3*	$\frac{-0.4(V+30)}{\exp[-(V+30)/7.2]-1}$	$\frac{0.124(V+30)}{\exp[(V+30)/7.2]-1}$	$\alpha/(\alpha+\beta)$	$\frac{0.6156}{\alpha+\beta}$
		q=1	$\frac{0.03(V+45)}{\exp[-(V+45)/1.5]-1}$	$\frac{0.01(V+45)}{\exp[(V+45)/1.5]-1}$	$\frac{1}{\exp\left[\frac{V+50}{4}\right]+1}$	$\frac{0.6156}{\alpha+\beta}$
I_{DR}		*p=1*	$\exp[-0.1144(V-13)]$	$\exp[-0.08(V-13)]$	$\frac{1}{1+a}$	$\frac{30.78\beta}{1+\alpha}$
I_H		*p=1*	$\exp[0.08316(V+75)]$	$\exp[0.033264(V+75)]$	$\frac{1}{\exp\left[\frac{V+81}{8}\right]+1}$	$\frac{\beta}{0.0473(1+\alpha)}$
I_M		*p=2*	$\frac{0.016}{\exp[-(V+52.7)/23]}$	$\frac{0.016}{\exp[(V-52.7)/18.8]}$	$\alpha/(\alpha+\beta)$	$1/(\alpha+\beta)$
I_{Ca}		*p=2*	$\frac{-15.69(V-81.5)}{\exp[-(V-81.5)/10]-1}$	$0.29\exp[-V/10.86]$	$\alpha/(\alpha+\beta)$	$1/(\alpha+\beta)$
		q=1	—	—	$\frac{0.001}{0.001+[Ca]_i}$	—
I_A	**soma**	*p=1*	$exp\left[0.0381(V-11)\left[-1.5 - \frac{1}{\exp[(V+40)/5+1]}\right]\right]$	$exp\left[0.021(V-11)\left[-1.5 - \frac{1}{\exp[(V+40)/5+1]}\right]\right]$	$\frac{1}{1+\alpha}$	$\frac{6.4826\,\beta}{1+\alpha}$
		q=1	$\exp[0.1144V+56]$	—	$\frac{1}{1+\alpha}$	$0.26(V+50)$
	dend	*p=1*	$exp\left[-0.0687(V+1) + \frac{0.0382(V+1)}{\exp[(V+40)/5]+1}\right]$	$exp\left[-0.026793(V+1) + \frac{0.014898(V+1)}{\exp[(V+40)/5]+1}\right]$	$\frac{1}{1+\alpha}$	$\frac{3.2413\beta}{1+\alpha}$
		q=1	$\exp[0.1144(V+56)]$	$\exp[0.1144V+56]$	$\frac{1}{1+\alpha}$	$0.26(V+50)$
I_{sAHP}		*p=1*	$\frac{0.0048}{\exp(-5\log_{10}([Ca]_{i2})-17.5)}$	$\frac{0.012}{\exp(2\log_{10}([Ca]_{i2})+20)}$	$\alpha/(\alpha+\beta)$	1000-2000

Table S2. Maximal conductance densities of ion channels.

Conductance (mS/cm^2)		I_{Na}	I_{DR}	I_M	I_H	I_{Ca}	I_A	I_{sAHP}	τ_{Ca}
Principal cell - Type A	Soma	54	3	0.55	-	0.2	1.43	-	-
	Dend	27	3	0.55	0.0286	0.2	0.32	7	1000
Principal cell - Type B	Soma	54	3	0.39	-	0.2	1.43	-	-
	Dend	27	3	0.39	0.0286	0.2	0.32	0.45	1000
Principal cell - Type C	Soma	54	3	0.4	-	0.2	1.43	-	-
	Dend	27	3	0.4	0.0286	0.2	0.32	0.36	1000
Interneuron	Soma	35	8	-	-	-		-	-
	Dend	10	3	-	-	-		-	-

Table S3. Variations in maximal conductances to model neuromodulator effects.

NM	Receptor	Channel	Low level of NM (during trials 2-10 of conditioning)	High level of NM (during trials 11-16 of conditioning and trails 1-4 of extinction)	Highest level of NM (during shock)
Dopamine	D_1Rs (Low affinity)	I_{Kdr}	-	Decrease *gKdr* by 10%	Decrease *gKdr* by 20%
		AP threshold	-	Change activation of Na^+ channel by -0.5mV	Change activation of Na^+ channel by -1.5mV
		NMDA (pyr-pyr)	-	Decrease *gNMDA* by 5%	Decrease *gNMDA* by 20%
		GABA (interneuron-pyr)	-	Increase *gGABA* by 40%	Increase *gGABA* by 60%
	D_2Rs (High affinity)	Input Resistance	Decrease *gleak* by 5%	Decrease *gleak* by 10%	Decrease *gleak* by 20%
		GABA (interneuron-pyr)	Decrease *gGABA* by 20%	Decrease *gGABA*, by 20%	Decrease *gGABA*,by 30%
Norepinephrine	NE-α (High affinity)	NMDA (thalamic input to interneuron)	Increase *gNMDA* by 5%	Increase *gNMDA* by 10%	Increase *gNMDA* by 30%
		NMDA (Cortical input to principal cells)	Decrease *gNMDA* by 10%	Decrease *gNMDA* by 30%	Decrease *gNMDA* by 30%
	NE-β (Low affinity)	I_{sAHP}	-	Reduce *gK,sAHP* by 20%	Reduce *gK,sAHP* by 30%
		NMDA (Cortical input to principal cells)	-	Increase *gNMDA* by 20%	Increase *gNMDA* by 50%
		NMDA (Cortical input to interneurons)	-	Decrease *gNMDA* by 20%	Decrease *gNMDA* by 30%

Table S4. Model synaptic strengths and learning parameters.

Connection	Initial Weight	f_max (f_min=0.8 for all)	Learning factor		Ca^{2+} Threshold	
			scaling	Decay	Low	High
Tone to Pyr (Thalamic)	5.5	3.5	80	0.04	0.40	0.53
Tone to Pyr (Cortical)	6	3.5	10	0.04	0.40	0.53
Tone to Inter (Thalamic)	4.5	4	5	0.01	0.45	0.5
Tone to Inter (Cortical)	4	4	20	0.01	0.45	0.5
PyrD to PyrD	0.7	4	80	0.03	0.3	0.55
PyrD to PyrV	0.7	4	10	0.03	0.3	0.55
PyrV to PyrD	0.7	4	80	0.03	0.3	0.55
PyrV to PyrV	0.7	4	10	0.03	0.3	0.55
InterD to PyrD	4.5	4	4	0.01	0.47	0.52
InterD to PyrV	4.5	4	2	0.01	0.47	0.52
InterV to PyrD	4.5	4	4	0.01	0.47	0.52
InterV to PyrV	4.5	4	2	0.01	0.47	0.52
PyrD to InterD	1	3	3	0.01	0.4	0.45
PyrD to InterV	1	2	2	0.01	0.4	0.45
PyrV to InterD	1	3	3	0.01	0.4	0.45
PyrV to InterV	1	3	2	0.01	0.4	0.45

- Shock synapses do not potentiate (weight =10 for synapses onto both principal cells and interneurons, in thalamic and cortical pathways).

1 Compartment LA Model

Range: Vrest : -69±1 mV Rin: 150±10 MΩ

Type C :

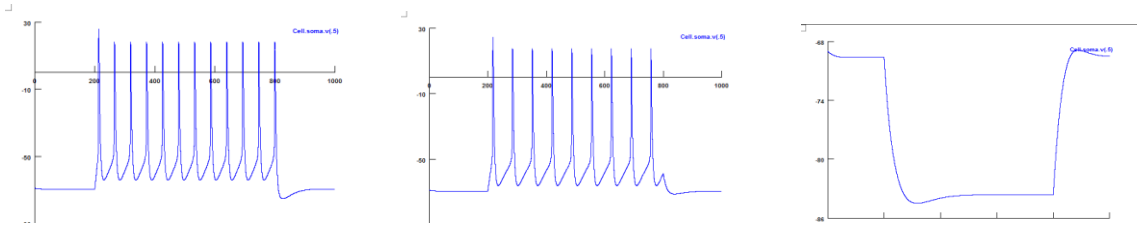

Current injection response of Type C cell to 400pA (left), 300pA (middle) and -100pA (right).

Vrest = -69.58 mV Rin = 149.2 MΩ

Type B :

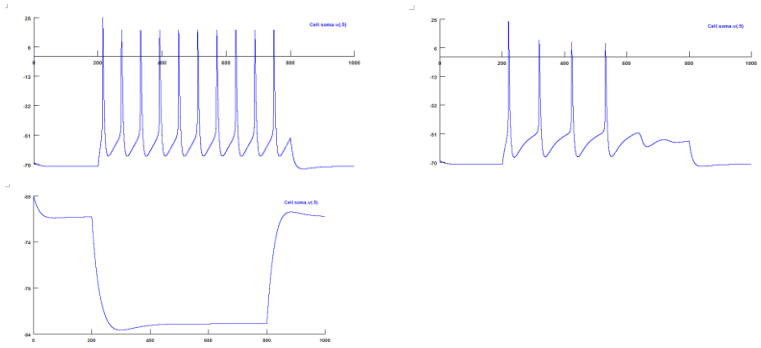

Current injection response of Type B cell to 400pA (left), 300pA (middle) and -100pA (right).

Vrest = -71.29 mV Rin = 122.6 MΩ

Type A :

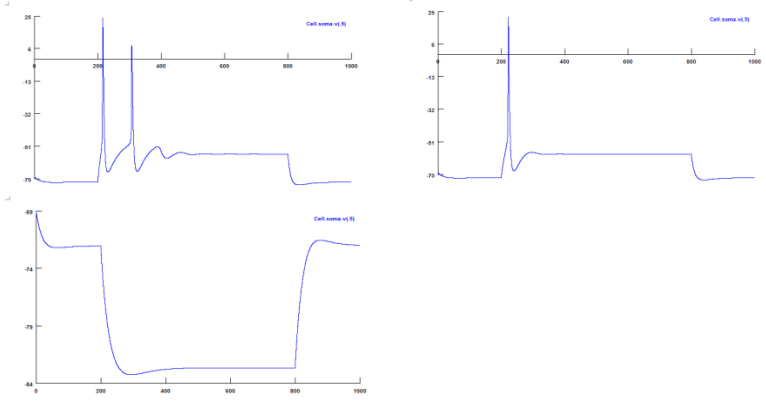

Current injection response of Type A cell to 400 pA (left), 300pA (middle) and -100 pA (right).

Vrest = -72.06 mV; Rin = 111.8 MΩ

Limitations of 1-compartment model:

- Input resistance and Vrest out of range: The spiking behavior of type B and type A cell can only be achieved if input resistance and Vrest are let go beyond their bounds. This may be due to the fact that as it does not have dendritic compartments, all conductances are at same location and interact with each other causing problems.
- Reduction in spike amplitude: The amplitude of spike decreases for type B and type A cell.

Table S5. the comparison the three compartmental model with other models

	Ch	**g** [mS/cm^2]	Multi- Cmpt		3-Cmpt	1-Cmpt
			Total	Selected apical dend		
Axon	I_{Na}	g_{Na}	36		×	×
	I_{Ca}	g_{Ca}	0.2		×	×
	I_{Kdr}	g_{Kdr}	3		×	×
	I_A	g_A	1.55(avg)		×	×
	I_{leak}	g_{leak}	0.0286		×	×
	SIZE	L [μm]	75(Initial), 250(main)		×	×
		Diam[μm]	1.25(Initial), 0.5(main)		×	×
		Total Area [μm^2]	218.75π = 93.75π[I] + 125π[M]		×	×
	R_a [ohm-cm]		50		×	×
	C_m [μF/cm^2]		1		×	×
Soma	I_{Na}	g_{Na}	18		54	27
	I_{Ca}	g_{Ca}	0.2		0.2	0.2
	I_{Kdr}	g_{Kdr}	3		3	3
	I_h	g_h	0.0021		×	0.0285993
	I_A	g_A	14.3		1.43	×
	I_M	g_M	×		0.55 (type A), 0.39 (type B), 0.4 (type C)	1.74 (type A), 1.42 (type B), 1.4 (type C)
	I_{leak}	g_{leak}	0.0286		0.0182	0.0933
	SIZE	L [μm]	20		25	58
		Diam[μm]	20		24.75	24.5
		Total Area [μm^2]	400π		618.75π	1421 π
	R_a [ohm-cm]		200		146.969697	200
	C_m [μF/cm^2]		1		1.4	4.5
Dendrite	I_{Na}	g_{Na}	18		27	×
	I_{Ca}	g_{Ca}	0.2		0.2	×
	I_{Kdr}	g_{Kdr}	3		3	×
	I_h	g_h	0.0123(avg)	0.00985993	0.0285993	×
	I_A	g_A	37.4(avg)	31.913796		×
	I_M	g_M	×		0.55 (type A), 0.39 (type B), 0.4 (type C)	×
	I_{sAHP}	g_{sAHP}	2.318144e-05		7 (type A), 0.45 (type B), 0.36 (type C)	100 (type A), 71.2 (type B), 0.015 (type C) in Soma
	τ_{Ca} (ms)		×		1000	×
	I_{leak}	g_{leak}	0.0565	0.0481	0.0481	×
	SIZE	L [μm]	Various		118.5(apical) 400 (p_dend)	×
		Diam[μm]	Various		2.5(apical) 5(p_dend)	×
		Total Area [μm^2]	3577π	296.25π	296.25π(apical) 2000 π(p_dend)	×
	R_a [ohm-cm]		200		200	×
	C_m [μF/cm^2]		1.3-2		1.4-2.8	×

CHAPTER 6

SUMMARY, CONTRIBUTIONS, AND FUTURE WORK

6.1 SUMMARY

Neuroscience spans several levels from genetic and proteomic to metabolomic, cellular, network and systems, to behavioral and clinical levels. Scientists typically study such systems at one level. Neurophysiological data are accumulating rapidly at several of these levels, and so the time is ripe for the development of computational tools to integrate such data and reverse engineer how brains work, to complement experimental investigations in furthering our understanding of how brains work. Another trait that makes computational modeling attractive is that it is very cost-effective compared to biological experimentation. The synergy of modeling and experimental techniques thus has the potential to inform one another and accelerate scientific discovery. Here we have presented four studies that demonstrate the utility of modeling to address hypotheses in a region of the human brain circuit that has implications for post-traumatic stress and a variety of anxiety disorders.

CHAPTER 2

In chapter 2, a large scale biophysical model of LAd is developed using biological data, and used to shed light on an outstanding issue related to auditory Pavlovian fear conditioning: the relative contributions of plasticity in auditory afferent (thalamic, cortical) neurons vs. within LA. Model experiments investigated whether fear memories depend on (1) training-induced increases in the responsiveness of thalamic and cortical

neurons projecting to LA, (2) plasticity at the synapses they form in LA, and/or (3) plasticity at synapses between LA neurons. These tests revealed that training-induced increases in the responsiveness of afferent neurons are required for fear memory formation. However, once the memory has been formed, this factor is no longer required because the efficacy of the synapses that thalamic and cortical neurons form with LA cells has augmented enough to maintain the memory. In contrast, our model experiments suggest that plasticity at synapses between LA neurons plays a minor role in maintaining the fear memory.

CHAPTER 3

The issue related to the formation of fear memory is a more general finding since it has applicability to other regions of the brain including the hippocampus. In that study, we examined how particular LA neurons are assigned to the fear memory trace, i.e., of the 24,000 neurons in the rodent lateral amygdala, which 20% are assigned to the fear memory trace and why. This study revealed that cells with high intrinsic excitability are more likely to be integrated into the memory trace via competitive synaptic interactions. We found that subsets of projection cells effectively band together by virtue of their excitatory interconnections to suppress plasticity in other principal neurons via the recruitment of inhibitory interneurons.

Future work: The model should be investigated to determine its 'limits' of performance, i.e., when might the model fail. For instance, is there a level of connectivity below which the principal cells cannot effectively band together to suppress other cells. Similarly, different connectivity configurations should also be investigated, e.g., uniform

connectivity, to determine whether competition might still hold. Also, the recruitment of neurons into a memory trace due to their intrinsic properties and connectivity could be applicable to several other regions of the brain including the neocortex and the hippocampus. Models with neurons from these regions could investigate whether such 'competition' underlies memory formation in the brain in general.

CHAPTER 4

This chapter suggested how intra-amgydalar plasticity might implement competition, and that competition and stimulus specificity may be inter-related. The model suggested that plasticity in both excitatory and di-synaptic inhibitory connections from principal cells involved in the memory formation were necessary for the competition. The model also suggested that plasticity between principal cells promotes while disynaptic inhibition opposes stimulus generalization, and that the plasticity configuration imprinted in the network for a particular memory by competition also ensures specificity to that memory. *Future work:* Different network sizes and connectivity configurations should be considered to determine the generalizability of the ideas revealed by the study.

CHAPTER 5

In Chapter 5, we considered the more focused problem of how to develop a single cell conductance-based biophysical model that provides 'acceptable biological behavior' for network studies. Should they have 1-, 2- or multiple compartments? Although other model such as the Izhikevich model that preserves neuro-computational properties do provide attractive alternatives, they are not suited for detailed biological studies that

require realistic synapses, neuromodulation, and morphology to represent transmission of signals from dendrites to soma and vice versa. We developed a 3-compartment single cell model that seems to provide a good compromise between biological realism and ease of computation. The model was then compared with 1-, 2- and 69-compartmental models to highlight the differences, and provide users with guidance of when to use which model.

Future work: More detailed studies of the synaptic transmission properties of the 3-compartmental model should be conducted, particularly as it impacts plasticity. This could include a study of the various plasticity models, including the role of dendritic spikes and back propagating action potentials on modulating such plasticity.

VITA

Dongbeom Kim was born and raised in Seoul, South Korea, and graduated from Chung-ryang High School in February of 1994. During his undergraduate studies at the Korea Military Academy (KMA), Dongbeom studied electrical engineering while preparing to be an army officer in KMA. In March of 1998, he received his BS in Electrical and Computer Engineering from KMA and was commissioned as a second Lieutenant of Army. After 10 years service in army, he entered graduate school at Seoul National University, completing his MS in ECE in February 2007 with an emphasis in Missile navigation, control and guidance technology.

Dongbeom then entered a Ph.D. program at University of Missouri-Columbia in the fall of 2008 to study computational neuroscience. He has authored or co-authored two conference papers, with one journal paper accepted, two others ready to be submitted, and one in preparation. He has presented three posters at the annual Society for Neuroscience Meetings. All the publications and presentations are listed below. He continues to be an officer, a Major in the Korean army, and is scheduled to return after graduation to work for the Korean government agency, Defense acquisition program agency.

PUBLICATIONS

Refereed Journal and Conference Articles

- Pendyam S, **Kim D**, Quirk GJ, Nair SS (2010) Acquisition of fear and extinction in lateral amygdala-a Modeling Study. *Proceedings of the Dynamic Systems and Control Conference*, Cambridge, MA, DSCC 2010-4218 pp. 413-421.
- **Kim D**; Samarth PS, Chen Y, Nair SS (2012). Computational study of the impact of neuromodulation and dendritic morphology on synaptic plasticity. *Proceedings of the Dynamic Systems and Control Conference.*
- **Kim D,** Pare D, Nair SS (2013) Mechanisms contributing to the induction and storage of pavlovian fear memories in the lateral amygdala, *Learning & Memory* (in press).

- **Kim D,** Pare D, Nair SS (2013) Assignment of lateral amygdala neurons to the fear memory trace depends on competitive synaptic interactions. To be submitted to *Journal of Neuroscience* (in press)
- **Kim D,** Nair SS (2012) Synaptic mechanisms related to competition and specificity of amygdalar fear (in preparation)
- **Kim D,** Pranit S, Chen Y, Nair SS (2012) Development of reduced order biologically realistic cell models (in preparation).

Posters and Presentations

- **Kim D,** Pendyam S, Pare D, Nair SS (2011) Modeling acquisition and extinction of auditory fear in the lateral amygdala– a computational modeling study. 41th *Society of Neuroscience (SfN) Annual Meeting*, Washington, DC, November, 12–16.
- **Kim D,** Pare D, Nair SS (2012) Assignment of lateral amygdala neurons to the fear memory trace depends on competitive synaptic interactions. 42th *Society of Neuroscience (SfN) Annual Meeting*, New Orleans, LA, October, 13–17.
- **Kim D,** Pranit S, Chen Y, Nair SS (2012) Development of reduced order biologically realistic cell models. 42th *Society of Neuroscience (SfN) Annual Meeting*, New Orleans, LA, October, 13–17.